



universität
wien

MAGISTERARBEIT

Titel der Magisterarbeit

BINARY AGB STARS OBSERVED WITH HERSCHEL

Verfasser

Klaus Kornfeld, Bakk.rer.nat.

angestrebter akademischer Grad

Magister der Naturwissenschaften (Mag.rer.nat.)

Wien, 2012

Studienkennzahl lt. Studienblatt:

A 066 861

Studienrichtung lt. Studienblatt:

Astronomie

Betreuer:

Ao. Univ.-Prof. Mag. Dr. Franz Kerschbaum

Every atom in your body came from a star that exploded. And the atoms in your left hand probably came from a different star than your right hand. It really is the most poetic thing I know about physics: You are all stardust. You couldn't be here if stars hadn't exploded, because the elements - the carbon, nitrogen, oxygen, iron, all the things that matter for evolution - weren't created at the beginning of time. They were created in the nuclear furnaces of stars, and the only way they could get into your body is if those stars were kind enough to explode. So, forget Jesus. The stars died so that you could be here today.

- Lawrence Krauss

Contents

Kurzbeschreibung/Abstract	9
Danksagung/Acknowledgement	13
1 Introduction	17
1.1 The Herschel Space Observatory	17
1.1.1 The satellite	18
1.1.2 On-board instrumentation	18
1.1.3 The Herschel Interactive Processing Environment	21
1.1.4 The Herschel Key Program MESS	22
1.2 The Asymptotic Giant Branch	23
1.2.1 AGB stars	25
1.3 The atmosphere and outer CSE	29
1.3.1 Observational properties	30
1.3.2 Mass loss	32
1.3.3 Geometry of the CSE	33
1.4 Outflow morphology	35
1.4.1 Morphology as seen by Herschel	36
2 Binary AGB stars	45
2.1 Binary stars	45
2.1.1 Classification	45
2.2 Properties of binary stars	50
2.2.1 Frequency	50
2.2.2 Age	51
2.2.3 Separation and period	51
2.2.4 Eccentricity	52
2.2.5 Spin-orbit alignment	53
2.2.6 Orbit-orbit alignment	54
2.2.7 Mass ratio	54
2.2.8 Multiple systems	54
2.3 Formation scenarios of binary systems	55
2.3.1 Separate nuclei	55
2.3.2 Capture	55

2.3.3	Fission	57
2.3.4	Fragmentation	57
2.3.5	Cloud clump collisions	61
2.3.6	Eccentric disk instability	62
2.4	Interacting binary stars	63
2.4.1	Circumstellar envelopes	64
2.4.2	Circumbinary envelopes	65
2.4.3	Mass loss through wind	65
2.5	Binary AGB stars	65
2.6	The Roche equipotential	66
2.6.1	The Roche lobe	66
2.6.2	Limitations of the Roche lobe concept	68
2.7	Detecting binaries with AGB stars	70
2.7.1	Radial-velocity variations	72
2.7.2	A visual companion	74
2.7.3	Composite nature of the spectrum and/or symbiotic activity	74
2.7.4	X-ray emission	75
2.7.5	Shallow light curves from Mira variables	76
2.7.6	Lunar occultations	76
2.7.7	Imaging of CSE asymmetries	77
2.7.8	Interferometric detection	77
2.8	AGB mass loss in a binary system	78
2.8.1	Funneling through L_1	78
2.8.2	The spiral arm	79
2.8.3	Disk	80
2.8.4	Dust formation in the outflow zone	80
2.9	The successors of AGB stars in binary systems	80
2.9.1	Technetium and intrinsic/extrinsic S stars	81
2.9.2	Successors	81
3	Binary AGB candidates in the Herschel MESS sample	85
3.1	U Cam	86
3.2	VY CMa	88
3.3	TX Cam	89
3.4	VY UMa	91
3.5	V Eri	92
3.6	W Aql	93
3.7	EP Aqr	93
3.8	LL Peg	95
3.9	R Aqr	96
3.10	θ Aps	98
3.11	TW Hor	99

3.12 π^1 Gru	100
3.13 o^1 Ori	101
3.14 o Cet (Mira)	102
4 Discussion	109
4.1 Chemistry	110
4.2 Magnetic field	110
4.3 Stand-off distance of the bow shock	110
4.4 The ISM density	112
5 Conclusions	115
Bibliography	116
Appendix	129

Kurzbeschreibung

Sterne am Asymptotischen Riesenast (AGB) sind Objekte mit niedrigen bis mittleren Massen und am Ende ihrer Lebensdauer angelangt. Sie sind besonders wichtig im galaktischen Kontext, weil sie das meiste Material, sogar mehr als Supernovae, zur chemischen Entwicklung des interstellaren Mediums (ISM) beitragen und so die Evolution der Galaxie beeinflussen. Viele AGB Sterne zeigen ungewöhnliche Morphologien auf, verursacht durch Massenverlustprozesse der Sterne. Der ausströmende Wind von AGB Sternen kollidiert mit dem umgebenden ISM und daraus resultiert in den meisten Fällen eine Bugstosswelle in Richtung der stellaren Raumbewegung, die auch Kelvin-Helmholtz und Rayleigh-Taylor Instabilitäten aufweisen kann, oder eine ringförmige Struktur, die den Stern umgibt, wie in den neuesten Aufnahmen des Infrarot-Weltraumteleskops Herschel zu sehen ist. Mit Hilfe dieses Weltraumobservatoriums untersuchte man im Rahmen des MESS (engl.; Massenverlust von entwickelten Sternen) Programms ein Sample von 78 AGB Sternen. Dabei wurden 4 verschiedene morphologische Typen festgestellt: “*fermata*”, “*eye*”, “*ring*”, und “*irregular*”. Auch Punktquellen sind im Sample zu finden. Um herauszufinden, ob bestimmte Morphologien auf einen Begleitstern hinweisen, kann man die von Herschel gefundenen Ausströmungen mit in Doppelsternen bekannten morphologischen (A-)Symmetrien vergleichen. Diese Magisterarbeit beschäftigt sich mit 14 AGB Doppelsternkandidaten aus dem MESS Sample und vergleicht frühere Ergebnisse mit den neuesten Entdeckungen durch Herschel. Das Herschel Weltraumteleskop kann, dadurch, dass es im Infraroten beobachtet, durch die Staubschicht, die durch den Massenverlust sich um den AGB Stern bildet, hindurchsehen. Ein AGB Doppelsternsystem zu identifizieren kann sehr schwierig sein, weil der AGB Stern starke stellare Winde, in dem Staub gebildet wird, aufweisen kann, was die direkte Detektion eines Begleiters stark einschränkt. Um dennoch einen solchen nachzuweisen, bedient man sich anderer Methoden wie Photo- und Spektroskopie, CO Linien-Messungen oder das Analysieren von Komposit-Spektren.

In der Einleitung ist eine kurze Beschreibung der Herschel Cornerstone-Mission des Horizont 2000-Programms der ESA und eine Beschreibung des MESS Programms gegeben, gefolgt von einer Zusammenfassung über AGB Sterne, die verschiedene Morphologien aufweisen. Bevor 14 Objekte im Detail beschrieben werden, geht Kapitel 2 auf die Theorie der AGB Doppelsterne ein. Am Ende werden alle alten und neuen Erkenntnisse diskutiert und verschiedene Rückschlüsse gezogen, wie die Morphologie mit der Chemie (sauerstoff- oder kohlenstoffreiche Atmosphäre), mit der Distanz des Sterns zur Bugstosswelle (im Allgemeinen < 1 pc) und der lokalen ISM Dichte zusammenhängt.

Abstract

Asymptotic Giant Branch stars are stars at the end of their lifetime with low to intermediate masses. They are important in the Galactic context, since they contribute a lot of dust to the interstellar medium (ISM) and influence the chemical evolution of the Galaxy. Many AGB stars show peculiar outflow morphologies depending on their mass-loss rates. The outflowing wind of these stars collides with the surrounding interstellar medium (ISM). The collisions with the ISM result in the formation of bow shocks or rings, well visible in the latest Herschel Space Observatory images made with the on-board PACS instrument. Kelvin-Helmholtz and Rayleigh-Taylor instabilities were found in the bow shock regions. With the help of Herschel and within the framework of the MESS (Mass loss of Evolved StarS) Guaranteed Time Key Program it was tried to distinguish between the different morphologies. The outflow morphologies were categorized in 4 main classes: “*fermata*”, “*eye*”, “*ring*”, and “*irregular*”; also point sources showing no resolved circumstellar envelopes (CSEs) were found. Some of the AGB stars in the MESS sample are known binary stars and the binary state of some other objects is still in discussion. A new attempt to clarify the binarity of the objects can be made by checking their outflow morphology and to compare the results with known morphological (a-)symmetries in binary systems. This Thesis discusses 14 binary AGB candidates from the MESS sample, the previous findings and the Herschel results. Herschel observes at infrared wavelengths. Light at this wavelengths can be seen through the dust, which is formed in the surrounding environment of these stars. For the unknown cases it is difficult to determine the binary state, because AGB stars can have very strong wind outflows, making the detection of a companion difficult. Photo- and spectroscopy, CO line outflow measurements or composite spectra can be used to identify features caused directly or indirectly by the interaction of a primary with a secondary.

At first a brief description of the Herschel mission and the MESS program is given, followed by a short introduction to AGB stars and their mass outflow. Before the objects are introduced in detail, the theory behind binary AGB stars is presented. At the end all the available findings are discussed and conclusions about the dependency of the outflow morphology on the chemistry (C or O), the stand-off distance of the bow shock (in general < 1 pc) and the local ISM density (depending on the height above the Galactic plane) are tried to be made.

Danksagung

Ganz besonders möchte ich mich bei meinem Supervisor Franz Kerschbaum bedanken, der es möglich gemacht hat, an einem sehr aktuellen Thema zu arbeiten. Mein Dank gilt auch Andreas Mayer, der mich ohne Probleme in seine aktuelle Publikation miteinbezogen hat, was ich als Magister Student nicht als selbstverständlich halte. Ich danke auch Roland Ottensamer, der immer eine Antwort auf Fragen betreffend der Herschel PACS Software parat hatte. Ich möchte auch meinen Kollegen, mit denen ich viele Arbeitsstunden im Raum 126-127 im Westtrakt der Universitätssternwarte verbrachte, meinen Dank aussprechen für die vielen ergiebigen Diskussionen, die wir im Laufe der Zeit hatten. Für die konstruktiven Kritiken aus der AGB Arbeitsgruppe bin ich dankbar. Ich danke meinen Eltern, die mir das Studium ermöglicht haben und meine Pläne im Ausland zu studieren verwirklichen konnten.

Zu allerletzt möchte ich mich bei meinen Kollegen, die mit mir studiert haben, bedanken für all den Enthusiasmus während der gemeinsamen Lernstunden. Auch meine Freunde vom International Astronomical Youth Camp (IAYC), an dem ich mehrmals während der Sommerferien teilgenommen habe, sollen an dieser Stelle erwähnt werden. Durch sie lernte ich junge Wissenschaftler in einer internationalen Atmosphäre kennen, die ich vorher nicht kannte.

Ad astra!

Acknowledgement

Foremost i would like to thank my supervisor Franz Kerschbaum, who gave me the chance to work on a current research topic in combination with the newest results obtained with the PACS instrument on-board the Herschel Space Observatory. With his and Andreas Mayer's help i had the pleasure to contribute to a scientific publication as coauthor, what i consider as privilege being a Magister student. I also want to thank Roland Ottensamer for helping me with whatever question i had about software specifications. I am also very grateful for all the discussions with my colleagues in Room 126-127 in the west wing of the University Observatory Vienna and for all constructive criticism of the members of the AGB Working Group.

I thank my parents, who made it possible to let me study Astronomy and met my wish to study abroad in Sweden. The time as exchange student was one of the best experiences i could have wished for.

Finally i would like to thank all my colleagues, who accompanied me during the last years, and the friends i met at the International Astronomical Youth Camp, which i attended several times during the summer holidays, where i for the first time met Astronomy and science students from other countries and learned to enjoy an international atmosphere. This camp certainly changed my way of thinking about Astronomy and science in general.

Ad astra!

1 Introduction

1.1 The Herschel Space Observatory

The Herschel Space Observatory¹ (Herschel, Jewell et al. (2010); Pilbratt et al. (2010)) was launched on May 14th 2009 and is since then the largest telescope in space; at least until the James Web Space Telescope (JWST) takes over this title. It is the only telescope being able to cover a spectral range from the far-infrared (far-IR) to the sub-millimeter (sub-mm) wavelengths (55-672 μm). Its dimensions are 7.5 meters (height) x 4 meters (width), and it had a launch mass of more than 3 tonnes because of the superfluid liquid helium cryostat and the 3 scientific instruments, which will be introduced later in this section. The helium cools down the instruments to a temperature close above absolute zero.

Herschel was originally introduced as FIRSAT, the Far InfraRed and Submillimeter space Telescope. The planning process already began in July 1982 and it was part of the “Horizon 2000” long-term plan of the European Space Agency (ESA). Finally it was implemented as the fourth “cornerstone” mission. The instruments for this mission were chosen by the ESA Science Programme Committee (SPC) in May 1998. During a meeting of the involved institutions with industry, the satellite mission was renamed Herschel in recognition of the 200th anniversary of William Herschel’s detection of infrared light. The ESA facility Herschel is the successor of a number of infrared space telescopes with cryogenic tanks, namely IRAS (InfraRed Astronomical Satellite), ISO (Infrared Space Observatory), Spitzer Space Observatory and AKARI and is thought to build a bridge to the radio range, which was scanned and sampled by SWAS (Submillimeter Wave Astronomy Satellite) until 2004. Herschel’s successor mission, for now named SPICA (Space Infra-Red Telescope for Cosmology and Astrophysics), a mission suggested by the Japanese space agency JAXA, was classified as “mission of opportunity” by ESA. Herschel’s scientific goal is to gain more insight into the physics and processes in the ISM, therefor observing a range of objects from solar type stars to more evolved ones (like on the AGB). The observations are supposed to give new ideas about the star formation history in our Galaxy and to renew our understanding of the physics in the cosmos. The 3 on-board instruments were designed and constructed with the ulterior

¹This Section is based on http://herschel.esac.esa.int/Publ/2008/SPIE2008_Herschel_paper.pdf, which describes the Herschel mission in more detail.

motive to conduct a wide-area photometric survey of the extragalactic and Galactic sky for measuring dust-enshrouded star formation activity, to make a detailed study of the physics and chemistry of the ISM via photometric and spectroscopic surveys, to understand the stellar and interstellar life cycle via an investigation of early- and late-type stars, and also for satellite calibration purposes, to study comets, asteroids and outer planet atmospheres and their respective satellites.

21 Guaranteed Time Key Programs (GTKPs) were approved with a total observing time of 5878.9 hours, divided in the science categories: solar system, ISM/star formation, stars, galaxies/AGNs and cosmology (see Table 1 in the description by Pilbratt¹).

1.1.1 The satellite

Herschel consists of 2 modules, the Payload Module and the Service Module as shown in Figure 1.1. The Payload Module contains a large Cryostat Vacuum Vessel (CVV), which hosts 2 helium tanks, the optical bench with the focal plane unit, and the sunshield. The tanks are big enough for carrying 2360 liters of He II. The helium is important to cool down the satellite with its instruments HIFI, PACS and SPIRE to the needed temperatures of 1.75 to 15 K. The Service Module hosts the servicing systems, the necessary technology for providing power, attitude and orbit control, on-board data handling and command executions and communications with HIFI, PACS and SPIRE; it does not need to be cooled.

Herschel is thought to be able to operate for 3.5 years, relying on the cryostat technology already used with ISO. The satellite was positioned to have an orbit around the Lagrangian point L_2 in the Sun-Earth-Moon system. It has several advantages to place a satellite there, especially the design and construction of the cryotanks could be adopted, e.g. at L_2 the spacecraft always has a “warm” and a “cold” side, which lead to the possibility to construct it to have radiators on the “cold” side to make the cooling mechanism more effective and to reduce the helium boil-off rate for Herschel to extend the mission to the 3.5 years planned.

The Cassegrain-type telescope system consists of a primary mirror with 3.5 m diameter and a 30 cm diameter secondary mirror. For now the primary mirror is the largest SiC telescope operating in space. It consists of 12 segments, together forming a monolithic mirror, which was polished to a thickness of about 3 mm. The secondary mirror was constructed as a single piece. The hole telescope mirror system “just” has a weight of 320 kg.

1.1.2 On-board instrumentation

3 science instruments, able to analyse the light coming from the telescope in different ways, were constructed to provide broadband photometric and spectrometric imaging in six bands (70, 100, 160, 250, 350, 500 μm). This 3 instruments are PACS (Photoconductor Array Camera and Spectrometer), SPIRE (Spectral and Photometric Imaging

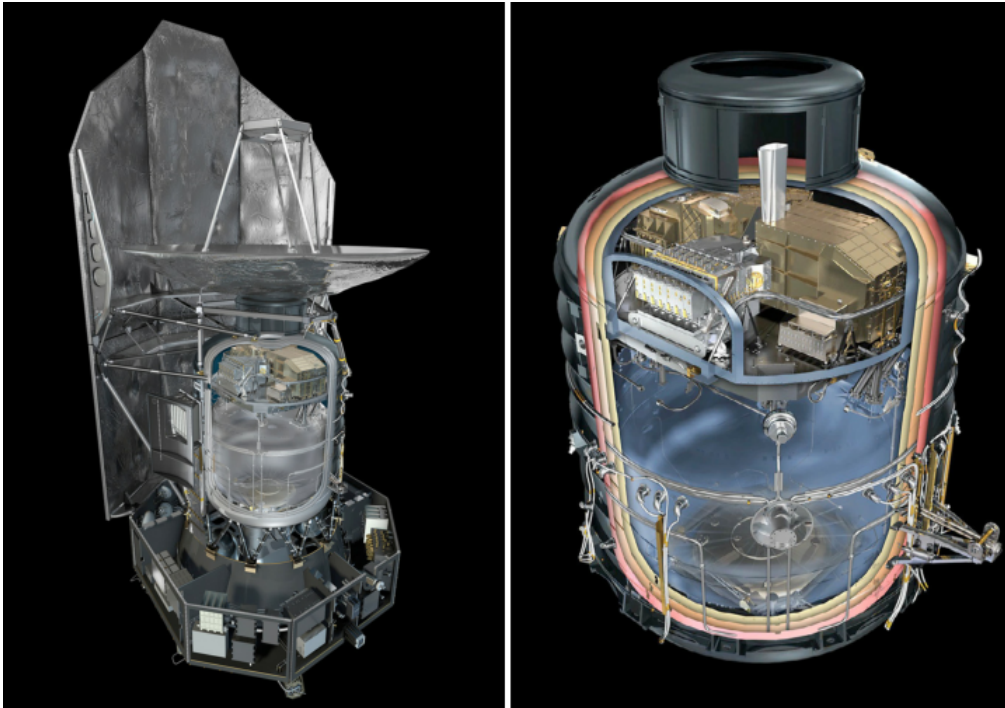


Figure 1.1: **Left:** The Herschel spacecraft featuring the Payload Module (PLM) with the cryostats focal plane unit, the telescope, the Service Module (SVM) and the sunshield/sunshade. **Right:** Payload Module with optical bench with the instrument focal plane units on top the main helium tank and the Cryostat Vacuum Vessel (CVV). *Image courtesy of ESA*

REceiver) and HIFI (Heterodyne Instrument for the Far-Infrared). The instruments were planned and built by 3 consortia of institutions with their respective Principal Investigators (PIs).

Photoconductor Array Camera and Spectrometer (PACS)

PACS consists of 4 detector arrays, 2 bolometer arrays used for photometry and 2 Ge:Ga photoconductor arrays used for spectroscopy. It can be used as an imaging photometer or as an integral field line spectrometer.

The photometer has 3 photometric bands at hand, a short wavelength array covering 60–85 and 85–130 μm (“blue”; sometimes described as “blue1” and “blue2”=“green”) and a long wavelength array covering 130–210 μm (“red”). For photometry the “blue” and ‘red’ bands can be used to observe simultaneously. The photometer gives you a 1.75'' x 3.5'' field of view with a predicted point source detection limit of ~ 3 mJy in all 3 bands.

Spectroscopic measurements with PACS cover a wavelength range of 55–210 μm in 3

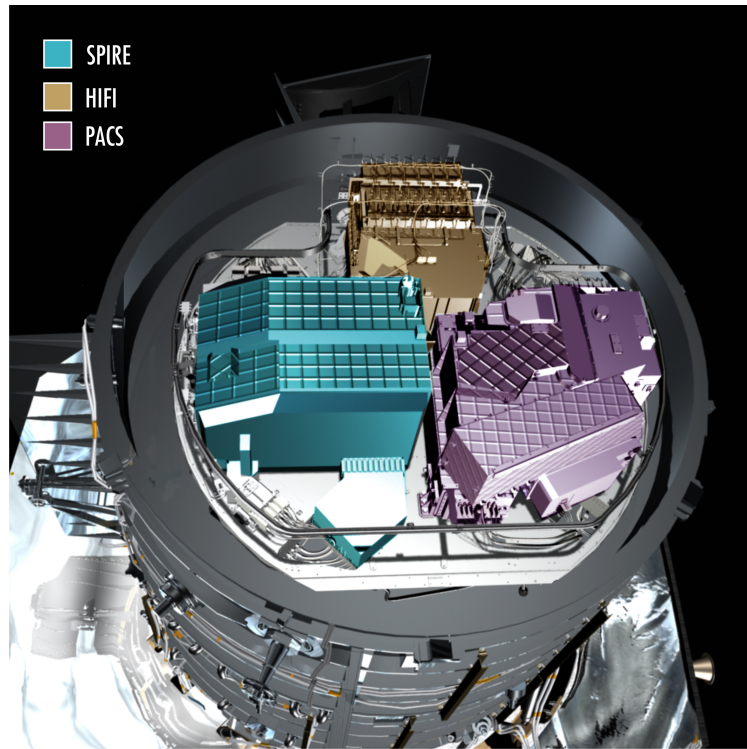


Figure 1.2: The assembly of the instruments PACS, SPIRE and HIFI in the focal plane.
Image courtesy of ESA

contiguous bands with different gratings, giving a resolution of $R \sim 1500\text{--}4000$ corresponding to velocity resolutions from 75 to 300 km s^{-1} with a coverage of $\sim 1500 \text{ km s}^{-1}$. The photoconductor arrays are cooled down to temperatures close to zero Kelvin. The predicted point source limit is $\sim 4\text{--}5$ to $8\text{--}10 \times 10^{-18} \text{ W m}^{-2}$ for longest and shortest wavelengths, respectively.

An extensive description of PACS can be found in Poglitsch et al. (2010). For getting new insights into the bow shocks, detached shells and the outflow morphology of (binary) AGB stars, within the framework of the MESS GTKP the PACS photometer (the “scan map” observing mode) was used to get new data.

Spectral and Photometric Imaging REceiver (SPIRE)

This instrument’s camera and spectrometer work above wavelengths of $200 \mu\text{m}$. It consists of an imaging photometer and a Fourier Transform Spectrometer (FTS), both using bolometer detector arrays, 2 of these arrays are for spectroscopy and 3 for photometry. The bolometers are cooled with the help of a ^3He sorption cooler to a temperature of $\sim 300 \text{ mK}$. The consortium that designed SPIRE, put its emphasis on the mapping speed, estimated to be about $0.25\text{--}0.5$ square degrees on the sky per day.

SPIRE's photometer is able to observe simultaneously in 3 colors (250, 350 and 500 μm), therefor taking images of a $4'$ x $8'$ field on the sky. The point source sensitivity was predicted to be about 8–11 mJy.

The spectrometer uses a broad-band beam divider to cut the incoming beam into 2 overlapping bands of 194–325 and 315–672 μm . The FTS then gives you an interferogram with its spectrum being encoded on the 2 spectroscopic bolometers. The spectral resolution for the spectrometer depends on the wavelength.

An extensive description of SPIRE can be found in Griffin et al. (2010).

Heterodyne Instrument for the Far-Infrared (HIFI)

HIFI is the very high resolution heterodyne spectrometer, offering a velocity resolution of 0.3–300 km s^{-1} . It is not supposed to image objects, it observes single pixels simultaneously in 2 polarisations, giving you enhanced sensitivity. A chopper mechanism splits the incoming beam into 7 bands. Also an oscillator splits the beam into 7 bands, so that you have 7 pairs of them. This pairs are then combined by 5 pairs of superconductor-insulator-superconductor (SIS) mixers and 2 pairs of hot electron bolometer (HEB) mixers, together covering a frequency of ~ 480 –1250 GHz. One pair of mixers covers one band. The mixers are part of the focal plane unit (FLU) that also houses the optics leading the beams to the mixers. Only one band is operating at a time to avoid failures in the processing.

HIFI has 4 spectrometers, 2 for every polarisation. The 2 on-board spectrometers are the high resolution (HRS) and the wide-band (WBS) spectrometer. The HRS is an Auto-Correlator Spectrometer (ACS) handling simultaneously the 2 signals from the 2 polarisations and working in a bandwidth of 235 MHz. The WBS is an Acousto-Optical Spectrometer (AOS) consisting of 2 independent spectrometers handling horizontal and vertical polarisation, respectively, in a bandwidth range of 4–8 GHz.

An extensive description of HIFI can be found in de Graauw et al. (2010).

1.1.3 The Herschel Interactive Processing Environment

The data reduction of images obtained with Herschel is done with HIPE, the Herschel Interactive Processing Environment². HIPE is written in Python and has a user interface giving one access to different tasks helping to get specific informations.

One can get data at different levels, depending on the reduction step. Raw data (produced by the on-board instruments) that can be downloaded from the Herschel Science Archive (HSA³) directly to a local store directory in HIPE, is designated as Level 0. To begin with the first data reduction, one also has to load a calibration tree. First of all calibration blocks, used for the PACS photometer, are to be marked and removed.

²A detailed description for the data processing can be found on http://herschel.esac.esa.int/Data_Processing.shtml

³http://herschel.esac.esa.int/Science_Archive.shtml

Damaged, saturated and dead pixels need to be identified and also to be removed. As it happens for electronic equipment, glitches need also to be taken care of. After this first reduction steps one has Level 0.5 data. The previous procedure has to be employed on all data, disregarding the instrument. However, from Level 0.5 on special tasks depending on the instrument need to be applied. To get Level 1 data, different basic Python scripts were written. According to the requirements and the scientific goal different tasks can be used to get specific results. If one reduces data further, Level 2 data can be produced. This data is then used for science.

For interpreting the outflow morphology via the detection of bow shocks and detached shells, Cox et al. (2012) used the *PhotProject* (with high-pass filter) and *Scanamorphos* map-making algorithms.

The *PhotProject* algorithm uses data processed by the high-pass filter to remove $1/f$ noise and detector drift. This task combines all the frames of an object into a single map. *PhotProject* also prepares the data for a Level 2-deglitching converting the image to a MapIndex object that contains information necessary to deglitch signal contributions for each pixel. Finally the map-making task reprojects the equatorial coordinates of the frames on the sky.

The *Scanamorphos* tool removes low-frequency noise to correct for additive brightness drifts. This brightness drifts can be derived directly from the data, since a portion of the sky is sampled several times by different bolometers at different times. This method is not depending on the noise model. By modifying instrumental parameters, the *Scanamorphos* algorithm can be used with all bolometers. This tool can be adapted to all spatial scales, that's why Cox et al. (2012) used it to restore the extended structures of the objects in Chapter 3. A detailed description of the *Scanamorphos* tool is given in Roussel (2012).

1.1.4 The Herschel Key Program MESS

The MESS Guaranteed Time Key Program⁴ is a collaboration of institutes from Austria, Belgium, Germany, The Netherlands, the UK, and USA. The latest Herschel images in Chapter 3 were obtained via this program, which has 3 main goals: (1) studying the time dependence of the mass-loss process, therefor resolving (multiple) shells around evolved objects to get an idea of the the amount of mass loss of low to high-mass stars, (2) studying the dust and gas chemistry in the CSEs (circumstellar envelopes), (3) studying properties and symmetries of low- and intermediate-mass stars (e.g. the Asymptotic Giant Branch (AGB) stars, post-AGB stars and planetary nebulue (PNe)), high mass post-main sequence objects (red supergiants (RSGs), Wolf-Rayet (WR) stars, luminous blue variables (LBVs)), and supernovae (SNe). In summary the dust evolution in galaxies (like our Milky Way) is tried to be figured out in more detail.

The mass-loss process has been studied already by IRAS, ISO, Spitzer or AKARI; the

⁴A detailed description of the MESS GTKP can be found in Groenewegen et al. (2011a)

basic questions, however, are still not answered in a satisfying manner. Herschel's scientific objective is (based on previous results) to find out more about the time evolution of the mass-loss rate, the geometry (a-symmetry) of mass loss and the resulting structures around stars in PNe or LBVs caused by interaction with the interstellar medium (ISM), and the formation of different dust species at specific locations in the outflowing wind. The geometry of the mass loss around stellar objects sometimes leads to the conclusion that one is in fact observing a binary star, therefore the outflowing morphology around this objects was a starting point to determine whether the observed object is a binary system or not. Compared with previous results for the objects in the MESS sample some binary AGB stars candidates were picked out and examined in more detail concerning their binary nature, which is part of this work. In total the MESS sample contains about 150 evolved stars that are observed with the PACS and SPIRE instruments (both photometric and spectroscopic).

At the end, the MESS consortium achieved observations of 103 evolved objects including AGB stars and post-AGB stars, RSGs, PNs, LBVs, WR stars and 5 SNRs (supernova remnants) with PACS in 70+170 μm with a subset observed with SPIRE. For spectroscopy 55 stars were observed with PACS and 23 with the SPIRE FTS. Concerning AGB stars, all chemical types (M-,S-, C-stars), variability types (irregular, semiregular, Miras) and the full range of periods and mass-loss rates were covered in the observing program. For more promising results the brightest objects with high IRAS fluxes and low background levels were chosen.

In the following Section an introduction to AGB stars is given with the goal to examine the circumstellar environment with the help of Herschel to detect detached rings, bow shocks and the wind-ISM interaction leading to different morphologies sometimes indicating binarity. The subsequent Chapter features binary stars and further focuses on the detection/identification of binary AGB stars, before binary AGB candidates in the MESS sample are discussed.

1.2 The Asymptotic Giant Branch

Asymptotic Giant Branch (AGB) stars were discovered a long time ago and are still full of mystery. In the past decades a lot has been learned about the interior and circumstellar structure of these objects, and about AGB stars being members in binary systems. They are considered as probes of stellar and Galactic evolution, since they are luminous (easily detectable) and defined as old and relaxed systems. A very detailed summary on AGB stars can be found in H. J. Habing (2003) and references therein, on which the following descriptions are based on. For some time now the AGB established itself as an own field of research. One of the interesting facts revealed is that these late-type stars contribute more dust to the Galaxy and so to the cosmic matter cycle than do SNe. It already has been known for a long time that different stars can have different colors.

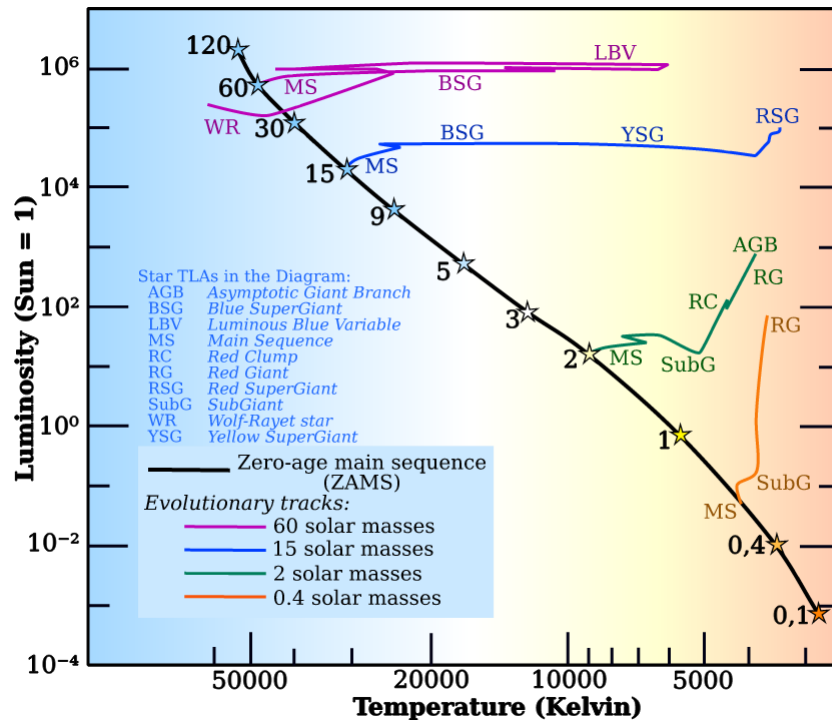


Figure 1.3: The Hertzsprung-Russell diagram. Description in the text. *Modified image under the GNU Free Documentation Licence. Original image courtesy of Jesús Maíz-Apellániz*

Around 1900 the “Planck equation” successfully connected the appearance of colors with thermodynamics and electromagnetic radiation, which pointed out a clear difference between a red giant and a dwarf. Before the first Hertzsprung-Russel diagrams came up, Henry Draper carried out a large survey of a few 100,000 stars to obtain spectra. This survey led to the creation of the Henry Draper (HD) catalogue. Maury, one of Draper’s team members, found a subclass of stars with narrower and deeper absorption lines and called them c stars. Hertzsprung found these c stars to have much smaller proper motions and concluded that they are more distant and have higher luminosities. Russell’s first diagram just considered main-sequence stars, and also included some red giants and a WD. He knew about the latter stars and suggested that their spectra were misinterpreted, which in fact they were. After it was clear that there is a difference between red giant stars and dwarfs, the question about the evolution of stellar systems arose.

In the Hertzsprung-Russell diagram (Figure 1.3) the AGB is the region populated by evolving low- to intermediate-mass stars. All stars with masses of 0.6 to 10 M_{\odot} undertake this evolution late in their lives. When the star runs out of hydrogen (H) produced by nuclear fusion, the core begins to contract and the inner temperature increases. This

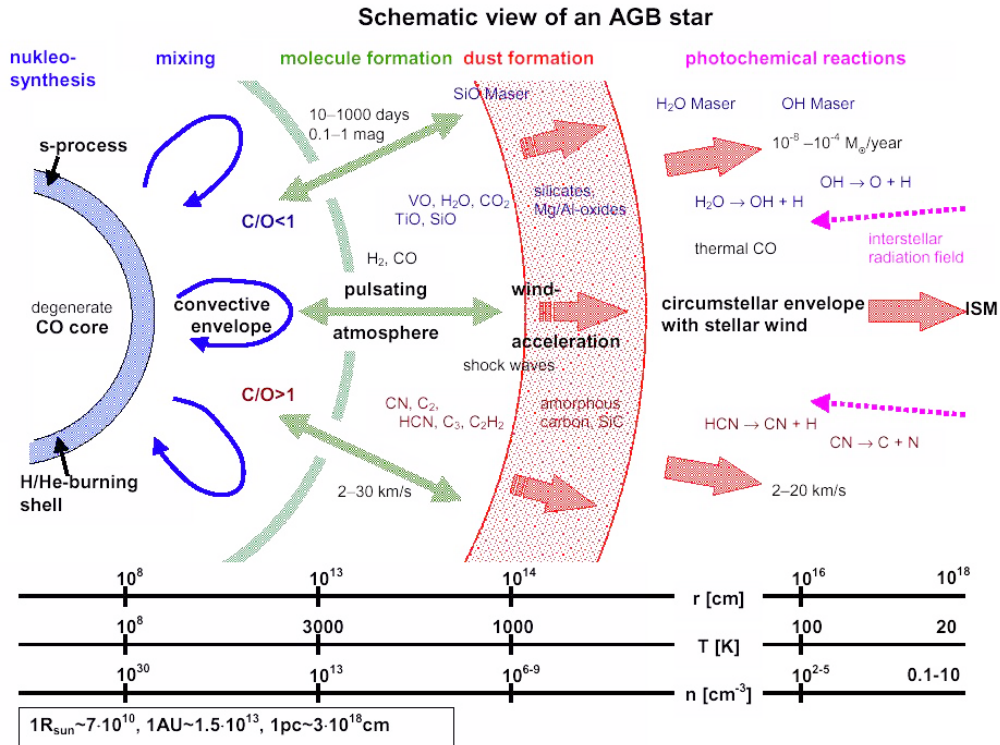


Figure 1.4: Structure of a TP-AGB star with an O-rich (upper half) and a C-rich (lower half) atmosphere. Radius, temperature and density dimensions are also indicated. Further description in the text. *Figure modified by J. Hron. Original courtesy of Th. Le Bertre*

causes the outer layers of the star to expand and to cool down. The expansion of the layers and the additionally increase in luminosity generates a big star, known as a red giant. Red giants can appear from yellow orange to red with the spectral types K and M, and also S and carbon stars (see the upper-right corner in the HR diagram in Figure 1.3). If the core temperature reaches $\sim 3 \times 10^8$ K, then helium-burning begins. He-burning causes the stars to halt the cooling and the luminosity increase, so that the star moves to the left side in the HR diagram (the horizontal branch). After all the He in the core is depleted, the star again moves to the right and upwards on the diagram. This ascending path is almost parallel to the Red Giant Branch track, so it is called the Asymptotic Giant Branch. Stars on this branch are therefor called AGB stars.

1.2.1 AGB stars

All stars with masses of $0.8-8 M_{\odot}$ undergo a last evolutionary step becoming AGB stars. In general, an AGB star consists of 4 major parts (as can be seen in Figure 1.4): (1) the

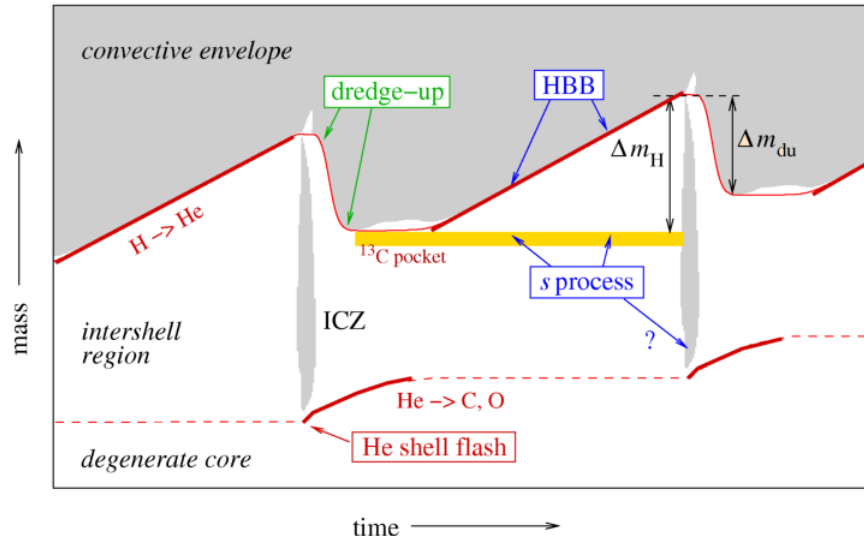


Figure 1.5: Schematic evolution through 2 thermal-pulse cycles. The grey area is the convection region. The ICZ (intershell convection zone) is driven by the He-shell flash. The thick red line indicates nuclear burning in the shells. The time axis is non-linear: The dredge-up and He-shell flash last ~ 100 yr, while the interpulse phase lasts 10^4 - 10^5 yr. Further explanation in the text. *Image courtesy of N. Langer*

core (small, hot, and dense), (2) the stellar envelope (large, hot and less dense), (3) the atmosphere (thin and warm) and (4) the circumstellar envelope (CSE; large, very diluted and cool). (3) and (4) will be discussed in an extra section. AGB stars cover a wide range of radii, densities and temperatures.

As described in the introduction at some point the star begins to burn He. That process forms carbon (via the 3α -process). This carbon (C) can partly be burned into oxygen (O) in the center. When the He in the core is depleted, the so called He-burning zone moves outward and the C/O core contracts until reaching the density of a white dwarf (WD). The beginning of the so-called **Early-AGB (E-AGB) phase** is determined by the contraction of the core and the expansion of the envelope leading to a rapid increase in luminosity. The He-burning shell produces most of the energy during that phase. During the E-AGB-phase the envelope becomes unstable and begins to pulsate. When the luminosity further increases to that of the tip of the Red Giant Branch ($3 \times 10^3 L_{\odot}$), then the star can burn He and H in the shells. On a regular basis the He-layer around the core burns into carbon to be added to the core's mass. The time, during this process occurs, is called a “thermal pulse” or a “He-shell flash” (Figure 1.5).

If it occurs, the luminosity modulates too. If one of those thermal pulses is over, the star burns H again. The phase between the occurrence of a He-shell flash and the

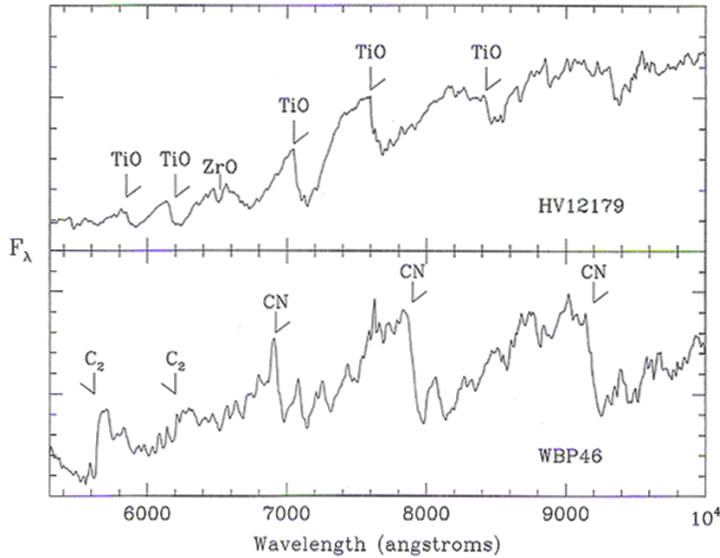


Figure 1.6: Spectra of an MS star (top) and a C star (bottom). These stars in particular are members of the Large Magellanic Cloud. Typical O-bearing molecules are CO, TiO, SiO, H₂ or VO. Typical C-bearing molecules are CO, C₂, C₃, C₂H₂, CN or HCN (H. J. Habing 2003).

H-burning is called the “**thermally pulsing AGB-phase (TP-AGB-phase)**”. During a TP-AGB phase the so-called “third dredge-up”-process can occur (the so-called “first dredge-up” occurs, when a main-sequence star begins to ascend the Red Giant Branch, convective mixing yields to elements produced by hydrogen fusion; the “second dredge-up” occurs in 4–8 M_⊙ stars, when the star runs out of helium and convection mixes the elements produced by the CNO cycle). A thermal pulse causes convective zones reaching layers where nuclear processes can take place and so gets material to the stellar surface. This surface then is enriched by newly formed carbon. Initially the atmospheres of AGB stars are oxygen-rich (C/O < 1), but if dredge-up-processes repeat often enough, the atmosphere will get carbon-rich (C/O > 1). This process is important for low- and intermediate-mass stars. Sufficient masses in stars lead to the carbon to be burned into nitrogen (Ni) before it reaches the stellar surface. The bottom of the convective envelope reaches temperatures of $T > 5 \times 10^7$ K. At this temperature H-burning is initiated within the convective envelope and is known as envelope-burning or “hot-bottom burning”.

Spectra

Spectra of M stars are dominated by TiO molecule bands, whereas C (carbon) stars show C₂ and CN molecule bands (Figure 1.6).

Additionally M stars have a C/O number ratio less than unity and C stars show a

ratio of $C/O > 1$. The CO molecule is the most important one in the atmospheres of cool stars, since it determines the chemistry of it. With a ratio of $C/O < 1$, surplus O atoms are available to form e.g. TiO. With $C/O > 1$, surplus C atoms are available to form e.g. the C_2 and CN molecules. Normally stars and the ISM show a ratio of $C/O < 1$, so there must be a process occurring in cool stars to explain C-rich atmospheres. This process is the previously mentioned “third dredge-up”

Some spectra show some peculiarities; enhanced bands of molecules involving s-process elements (e.g. ZrO). This indicates that s-processed material from the core has been brought to the surface (through the third dredge-up). If additionally to the TiO molecule ZrO is found, the star is referred to as MS star. During the dredge-up episode it can happen that the bands of the molecular oxides disappear because C is locking up the O in the CO molecule, leading to a pure S star. Again, if the process happens long enough C-rich molecules can appear in the spectra and the object becomes a SC star. In some atmospheres of AGB stars also technetium (Tc) was found, which lead to the conclusion that new elements are formed inside the stars, since Tc has no stable isotope and the isotope ^{99}Tc has a half-life of just $\sim 2 \times 10^5$ yr and is therefore thought to be brought to the stellar surface in the last few times 10^5 yr.

Variability

AGB stars strongly pulsate and this is the main reason for the variability of this stars. However, also episodic ejections of dust shells or orbiting dust clouds can cause it. Most of the AGB stars are long-period variables (LPV) showing variations in brightness over long time scales ranging from months to years. 3 main classes of LPVs can be distinguished:

- Mira variables: named after the prototype Mira (described in Chapter 3), showing long regular pulsation periods of 80 - 1000 d and luminosity variations of 2.5 - 11 mag.
- Semiregular variables: periods like Mira with lower and irregular amplitudes
- Irregular variables: like semiregular variables, but with very irregular light curves.

Most of the red giant variables are listed in the General Catalog of Variable Stars (GCVS). However, one class of AGB stars, dust-enshrouded infrared variables are too faint to be detected in the visible. Dust-enshrouded O-rich stars can be found by infrared surveys and by the 1612 MHz OH maser emission, in which case they are called OH/IR stars. The analogue C-rich stars can be found by infrared surveys. C stars do not produce OH maser emissions. The dust-enshrouded infrared variables are in a more advanced state than e.g. Mira variables, they show signs for stellar winds with higher mass-loss rates than Miras do. They also generally pulsate with larger amplitudes and longer periods than optical Mira variables. AGB stars also differ in mass. In globular

clusters the turn-off mass ranges from $\sim 0.85 M_{\odot}$ to $6\text{--}8 M_{\odot}$. In the local population Mira variables show masses of $> 1.1 M_{\odot}$ for periods $P > 300$ d and $< 1.1 M_{\odot}$ for $P < 300$ d. Miras with periods near to 200 d are found in more metal-rich globular clusters, so they are clearly of initial mass $\sim 0.85 M_{\odot}$. Semiregular variables have masses similar to Miras with $P > 300$ d. They also can be found in globular clusters (but of all metallicities), so the mass range is similar to that of the Miras.

Post-AGB-phase

Post-AGB objects are the result of stars leaving the AGB evolutionary phase caused by very strong mass-loss events. They evolve to hotter effective temperatures at more or less constant luminosity, but are not hot enough to ionize circumstellar material. For that reason they form planetary nebulae (PNe) and then cool down to WDs. For binary AGB stars it is more complicated, since the companion influences the process, as is described in section 2.

1.3 The atmosphere and outer CSE

The definition of an atmosphere for an AGB star is not very sharp. The question is how far outwards this region goes. Different approaches exist, so it can be simply defined as the region visible from the outside, the region where most of the electromagnetic emissions come from. The distinction of the atmosphere and the outflowing wind is another matter. The border could be defined as the region where the outflow velocity is higher than the escape velocity. The atmosphere is seen as the transition region between the stellar interior and the interstellar matter. The farther away from the stellar center, the more complex the atmosphere becomes, reflecting the relatively simple stellar core and the complexity of the ISM. Studying the composition of AGB star atmospheres is of importance, since the stars are producing heavy elements in their centers and via physical processes they are mixed out into the atmosphere.

In almost all cases the atmosphere is not perfectly spherical. Thermal pulses and He-shell flashes affect the atmospheric structure by inducing shock fronts. In this shock regions dust molecule formation occurs. Many physical and chemical reactions like convection, pulsation, radiation, molecule and dust formation and absorption together with the accelerating stellar wind need to be unified into a theory explaining the processes going on in the atmosphere. The formation of shock fronts and the interplay between the outflowing matter and the surrounding ISM was recently studied with the help of the Herschel Space Observatory.

1.3.1 Observational properties

AGB stars are very bright. Different observation opportunities exist. First of all, the majority of light is emitted in the infrared (IR). A lot of spectra have been obtained, since the IRAS and ISO satellites collected a lot of data for spectrophotometric studies in the infrared wavelength. The Earth's atmosphere is IR-opaque (and UV-opaque), so no ground-based observatory can observe in that wavelength(s). With the help of IR observations continuous flux spectra ranging from the visual to the far-infrared (far-IR) can be obtained and compared with stellar models. The systematic exploration of spectral lines and bands of water vapor, CO₂ or SiO is possible with IR satellites. Also emission features from atoms in the far-IR, dust components and polycyclic aromatic hydrocarbons (PAH) can be detected via space observatories. With the help of high-resolution spectrometers, Fourier transform spectrometers or cryogenic echelle spectrometers IR spectra can be recorded. Already the first generation of those instruments could give some insight in the structure, dynamics and chemistry of AGB atmospheres. A lot of photometry and polarimetry databases exist containing broadband fluxes and colors of AGB atmospheres. Interferometry is also a useful tool, since some AGB stars have very large diameters and are relatively nearby to measure their sizes with the help of phase or speckle interferometry or with the lunar occultation (LO) method. The diameter can be measured in different wavelengths to have an idea about the extension of the atmosphere compared to models. Through spectroscopic analysis one can calculate atmospheric velocity fields. A micro- and macroturbulence parameter may be calculated for the atmosphere. These parameters contain information about the velocity fields in an atmosphere. Shock waves obscuring in Mira stars can significantly change the velocity fields through the atmosphere. Velocity fields in the upper atmosphere can be calculated with the help of SiO masers. Masers also give an insight into the existence of magnetic fields in AGB stars. Very long baseline interferometry was used to map magnetic fields from SiO emissions e.g. around the Mira variable TX Cam; a field of the order of 10 Gauss was traced. Through observing the chromosphere of AGB stars it was found out that the upper atmosphere consists of a hot and cold component, what is not surprising, since it seems to be also the case for hotter stars. The hot layer was discovered through the observation of Ca II and Fe II lines. The standard theoretical model did not consider this. To model the findings in the chromosphere is difficult, because complex geometry of the velocity fields prevents a qualitative description yet. A newer method for studying the AGB CSE is to observe scattered stellar or interstellar light by circumstellar atoms, molecules and dust. The environment can then be studied with the help of high angular resolutions in optical and IR wavelengths. Atomic and molecular species can be detected at radio, IR and optical wavelengths. A minimum amount of atoms is required to observe a specific atomic line for a given sensitivity. Due to the mass-loss rate typical for cool stars like on the AGB the environment is for the most part dominated by molecules, not single atoms. Atoms can be found more outside the CSE, but the excitation in the outer region may not be high enough to be able to detect any emission at all. In a warmer

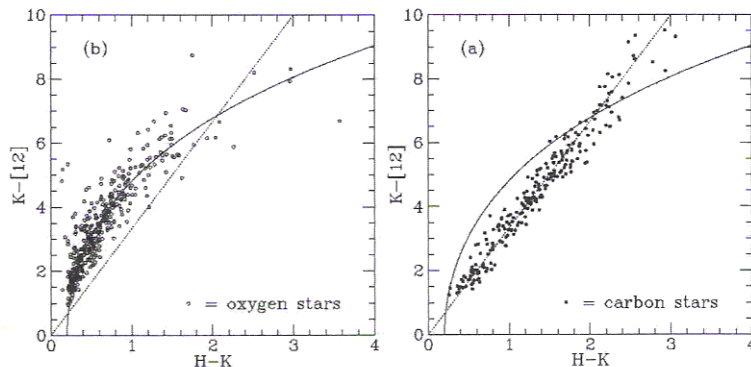


Figure 1.7: Color-color diagrams based on the $[H-K]$ and $[K-12]$ colors for O-CSEs (left) and C-CSEs (right) (van Loon et al. 1998).

star, like a supergiant, with high mass loss the situation would be different. A prominent element to search for in the CSE is H I, detected through the 21 cm hyperfine line, but it is still difficult to detect because of interstellar H I emission disturbing the spectrum. Fine-structure lines like for C I, contrary to hyperfine ones, can be detected easier, since they are much stronger. ISO spectra show fine-structured emissions of Fe I, Fe II, S I and Si II. Through light scattering Na I or K I were found in the CSE. In general, CSE molecules can be detected in absorption spectra in the near-IR or in emission spectra in the mid-IR and radio wavelengths. Tables for molecule detections in the radio, infrared and optical can be found in H. J. Habing (2003). Dust emissions are not perfect for estimating the chemical composition of the CSE, but they are useful to determine the C/O ratio. The main tool for estimating this ratio is still the color-color diagram based on IRAS $[12-25]$ and $[25-60]$ colors. A combination of mid-IR color (e.g. $[12-25]$ or $[K-12]$) and near-IR-color ($[H-K]$ or $[K-L]$) is very effective, because O-rich environments show larger excess at these IR wavelengths (Figure 1.7).

The temperatures of flux-forming regions of AGB stars can not be estimated trivially. For a star like the sun the flux distribution looks like the Planck function because of limited variations of the continuous absorption coefficient with wavelengths. Continuous absorption in the sun is dominated by H^- bound-free and free-free absorption. This is also true for AGB stars, but their flux distribution is far from Planckian. The flux in AGB stars is more affected by spectral lines and by the far-IR part of the flux distribution. Dust emission in the outer atmosphere or envelope may dominate and also introduce a broader flux distribution. Disregarding such an emission in the IR and trying to fit a Planck function to the flux in the visual and near-IR, one can estimate a temperature for AGB stars between 2000 and 3500 K.

1.3.2 Mass loss

Mass loss is an important part of the stellar evolution on the AGB. The mass loss at very high rates, rather than the nuclear burning process, may be the main process affecting the luminosity of the star. Mass loss is caused by stellar wind. Such stellar winds require momentum, an outward-directed force to overcome gravity. 2 types of stellar winds exist: **Thermal winds** and radiation-driven winds. Thermal winds are generated by gradients of the gas pressure. This pressure may be created by dissipation of sound waves or by radiative heating of the gas. **Radiation-driven wind** is driven directly by a radiation field by absorbing outward-directed stellar radiation and re-emitting photons in all directions creating a new force, the radiation pressure, pointing away from the star. Additionally gas in the CSE can also be accelerated through sound waves, shocks or magneto-hydrodynamic waves and so on.

AGB stars have slow winds with typical terminal velocities of 10–20 km s⁻¹. Terminal velocities are low, but the actual mass-loss rates are high, of the order of 10⁻⁷–10⁻⁴ M_⊙ yr⁻¹ (compare to the sun with a wind outflow of 500 km s⁻¹ and a mass loss of about 10⁻¹⁴ M_⊙ yr⁻¹). The values suggest high gas densities in the outflow of AGB CSEs and the wind must originate in the dense regions.

The understanding today is that the mass loss unifies the theories about the dynamical atmosphere extended by shock waves due to pulsation and the radiation pressure on dust grains. Models have been developed showing highest levels of self-consistency. Through them it is possible to predict the mass-loss rates from stellar parameters. Interior pulsation of the star causes large-scale motions of the outer layers in the form of waves that run outwards the atmosphere and so propagate density gradients resulting in strong radiating shocks. A shock front causes the gas to become compressed, heated and pushed outwards. Radiative cooling may cause the temperature to drop and a relatively cool, dense outward-moving shell develops. If the dust production via this process is not high enough, the gas may fall back and is hit by the next shock. If in this outflowing matter the density is high enough and the temperature is cool enough, dust grains can be formed. The gas density governs the time scale and efficiency for the grain growth and the temperature acts as threshold for the condensation. Though the model of a pulsation-enhanced dust-driven wind is favoured today, theories of stellar winds driven by Alfvén or sound waves were also suggested. This theories can not be excluded since for the shock wave-theory, many models assume LTE cooling. It is very efficient and leads to dense cool layers close to the photosphere, where dust grains can be formed. This assumption, however, does not seem to work behind a shock wave in the critical outer zones, where the wind accelerates, according to Willson & Bowen (1998). Their suggestion effects the understanding of the detailed atmospheric structure and the hole mass-loss process. An important factor concerning the driving mechanism of stellar winds is the high dust-to-gas ratio observed. Assuming a model that uses momentum, rather than radiation pressure, on dust to initiate a wind, it is often believed that grains form in the outer regions of the atmosphere, when the temperature is low

enough. As explained before, a low enough temperature allows a condensation process. Grain growth is a relatively slow process proceeding far from equilibrium. Concerning typical values for AGB atmospheres, dust formation based on this assumption is not very effective. The gas density is important for condensation to happen, but it may not be possible to produce enough dust as a normal by-product of an outflow, because the gas dilutes too fast to let significant condensation occur.

For understanding the mass loss the inner wind regions need to be investigated in more detail. Monitoring programs are necessary that cover at least one pulsation cycle of an AGB star. A time-dependent spacial study of the gas, the dust, the temperatures and the velocity fields lead to a better understanding of the mass-loss mechanism. This has been done already by e.g. ISO and Hubble.

The efficiencies of the mass loss and the wind acceleration vary depending on the stellar properties, leading also to variations in the CSE, so that the opaqueness, the geometry, the kinematics and the chemistry change on different time scales. Inner region mass-loss rates of up to $10^{-4} M_{\odot} \text{ yr}^{-1}$ have been found. This is a short time scale regarding the evolutionary path an AGB star takes. Such a mass loss can highly obscure the central star, so that all stellar radiation in the visual and near-IR is absorbed in a dusty CSE and then re-emitted at longer wavelengths. Higher mass loss may also directly influence the overall spherical symmetry. Finally it enriches the CSE with elements from the core. The circumstellar environment is the important starting point for the formation of post-AGB planetary, nebular structures. The structures of the new born PNe can also give an idea about the predecessor objects, e.g. the successors of binary AGB stars show a different morphology than do nebulae formed from single AGB stars.

1.3.3 Geometry of the CSE

To have an idea about the 3D density distribution, the geometry and the kinematics of the CSE are important for understanding the mass-loss process and the geometry of succeeding PNe. The trick is to learn about the 3D geometry from observed 2D brightness distributions. This process can be complicated by radiative effects, such as saturation or masers, or by excitation and the chemistry itself. Even if one considers the surrounding ISM and the space motion of an AGB star (a specific description of a sample observed with the Herschel Space Observatory is discussed in Chapter 3 including a more detailed explanation of outflow morphologies in the following Section), an overall spherical symmetry is assumed (it is actually very true for a nearly stationary star, but there is still some relative velocity difference between the stellar wind and the surrounding ISM). Interferometry is the best observational method to be used to study regions close to a star through observing molecular maser line emissions and near-IR dust emissions. It is difficult to obtain some information about the geometry with this method. Interferometers are sensitive to brightness distribution gradients, extended emission features may be missed. Maser emissions make problems in regions with large optical depths. With the help of SiO masers circular rings were resolved in regions inside the dusty CSE. On

small scales the mass loss is believed to be isotropic ($< 0.1''$), but the relative positions between the star and maser emissions are sometimes not very accurate to be sure. Maser emissions can also be used to determine the magnetic field of the AGB star or as a distance indicator using stellar parallax measurements of obscured objects. Magnetic fields may influence the shape of the outflowing matter on different scales.

On larger scales the OH (1612MHz) maser in general shows a spherical shell (for 15 O-rich CSEs in H. J. Habing (2003)) with some crudities in the brightness distribution. Symmetry is also shown in CO radio line emission maps (for 45 O-rich and C-rich CSEs in H. J. Habing (2003)). Scattered stellar light confirmed the observations of thin shells around this objects.

CW Leo: CW Leo (IRC +10216) is a very well-studied carbon star with a thick dust envelope. Several observations of its CSE exist. These early observations are presented here as a very brief example of how a CSE is identified with the help of different species and wavelengths.

A fair number of molecular species have been observed at high-angular resolution to show the geometry of the envelope at different sizes. Figure 1.10[d,e,f] shows CW Leo at different size scales. Multiple shells were found, expected to be caused by multiple mass-loss events. The shells are visible as circular arcs being part of a circularly, symmetric, reflection nebulosity. CW Leo also shows asymmetries on small scales.

To stay with CW Leo, the dust distribution for this object was found to be very inhomogeneous within 10 stellar radii, reflecting an asymmetry. Studies of some other O-rich CSEs also suggested asymmetries in the outflow and even clumpiness caused by several mass-loss events. CO radio line data showed a fraction of 30 % of the sample used in H. J. Habing (2003) to have some asymmetries in the CSE together with a surrounding, large symmetric envelope. α Cet, described in detail in Chapter 3, is an extreme example showing a CSE with a bipolar outflow. However, this outflow may have been partly caused by its companion star. Also objects with peculiar line profiles were observed, showing themselves as narrow central features centered on a broader component. The shape of PNe gave some hints to assume that at some point asymmetries must develop already on the AGB.

Information about the kinematics of a CSE can be gotten easier. Line profiles can be used directly to obtain gas expansion velocities. For all 3 classes of LPVs there exist CO surveys to calculate the thermal velocities for AGB CSEs. This velocities also were indicated to be dependant on the mass and the metallicity of the objects. In the CSE the final terminal velocities are believed to be reached within a few tens of stellar radii. The acceleration region is small and difficult to observe. However, high spectral resolution imaging is able to find a remedy.

Instabilities in the outflow may produce clumpy structures in the inner CSE, which are then accelerated to intermediate velocities. The “clump density” in the equatorial regions is much higher than in the polar regions of AGB stars, because the acceleration of the clumps is more effective on the poles. This can explain e.g. an hour-glass morphology of a PN.

1.4 Outflow morphology

Planetary nebulae are known successors of AGB stars. While transiting from the AGB to the PN stage, morphological changes of the CSEs are often accompanying the process. AGB stars (with low proper motion) in general have more or less spherical molecular envelopes, but many proto-planetary nebulae (PPNe) and PNe show axisymmetric (bipolar or elliptical), aspherical shapes. The change in the morphology begins during the AGB stage and is completed at the beginning of the PN phase. The non-spherical geometry of PNe gives hints for the morphological evolution of the CSE. Mastrodemos & Morris (1999) in particular presented their findings on the influence of detached binary companions of AGB stars (and red giants) on the dusty wind with the help of 3D smoothed particle hydrodynamics (SPH) simulations and the degree to which their results can reproduce observations of the asymmetric morphology of PNe.

With varying the parameters for the simulations like the binary separation, the wind outflow velocity, the binary-mass ratio (including the masses for both objects), the orbital eccentricity and the mass-loss rate and radius of the primary they found 3 main morphologies in their calculations: a bipolar, a quasi-spherical and an elliptical morphological structure. To describe the effectiveness of the binary separation to form aspherical or axially symmetric outflow, they distinguished between a slow, an intermediate and a fast wind. Depending on the separation and the outflowing wind velocity the 3 types of morphologies evolved in their calculations. Because of the number of parameters used in this calculations there could not be made a reliable statement, which morphology occurs for what separation, though they tried to draw a line. Overall Mastrodemos and Morris published a series of papers where they conducted research on bipolar proto-planetary nebulae and their properties,

IRAS observations already showed some low temperature circumstellar dust around AGB stars (van der Veen & Habing 1988). First observational evidence for a real detached shell was found by e.g. Olofsson et al. (1988), Stencel et al. (1988) or Hawkins (1990). After this discoveries IRAS and ISO were used to observe more AGB stars and actually found detached thermal dust emissions around many stars. In the following years detached shells were found through CO radio line emissions and in the optical and interferometric radio maps were used to study their structure, recovering spherical thick CO-line emitting, geometrically thin shells (for detailed information please look up the reference list of Chapter 7 in H. J. Habing (2003)). Intense mass loss on short time scales has been determined as the reason for these spherical shells. IRAS was the

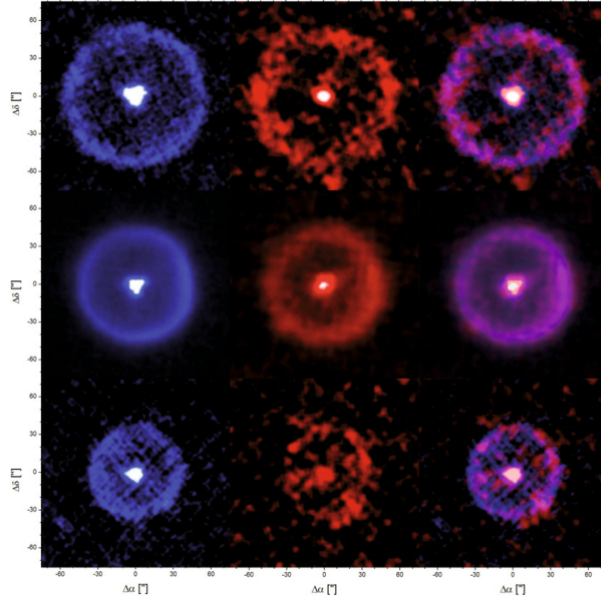


Figure 1.8: **left to right:** 70 μm , 160 μm , two colour composite PACS scan maps. top to bottom: AQ And, U Ant, TT Cyg (Kerschbaum et al. 2010).

first satellite observing the shells in the infrared (Stencel et al. 1988). The satellites Spitzer and AKARI revealed the shells in even more detail. The newest generation of infrared telescopes was introduced with the Herschel Space Observatory, leading to another revolution in high resolution imaging.

1.4.1 Morphology as seen by Herschel

This part describes the theoretical background and the used methods for the obtained Herschel images within the framework of the MESS program and is based on Cox et al. (2012). In Chapter 3 binary AGB candidates in the Herschel MESS sample are presented. Detached infrared shells in the Herschel data have already been discussed in Kerschbaum et al. (2010, 2011), and **bow shocks** in Ladjal et al. (2010) and Jorissen et al. (2011). Mayer et al. (2011) reported the newest insights on the morphology for Mira (see the last object in Chapter 3). For a more detailed description of the data reduction for the objects look up the publications and the references therein.

In Kerschbaum et al. (2010) (Figure 1.8) Herschel images of the detached dust shells of the carbon stars AQ And, U Ant, and TT Cyg were presented. AQ And is a semiregular C star with $T_{\text{eff}} = 2660$ K and an applied distance of 825 pc, U Ant is another semiregular pulsating star with $T_{\text{eff}} = 2810$ K and a distance of 260 pc (Hipparcos parallax), and TT Cyg is a SRb-type semiregular variable with $T_{\text{eff}} = 2825$ K and an uncertain Hipparcos distance of 510 pc (a calculated distance of 436 pc using PL-relations, but for

consistency with previous publications the calculated Hipparcos distance was used). For their analysis they assumed the stars having an attached and a detached shell reflecting present day mass loss and past mass loss, respectively. The images were taken with the PACS instrument on-board Herschel and the data reduction was executed with the help of HIPE. This resulted in the detection of circular rings of emission for the mentioned stars, pointing to an enhanced mass-loss period. The attached shells were estimated to have an age of thousands of years, as for the detached shells an age of 1000 to 10,000 years was estimated. To get more information about the shells, more observations with Herschel were requested by the authors. A sample of stars additionally consisting of AQ Sgr, RT Cap, Y CVn, U Cam, UX Dra, W Aql, W Ori and X TrA was presented in Kerschbaum et al. (2011). W Aql and U Cam are discussed in more detail in Chapter 3. Images of U Ant (Figure 1.10[a,b,c]) were obtained with SPIRE at longer wavelengths. Additionally to the shells a large filamentary structure was revealed at 250 μm . This structure was theorized to come from a wind-ISM interaction. SPIRE images of U Cam, known to have a detached shell, show an extended elliptical or double bow-like structure. Looking at the sample, some objects show signs of an extended, faint detached structure at longer wavelengths, which also revealed larger structures for e.g. Mira, probably caused by its space motion and the companion. For X TrA the age of the detached shell was estimated to be almost 30,000 yr, considering that the expansion velocities of the dust equals the values for the gas outflow.

To link to the previous example of CW Leo, Ladjal et al. (2010) presented Herschel PACS and SPIRE images of the object (Figure 1.10[g,h,i,j]). In the 160, 250 and 350 μm images an arc presenting itself as an extended emission is clearly seen, which is flattened in the easterly direction. Previous far-UV (UltraViolet) images show a nebulosity in the western part, which could not be seen in the Herschel images.

Detached shells are believed to be caused by mass-loss variations caused by thermal pulses. This shells can also be formed via AGB-ISM interaction scenarios. The AGB wind slows down and interacts with the ISM material forming a density enhanced region in the direction of the wind. If the space motion of the AGB star is large enough, shocks in the outflow can occur. To distinguish between the 2 possibilities, shells produced via the mass-loss mechanism should be more spherical and shells produced by the AGB-ISM interaction are more aspherical due to the space motion of the object. This also means that the material in a bow shock is a mix-up of atmospheric material (C-rich in the case of CW Leo) and ISM material. As already mentioned, a companion can in addition make the structure more complex.

Jorissen et al. (2011) like Ladjal et al. (2010) presented the newest Herschel images of bow shocks, this time for X Her, an O-rich M8III semiregular variable star, and TX Psc, one of the brightest and nearest C stars (Sra/b), which show axisymmetric shells. Ladjal et al. (2010) pointed out that this shells can be triggered by: (1) wind ejection in a binary system (spiral structure, see Chapter 2), (2) asymmetric mass loss in a single star (e.g. red giants with cool spots), (3) the existence of a stellar dipole magnetic field (a companion star may be needed to give the magnetic field significance for shaping the

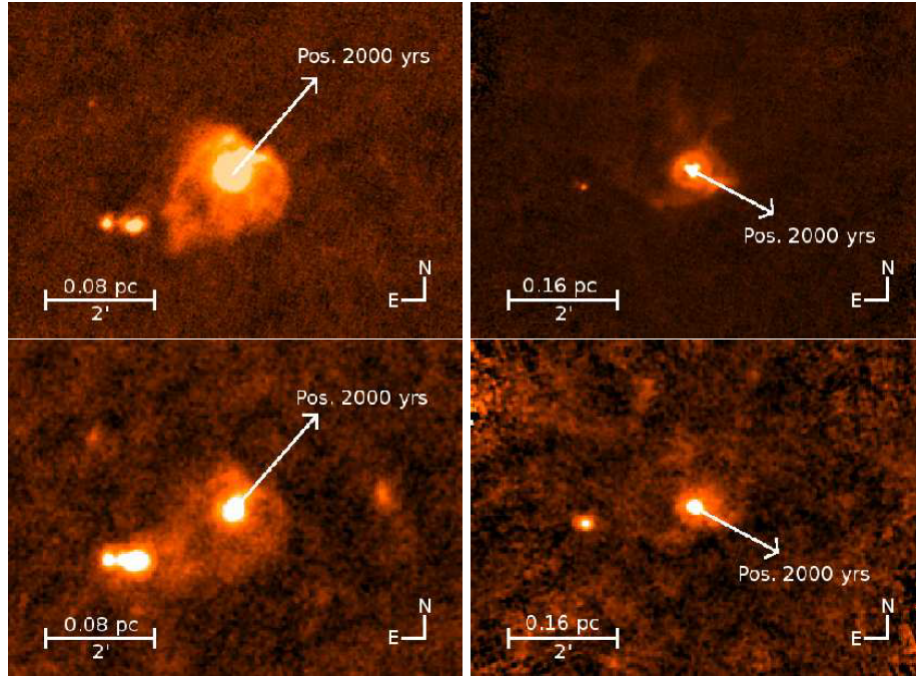


Figure 1.9: PACS images of X Her and TX Psc at $70 \mu\text{m}$ (upper image) and $160 \mu\text{m}$ (lower image). Arrow: direction of proper motion. The bright dots near to the objects are galaxies (Jorissen et al. 2011).

outflow) and (4) wind-ISM interaction, which is the trigger their paper is theorizing on. Images of X Her and TX Psc show complex structures (see Figure 1.9) and indicate a wind-ISM interaction. The images also show a clump along the direction of motion for both stars, it may be a direct indication of instabilities in the bow shock caused by AGB-ISM interaction. PACS images also revealed fainter clumps possibly associated with Kelvin-Helmholtz (KH) instabilities.

Cox et al. (2012) made a first complete study of the MESS sample regarding the morphology of bow shocks and detached shells around AGB stars and red supergiants. Some observations imply the existence of a companion. Some stars have been known before to have companions, for other stars the binary status is still a matter of discussion. They identified 4 shapes of detached far-IR emissions: (1) “*fermata*”, (2) “*rings*”, (3) “*eyes*” and (4) “*irregular*”. AGB stars not showing such an emission were classified as “*non-detection*” (see Figure 1.11[a-h]). “*Fermata*” class objects are identified as an elliptical arc (a shell-like structure) spanning an angle of at least 90° . Additionally in this class some objects show KH or Rayleigh-Taylor (RT) instabilities. X Pav, EP Aqr and X Her also show a bullet-shaped arc caused by material flowing back passing on both sides of the star, possibly caused by the relative motion to the ISM. VY UMa and U Cam show 2 arcs with some evidence for jet structures in the mid plane, identified as “*eye*” morphology. The 2 connected arcs for each object seem to purport a ring, caused by viewing at

the objects with an inclination other than 90° . Real circular structures are summarized as “*ring*” morphology. In this class one finds objects previously known for their detached shells with typical wind-wind interaction zones. Younger objects in this group also have a co-spatial counterpart molecular gas ring. Objects like AQ And, U Ant, U Cam, TT Cyg, R Scl, S Sct, V644 Sco, Y CVn or DR Ser belong to this group. As one can see, U Cam was marked as “*eye*” and “*ring*” type, because it shows both morphologies having a small detached ring and a bow shock region. Maybe the small detached ring could evolve in a low density medium, caused by an earlier mass-loss event sweeping out ISM material to create the bow shock, via wind-wind interaction. Another reason might be that the small (inner) ring is a transition region between a (back-flowing) termination shock and the free expansion zone. A second subset of objects, including CW Leo and α Ori, shows irregular multiple incomplete shells in the inner region. Objects, for which none of the above morphologies could be adopted to, were classified as “*irregulars*” if they show diffuse irregular extended emission. Objects with no found diffuse emission are “*non-detections*”. The category of the “*irregulars*” also consists of previously identified binary stars. Binarity is difficult to prove with PACS images. 4 binary candidates could be found for the “*ring*” morphology, 3 objects with “*irregular*” morphology are confirmed binaries, and so are 2 objects showing the “*eye*” morphology.

For estimating the radial distance of the arcs and the detached shells radial profiles (as can be seen for Mira in Chapter 3) were produced for the “*eye*” and “*ring*” morphological types. Sometimes very faint emissions hampered a correct calculation of the stand-off distance.

Bow shocks

Bow shocks can evolve, when 2 material flows with different density, velocity, or viscosity collide. Such bow shocks are seen around compact H II regions caused by stellar winds or also winds in binary stars, or simply between a fast and a slow wind or a stellar wind and the ISM. Concerning the last mentioned possibility, the bow shock forms, where the ram pressure and momentum flux of the wind and the ISM are equal (contact discontinuity). The standard model for a bow shock describes 3 parts: (1) the forward shock separating unshocked and shocked ISM, (2) the wind termination shock separating the free-streaming and the shocked wind, and (3) the contact discontinuity described before. However, real shocks just occur if the Mach number of a fluid velocity is $M > 1$, meaning that the relative motion between stellar wind and ISM needs to be higher than the speed of sound in the ISM. In general the thickness of the bow shock, compared with the stand-off distance, is negligible if the post-shock cooling is effective enough. The stand-off distance can be calculated as

$$R_0 = \sqrt{\frac{\dot{M}v_w}{4\pi\rho_{ISM}v_*^2}}, \quad (1.1)$$

where \dot{M} is the mass loss, ν_w the isotropic stellar wind velocity (with respect to the rest-frame of the star), ρ_{ISM} the local ISM mass density and ν_*^2 the relative (to the ISM) stellar space velocity. In what way a magnetic field plays a role forming bow shocks, has to be investigated in more detail.

In Cox et al. (2012) infrared emissions coming from the bow shock regions must contain dust on the order of 2×10^{-7} to $2.5 \times 10^{-4} M_\odot$. The masses of dust and gas in general are on the order of the swept-up ISM material. The formation and destruction of dust grains, however, may change the dust-to-gas ratio implying some deviation from that norm.

To overcome the fact that the relative star-ISM motion is inclined with respect to the plane of the sky, Cox et al. (2012) simulated a 3D bow shock surface, a hollow paraboloid surface. Such a surface can be created by rotating a 2D shape. With the help of the inclination angle the 3D surface is then projected onto the plane of the sky, so that the true shape of the bow shock in the direction of the stellar motion can be derived.

To have theoretical models to compare with, hydrodynamical simulations with the MPI-AMRVAC code (Keppens et al. 2012) were conducted. In such simulations all input parameters can be varied (in that case e.g. the mass-loss rate, the wind and relative space velocity, ISM parameters such as density and temperature). An important feature is the possibility to study emerging (KH and RT) instabilities. So-called RT-fingers are visible in the bow shock in some cases. KH instabilities are able to form more complex structures, so large that the instabilities could manipulate the large-scale morphology. RT and KH instabilities were found in the bow shock regions of e.g. UU Aur, R Hya, X Pav, μ Cep, Ep Aqr, R Leo, RT Vir, X Her or V1943 Sgr. Especially simulations, described in the following, with high mass-loss rates and a low ISM density pronounce stronger KH structures, RT instabilities seem to be more prominent in simulations with high mass loss rate too. Non-linear thin shell instability and transverse acceleration instability can also occur, as was shown numerically by Vishniac (1994) and Dgani et al. (1996), respectively. A total of 7 simulations was undertaken to observe the interaction of the stellar wind with the ISM. They described a basic model, one with high and a low mass loss, with low dust formation, with a high stellar space motion, with a low ISM density and with a warm ISM. Magnetic fields were not incorporated. Destruction and formation of dust was neglected as were radiative processes and photoionisation. The stellar space motion in the simulations was always faster than the stellar wind. As expected the simulated collision of the outflowing stellar wind with the ISM creates a bow shock. The region and morphology of the bow shock strongly depend on the input parameters. The bow shocks reach their final equilibrium distance in 50,000 to 150,000 yr. The basic model (Figure 1.11[i,j,k]) shows a typical bow shock with high density shocked wind with lower temperatures than the shocked ISM material. This typical morphology can be seen in all alterations except for the high stellar space motion and the warm ISM case, which reveal a chaotic bow shock with turbulence. A comparison of the observations with the simulations showed that the large arcs seen in the PACS images were reproduced in the simulations, when the shocks were adiabatic. What the simulations

could not resolve to their satisfaction was to show if the observations show the forward shock, the reverse shock or the contact discontinuity of the bow shock. The spatial resolution was limited and it is not clear what region the far-IR emission represents.

As mentioned before, if an AGB star has a companion, then the outflow morphology of the AGB wind could indicate it. There are, however, several other methods to detect a companion with an AGB primary. The following Chapter gives an overview of some binary AGB stars. The properties and formation scenarios are described with the goal to find detection methods, before Chapter 3 discusses previously known and AGB binary system candidates in the Herschel MESS sample.

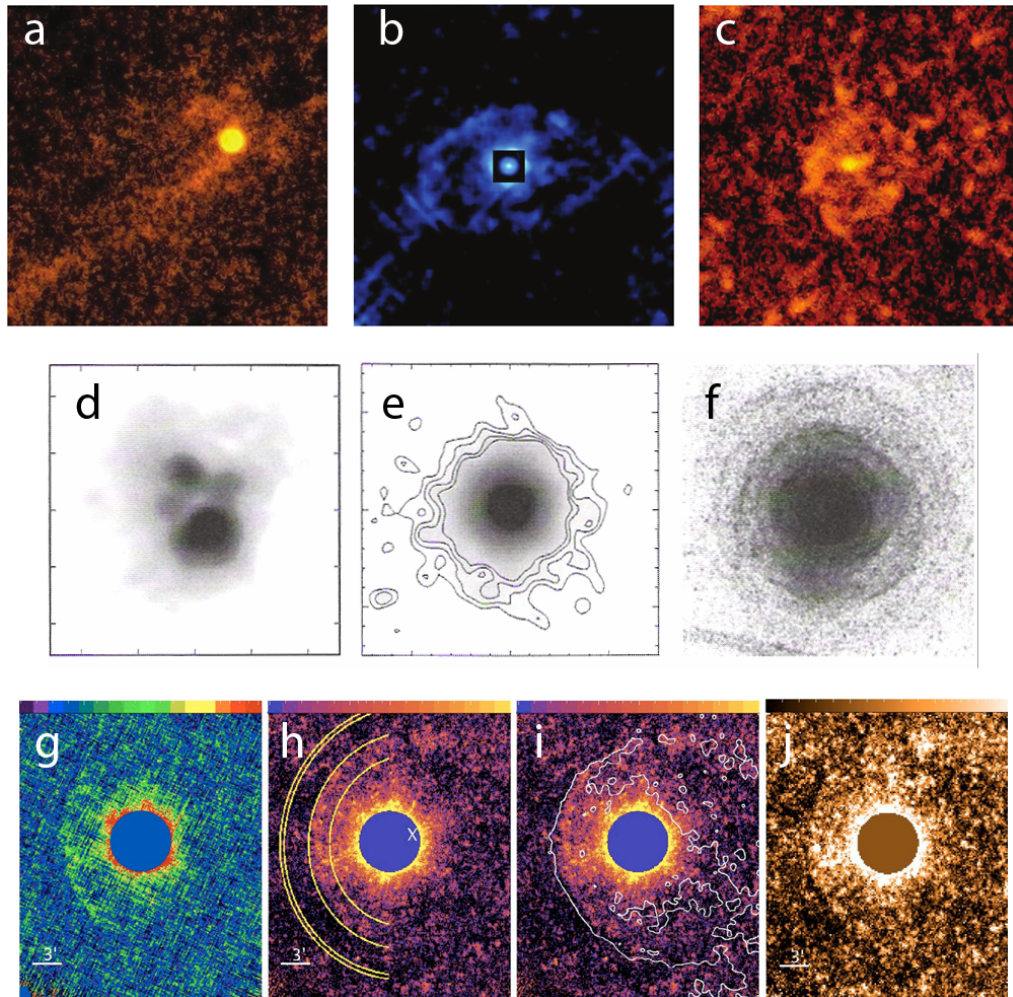


Figure 1.10: **a,b,c)** PACS images from left to right: U Ant ($250 \mu\text{m}$, $20'$, point source removed), U Cam ($70 \mu\text{m}$, $6'$, 2 different intensity scales), Y CVn ($250 \mu\text{m}$, $20'$, point source removed). Description in the text. (Kerschbaum et al. 2011)

d,e,f) CW Leo-CSE from left to right: $2.15 \mu\text{m}$ ($1''$, Weigelt et al. (1998)), 1.3 mm ($2.5''$, Groenewegen et al. (1997)), in B+V filter ($2.2''$, Mauron & Huggins (2000)). Description in the text.

g,h,i,j) Surface brightness maps (in Jy/pixel) of CW Leo-CSE from left to right: PACS $160 \mu\text{m}$, SPIRE $250 \mu\text{m}$ (inner and outer annulus representing the integrated flux for the extended emission and for the sky, respectively. The white cross is the ellipse-center), SPIRE $250 \mu\text{m}$ (white contours representing the far-UV map at $4.4 \times 10^{-5} \text{ mJy arcsec}^{-2}$ limit), SPIRE $350 \mu\text{m}$. $23' \times 27'$ FOV for all images. All background sources removed. Description in the text (Ladjal et al. 2010)

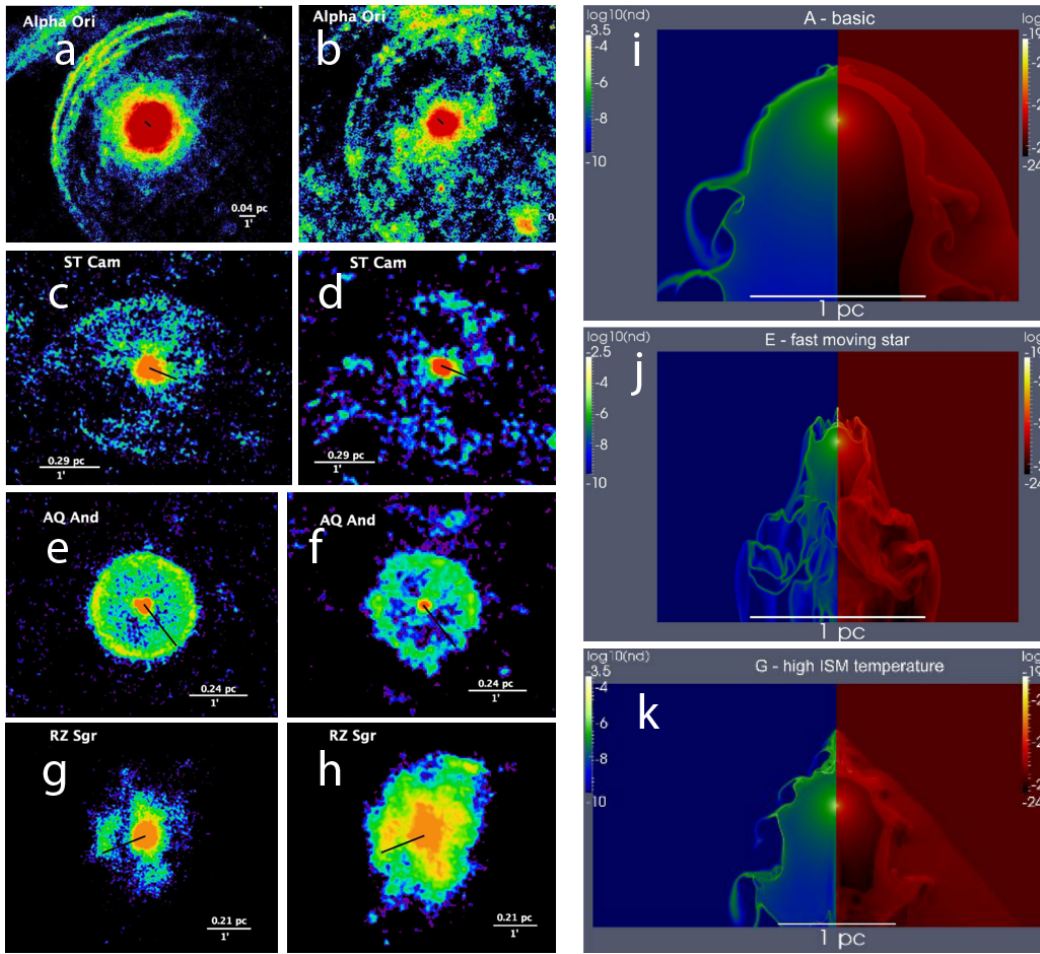


Figure 1.11: PACS 70 μm and 160 μm images of morphological types: **a,b)** “*fermata*” (α Ori); **c,d)** “*eye*” (ST Cam); **e,f)** “*ring*” (U Cam); **g,h)** “*irregular*” (RZ Sgr).

i,j,k) Hydrodynamical simulations of AGB CSEs (gas density on the right, dust grain particle density on the left) from top to bottom: basic model after 1.37×10^5 yr, high stellar space motion-model after 6.5×10^4 yr, warm ISM-model. Description in the text (Cox et al. 2012).

2 Binary AGB stars

2.1 Binary stars

The majority of stars in the universe are members in binary systems (or even multiple systems). Binaries are present among all types of stars. In this Thesis the emphasis is on variable stars, especially AGB stars evolving in binary systems. This Chapter is for the most part based on S.N. Shore (1992); J. Sahade (1993); H. Zinnecker (2001); H. J. Habing (2003).

The term “binary” was first mentioned in the Catalogue of 500 New Nebulae, Nebulous Stars, Planetary Nebulae, and Clusters of Stars (Herschel 1802), as follows:

“If, on the contrary, two stars should really be situated very near each other, and at the same time so far insulated as not to be materially affected by the attractions of neighbouring stars, they will then compose a separate system, and remain united by the bond of their own mutual gravitation towards each other. This should be called a real double star; and any two stars that are thus mutually connected, form the binary sidereal system which we are now to consider.”

Binary stars have proven to be important to astrophysics, since they gave us an idea about the structure and evolution of stars and were the starting point for e.g. the development of the hydrodynamics and radiative transfer theories. In the nineteenth century there was a huge progress due to the better understanding of celestial mechanics outside our solar system.

2.1.1 Classification

A binary star is a system with 2 stars orbiting a common center of mass. To distinguish the stars, the brighter star is always called the primary and the other star is the companion star, or secondary. One has to take care using the phrase “double star”, since this is normally referred to 2 stars observed to be very close, but not showing any interaction at all. A closer look at double stars reveals different distances, motions or velocities of

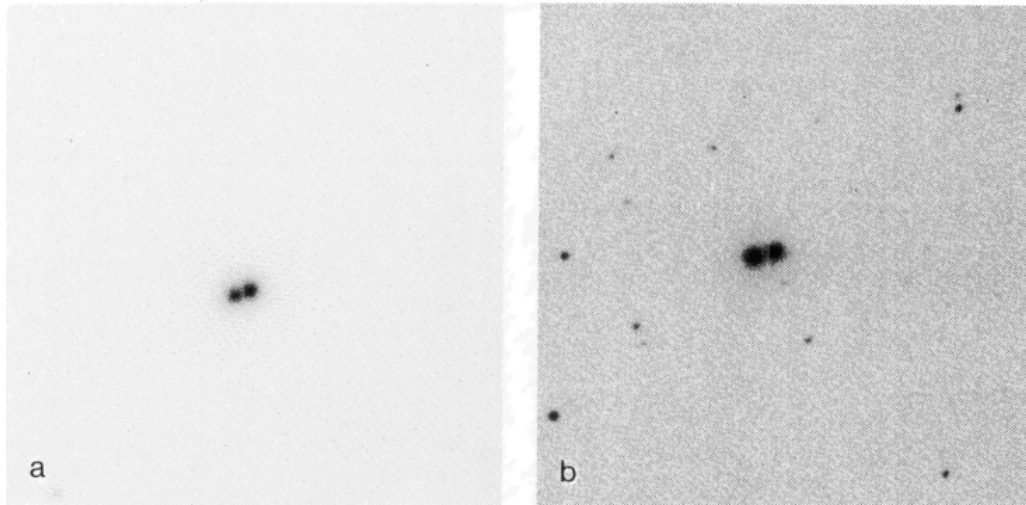


Figure 2.1: Examples for visual binaries (a $70'' \times 70''$ field). **a)** Glass-I in front of the Chamaeleon I molecular cloud. **b)** Sz 60 in the outskirts of the Chamaeleon II cloud. Faint background stars can be seen (Reipurth & Zinnecker 1993).

the 2 objects.

In 1767 John Michell was the first one publicly thinking about binaries being physically attached to each other. William Herschel was the first one publishing a catalogue with 700 double stars and later suggested some of them being binary systems. After 1800 a lot of double and binary stars were known, but the distinction was yet difficult.

Different observational techniques lead to the classification of different binary systems: visual binaries, spectroscopic binaries, eclipsing binaries and astrometric binaries.

A visual binary (Figure 2.1) is simply a pair of stars seen with the telescope. One has to take care with observations, since the plane of the orbits of the 2 stars in the binary system is normally inclined to the plane of the sky (The 7 elements describing an orbit are the semi-major axis a , the eccentricity e , the orbital period P , the time of passage (at periastron for a non-circular orbit) T_0 , the orbital inclination on the plane of the sky i , the longitude of periastron (for non-circular orbits) ω , and the position angle of the ascending node Ω). Concerning bright long-period variables the direct visual discovery of binarity is promising for close companions. Separations of less than $1''$ have been found for e.g. α Ceti (Mira) or X Ophi. For fainter variables, the minimum angular separation to detect binarity increases.

A spectroscopic binary is a binary identified through oscillations in its spectral lines. If 2 stars of a binary system are moving along the line-of-sight, then one can see 2 sets of lines, since the lines of one star are shifted towards the red and of the other star towards the blue. This is visible in the spectrum in the form of oscillations (for both stars). One has to distinguish between a single-lined (SB1) and a double-lined (SB2) spectroscopic binary. One normally observes double-lined spectroscopic binaries

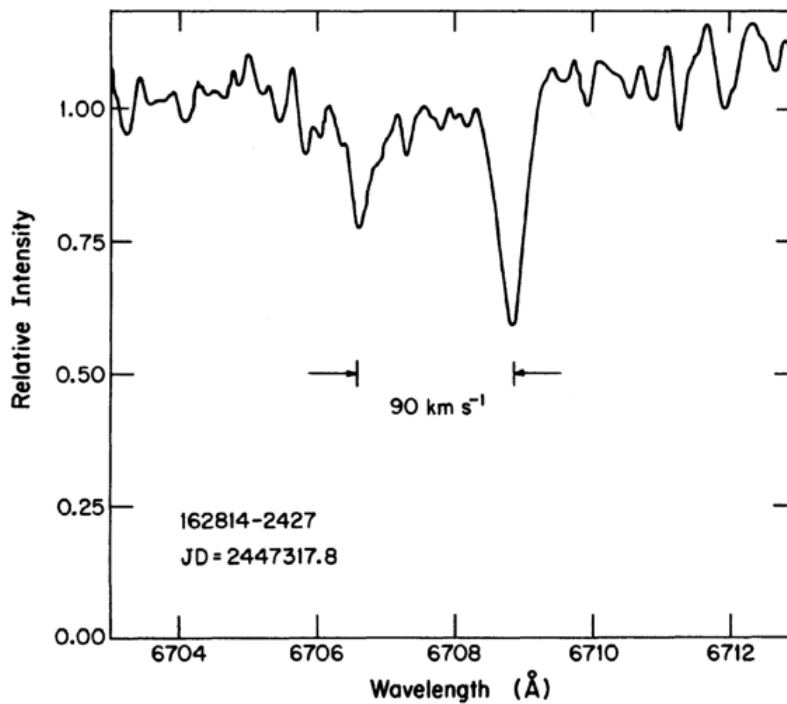


Figure 2.2: High resolution spectrum (10 km s^{-1}) of the Li (6707 \AA) lines in the double-lined binary 162814–2427. Two absorption features are evident at the appropriate velocities for each of the binary components, with the primary absorption line being the redder of the two (Mathieu et al. 1989a).

(Figure 2.2). If, however, just one star is visible in the spectrum shifting towards the blue and then towards the red, then this is a single-line spectroscopic binary. A spectroscopic inspection of long-period variables spectra can lead to the detection of a companion, but just if the spectral types of the variable and the companion are sufficiently different.

Eclipsing binaries (Figure 2.3) are visible as a single object, but considering observed brightness variations and spectroscopic measurements one can identify it to be 2 stars in close orbit.

An astrometric binary can be discovered by observing the primary star getting gravitationally influenced by the companion. This method becomes important if e.g. the system is too far away to identify it visually (Figure 2.4).

Other means of detecting binarity for long-period variables are the examination of the light curve or an emission nebulosity like can be seen around R Aqr. In the light curve a companion can be seen if it is bright enough, revealing itself via an extended flat section around minimum light or by a decrease in amplitude. The emission nebulosity around R Aqr is unique. No other variable star shows such an emission, supporting the

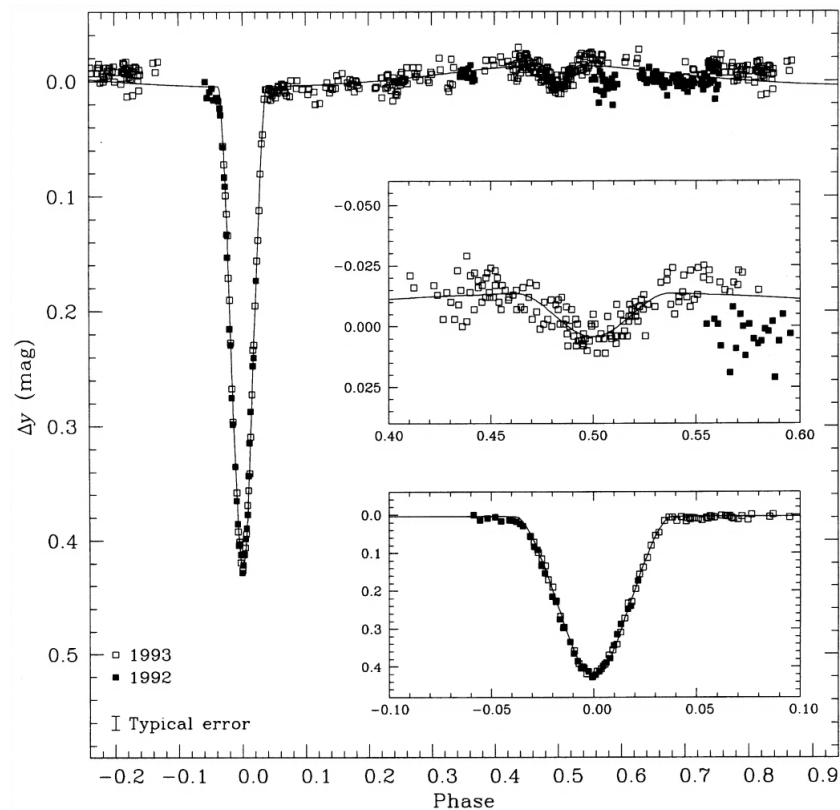


Figure 2.3: Light curve for TY CrA during 1992 and 1993. The magnitude is the offset from y measured near quadrature. The typical error of 0.006 mag is indicated. Note the shallow secondary eclipse at phase 0.5 and the strong reflection effect. The inset figures expand the regions around the primary and secondary eclipses (Casey et al. 1998).

idea that R Aqr must be different. The occurrence of a companion orbiting a common center of mass with R Aqr can be an explanation (see Chapter 3.9). To determine what is the best method to detect the visual, spectroscopic, eclipsing or astrometric binaries, one should know something about the properties this binaries have.

The Hipparcos survey

Hipparcos (High Precision Parallax Collecting Satellite) was a satellite for the astrometric measurement of about 1 million stars. It was launched in 1989 and collected data until 1993.

The Hipparcos satellite could give some hints on the binary distribution, especially on mass ratio and semi-major axis, and on the orbital evolution of stellar systems. This three are considered important parameters for star formation in a binary system.

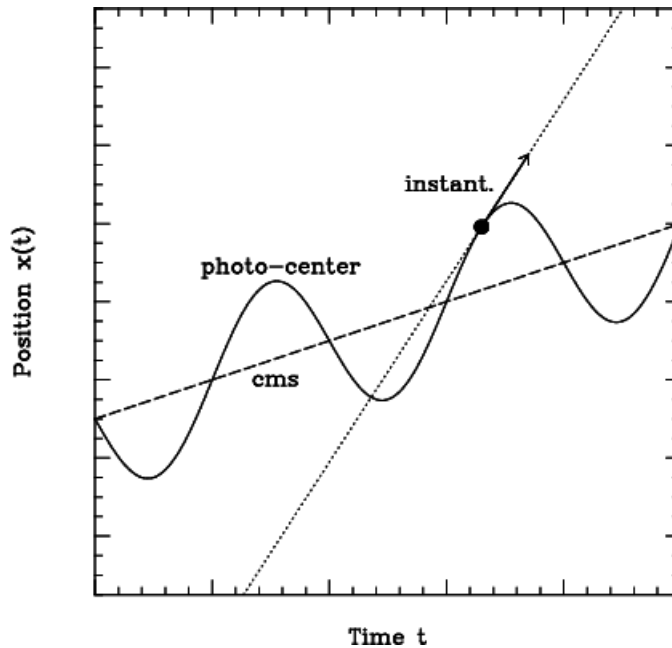


Figure 2.4: Wave motion of the photo-center of an astrometric binary (solid curve) around the linear motion of its center-of-mass (cms; dashed line). An instantaneous position and an instantaneous proper motion are indicated (filled dot; arrow). The linear prediction based on the instantaneous values is shown as a dotted line. The long-term averaged “mean” proper motion is equal to the motion of the cms (Wielen et al. 2001).

Duquennoy & Mayor (1991) studied solar-type field stars data obtained with Hipparcos and came to the following conclusions: (1) they calculated log-normal distribution of orbital periods with a median value of $P = 180$ yr; (2) they found a mass-ratio distribution increasing towards small values of the mass ratio q ; (3) they found a total multiplicity of 57 %. With Hipparcos it was possible to study the multiplicity in the 1-10 AU range for the first time with a satellite because of the sensitivity of its instruments.

The Hipparcos Catalogue includes 5 types of binary solutions, to which Quist & Lindgren (2001) added a sixth possibility ($\Delta\mu$). The standard solution of the Hipparcos satellite contained 5 parameters, namely the position (2), proper motion (2) and the trigonometric parallax (1). The additional binary solutions (including $\Delta\mu$) were:

- Component Solution (C): Double and multiple stars including objects with $p > 0.1''$ and $\Delta m < 4$ mag. The 5-parameter solution could be applied to each component.
- Acceleration Solution (G): Hipparcos could not resolve a separation less than $0.1''$, but still could identify binarity through the curved motion of the photo-center. 2 or 4 more parameters were added for the quadratic and cubic polynomials of time in each coordinate (α, δ).

- Orbital Solution (O): The seven Keplerian elements of the orbit of the photo-center around the center of mass could be resolved.
- VIM Solution (V): Variability Induced Movers show non-linear motions of the photo-center due to variability.
- Stochastic Solution (X): The 5-parameter fit sometimes gives too large residuals not explicable by observation errors, multiplicity is implied in those systems representing 1% of the Hipparcos objects.
- Delta-mu binaries ($\Delta\mu$): This binaries were found comparing quasi-instantaneous proper motions by Hipparcos with long-term averaged, ground-based proper motions, showing a statistically significant difference between the 2 measurement methods.

2.2 Properties of binary stars

The following describes the physical and dynamical properties of pre-main-sequence and main-sequence stars, which were obtained by observations. With the knowledge of the properties one can think about the origin of binary stars.

There is a small sample of pre-main-sequence stars available, but the important informations can be interpreted already. Foremost Reipurth (1988), Zinnecker (1989), and Boss (1993) collected statistical samples. Wootten (1989) and Sasselov & Rucinski (1990) were the first suspecting the presence of binary protostellar objects. Protostellar objects being members in binary systems gave rise to new theories of star formation.

For main-sequence stars Duquennoy & Mayor (1990) have obtained data from all F7-G9 dwarfs within 22 pc of the sun. Their sample consists of 166 primaries and 44 secondaries.

2.2.1 Frequency

Mathieu et al. (1989b) discovered 6 spectroscopic pre-main-sequence binaries T Tauri stars (a class of variable stars named after the prototype - T Tauri; see e.g. Ratzka et al. (2009)) in their sample and found a binary frequency of $F = 0.10$ with periods smaller than $P = 100$ d (compare to the main-sequence frequency of $F = 0.12$ for the same periods). Chen et al. (1990) detected a binary frequency of $F = 0.29$ observing 9 double systems in 31 pre-main-sequence stars through the lunar occultation method (compare to the main-sequence frequency of $F = 0.28 - 0.33$). The frequencies here suggest that all binaries are already formed during the pre-main sequence. Also a very small number of triple pre-main-sequence systems has been found.

Duquennoy & Mayor (1990) found in their sample of main-sequence stars 65 % having a companion with a mass ratio of $q = M_2/M_1 \geq 0.1$. The half of the other 35 % could

have a companion, but with a very low mass with the ratio $q = 0.01 - 0.1$. This means, that less than 25 % are thought to be single stars. This reflects the idea of most of the stars in the universe being part of binary or multiple systems. They also found 9 triple and 5 quadruple systems.

Frankowski et al. (2009) found 6.3 % of their Hipparcos M giants with few velocity measurements to be spectroscopic binary systems, this being less than half of the analogous rate for their field K giants. This difference may be explained by the difficulty of finding binaries among M giants, because they have smaller orbital velocity amplitudes and larger intrinsic jitter. Also M and K giants are differently distributed in the eccentricity-period diagram (Figure 2.5). For M giants with more than 2 velocity measurements 11.1 % were found to be confirmed binaries and additional 2.7 % are possible detections.

2.2.2 Age

The ages for pre-main-sequence binary T Tauri systems range from 10^5 yr (Boss 1993) to 10^6 yr (Mathieu et al. 1989b). The older stars were calculated to be very close to the birthline in the Hertzsprung-Russell diagram (Stahler 1988). DF Tau, a younger binary was also found to be close to this birthline (Chen et al. 1990). Another young binary was found to be deeply embedded in a NH_3 cloud clump (Zinnecker 1989). The detection of binary systems in early epochs of star formation leads to the conclusion that binarity plays a role in the stellar evolution. To determine the age of stars in binary systems is not an easy task, considering how many types of stars are members in those systems. Depending on the knowledge of the evolution of different binary stars one can estimate the age knowing the exact stellar type, e.g. knowing that T Tauri stars are pre-main-sequence objects or AGB stars are late-type stars, but if these stars are members in multiple systems, then the age determination is difficult because of the physical and chemical processes “accelerating” the evolution of the objects.

2.2.3 Separation and period

Cohen & Kuhl (1979) found 34 close pre-main-sequence T Tauri stars and suggested because of the similar luminosities of primary and secondary them to be physical binaries. Reipurth (1988) calculated a separation of $p = 200 - 2400$ AU for their 28 visually detected pre-main-sequence binaries. Chan and Simon (1990) found 7 T Tauri binaries with separations around 500 AU. Chen et al. (1990) found 5 of their 7 binaries detected through lunar occultation to have projected separations of $p = 1 - 80$ AU. T Tauri stars identified as spectroscopic binaries were found to have periods on the order of days to months (Boss 1993). The separation of binaries in the pre-main-sequence sample covers a wide range comparable to their main-sequence counterparts.

The sample of main-sequence stars of Duquennoy & Mayor (1990) shows a roughly Gaussian distribution in orbital period, which ranges from days to millions of years,

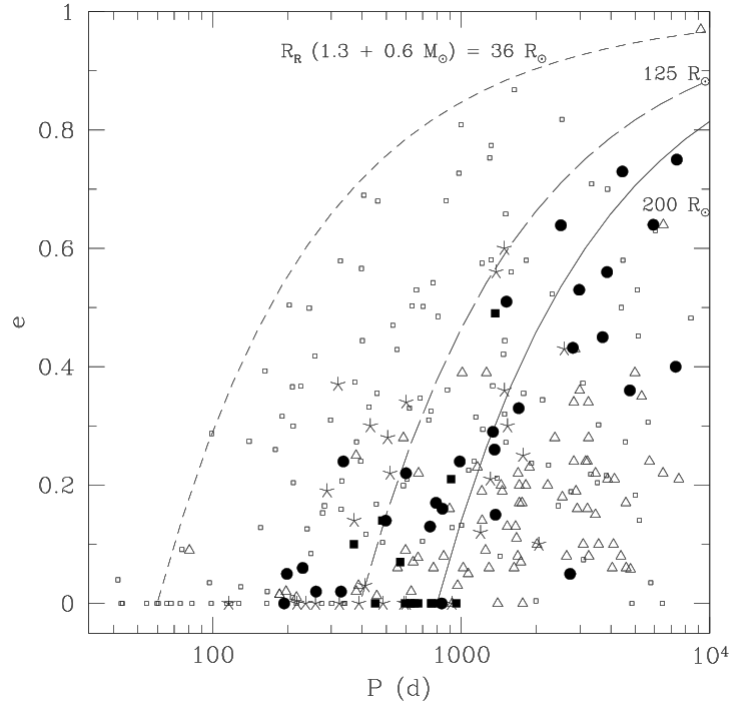


Figure 2.5: The $(e\text{-log } P)$ diagram for spectroscopic binaries involving M giants (black dots), K giants in open clusters (small open squares), barium and S stars (open triangles), symbiotic stars involving a M giant (and yellow symbiotics, filled squares) and post-AGB stars (star symbols). The short- and long-dashed lines correspond to loci of constant periastron distance (78 and 280 R_{\odot}), translating into Roche radii of 35 and 125 R_{\odot} , respectively (assuming masses of 1.3 and 0.6 M_{\odot} for the 2 components). The solid line corresponds to a periastron-distance of 450 R_{\odot} and a Roche radius of 200 R_{\odot} . The data was taken from the literature and the own study of Jorissen et al. (2009).

with a peak at $P = 300$ yr, with a separation from a few solar radii to $p = 0.1$ pc, peaking at $p = 10$ and 100 AU. For Hipparcos M giant binaries Famaey et al. (2009) found periods ranging from $P = 193 - 4500$ d. The Hipparcos binaries separations statistics show $\approx 25\%$ in the 1 - 10 AU range, 43 % in the 10 - 100 AU range (Quist & Lindegren 2000).

2.2.4 Eccentricity

Pre-main-sequence binaries with shorter periods than 4 days in general have circular orbits, systems with longer period have eccentricities ranging from $e = 0.1 - 0.5$ (Mathieu et al. 1989b). Systems with circular orbits undergo a very rapid evolution due to

the strong tidal forces, so it can be assumed that stars in those systems are very young a.k.a. in an early evolutionary state. Despite of this binaries tend to form with large eccentricities, whatever the separation is.

The main-sequence sample of Duquennoy & Mayor (1990) shows systems with less than 11 d periods heaving a very low eccentricity close to zero. This was expected considering the orbit circularization by tidal effects for stars having the same age as Galactic disk stars. Long period systems with periods larger than 1000 d have eccentricities ranging from $e = 0.2 - 1$. Systems with intermediate periods show a mean eccentricity of $e = 0.35$. This seems to be particularly true for halo and disk populations and especially for low mass secondaries. As interesting side information concerning the eccentricities of stars in binary systems and planets around stars, one can say that stars form in highly eccentric systems, and planets do not.

Today a typical eccentricity for binary stars (on the pre-main sequence and main sequence) of $e = 0.2 - 0.6$ is considered (Duquennoy & Mayor 1991; Mathieu 1994). Looking at the gravitational interaction in the eccentricity evolution in binary systems, Lubow & Artymowicz (1996, 2000) found the relation $e\dot{e} = -(1/2)\dot{a}/a$ for $e > 3$ (where $\dot{e} = e$) in most binary systems being in agreement with SPH calculations. Concerning spectroscopic binaries among Hipparcos M giants Jorissen et al. (2009) found that binary systems with $e < 0.4\log P - 1$ (periods P in days) are mostly post-mass-transfer systems, because of the vast majority of barium and S systems matching this condition, and these systems have companions with masses around $0.6 M_{\odot}$ as expected for WDs. Famaey et al. (2009) found eccentricities for Hipparcos (non-symbiotic) M giant binaries ranging from 0.0 to 0.7.

The eccentricity in multiple systems was not that much of a topic yet. Shatsky (2000) suggested that the wide outer sub-systems of multiple stars show a tendency towards circular orbits.

2.2.5 Spin-orbit alignment

Pre-main-sequence stars can have circumstellar disks and bipolar outflows as well. The disks are mostly aligned perpendicular to the rotation axis and the bipolar outflows with the rotation axis. Further observations of binary systems should give a hint of the spin orientation in the systems.

Spin rotating axes tend to be aligned parallel to the orbital rotation axes, as was already shown in Weis (1974). For main-sequence stars this correlation is even stronger for F than for A stars. Tidal forces are able to take some spin out of the system, though this tidal effects are not important for visual binaries. With observing eclipsing binaries the simultaneous calculation of the spin rotation and the orbital rotation is possible. In close binaries the tidal effects are very strong, but not strong enough to e.g. reverse the sense of rotation, the spin-orbit alignment therefore has to be primordial.

2.2.6 Orbit-orbit alignment

Weis (1974) theorized about the tendency towards coplanarity between visual and spectroscopic components in multiple systems. For 20 close visual multiple systems Fekel (1981) found 66 % of the systems to be coplanar (meaning an inclination smaller than 15°).

2.2.7 Mass ratio

The masses of pre-main-sequence stars in binaries are difficult to determine, since not much eclipsing pre-main sequence binaries have been found yet. Mathieu et al. (1989b), however, set lower limits on masses of the primaries and secondaries in double-lined spectroscopic binaries to $1.02 \pm 0.06 M_\odot$ and $0.94 \pm 0.05 M_\odot$, respectively.

Halbwachs (1986, 1987) had a sample of 205 spectroscopic binaries (trying not to include systems with mass exchange). The mass ratio for close spectroscopic binaries was calculated to be almost the same as for visual binaries, with $q = 0.2 - 1$, with a peak at $q = 0.4$. The sample of Trimble (1990) with 164 spectroscopic binaries showed a peak at $q = 0.2$ with a minor peak $q = 1$. Duquennoy & Mayor (1990) had the maximum peak around $q = 0.3$ with a minor peak around $p = 1$. The three previous examples are in good agreement.

Duquennoy & Mayor (1991) found for binaries of all separations a mass ratio distribution rising towards low mass ratios (i.e. unequal masses). For close binaries Mazeh et al. (1992) and Halbwachs et al. (1998) found for periods < 3000 d or separations $p < 5$ AU a uniform mass ratio distribution (i.e. biased towards equal masses compared to wider systems)

Concerning the binaries's total mass new results show that massive stars frequently have low-mass companions. Before the new results came up, the total mass was somehow believed to be connected to the separation, which turned out not to be true.

For Hipparcos M giant binaries mass ratios of 0.0034 to 0.203 could be found (Famaey et al. 2009).

2.2.8 Multiple systems

Multiple systems show very different periods for the closest and widest members in the system (Fekel 1981), they are hierarchical systems. Trapezium type systems can occur, with approximately the same distance of stars to each other, but do not survive long due to the rapid orbital evolution to more stable configurations or simply due to mass ejection (Anosova 1989). Duquennoy & Mayor (1991) showed that the fraction of triples, quadruples, and even sextuples and septuples relative to binaries is very small (a fraction of 0.11 ± 0.04 for triples and even less for systems with more stars).

Knowing the properties of binary systems, it is easier to think about formation sce-

narios. The more knowledge we gained over the years, the more precise (and complex) these theories became.

2.3 Formation scenarios of binary systems

There exist some theories about the formation of systems containing 2 or more stars. They are listed in order of appearance. The newest and most likely scenarios are presented at the end of this Section.

2.3.1 Separate nuclei

Laplace was the first one coming up with a suggestion of how binary systems form in 1789. He thought of double stars being formed by condensation of nuclei that began to orbit each other (Tassoul 1978). In the eighteenth century nobody investigated this idea further, but today the separate nuclei theory is being considered again, because nowadays we know a lot more about molecular clouds with its dense cores. These clouds are thought of being a place of frequent star formation. Molecular clouds can become highly structured to produce dense cores, which can have masses ranging from 0.3 to 10 M_{\odot} . Infrared observations also indicate star formation in these regions. A collapse in these clouds was never observed on a large scale. The cores may be formed by magnetic fields and therefore be quasi-static (Shu et al. 1987).

It's not known precisely, how the cores form, but it was shown that star formation happens afterwards. The **dynamics** behind the core formation is not yet understood, but there has to be one to explain the star formation.

The separate nuclei theory has a plausibility of arguments, but some facts copy this theory, however.

The youngest binary systems found could be explained very well due to binary molecular clouds existing in early phases. The range in core masses as mentioned before could lead to a variety of mass ratios, that were actually found in binaries.

In practice, however, the separate nuclei theory is not very likely due to radio **observations**. Separations of $p = 0.2$ pc and more were found and this is far too much separation for binary systems, that were found to have a maximum separation of 0.1 pc. Another problem is that we do not know yet if the cores are gravitationally bound or if we see physical or just optical binary stars evolving in the clouds. The third problem is the explanation of how the spin-orbit and orbit-orbit alignments arise in those systems.

2.3.2 Capture

In 1867 Stoney suggested the formation of binary stars through capture of single stars (Tassoul 1978). In order to consider this theory, one has to know the source of energy

dissipation, since a star has to be bounded in an orbit. 3 basic theories exist: Three-body encounters, tidal dissipation and gas disk interaction.

Mansbach (1970) was the first one actually calculating the formation rate of binary stars through **three-body encounters**. The theory works as follows: 3 unbound single stars undergo an encounter; one of 3 stars absorbs enough kinetic energy from the other 2, so that they gravitationally bound themselves. Mansbach assumed a Maxwell-Boltzmann distribution in phase space, so he found that the formation rate varies with the stellar number density to the third power and is directly dependent on powers of the final binary separation and the stellar masses. It is logical that three-body encounters happen mostly in regions of high stellar density. Preferably wide binaries form, but this contradicts observations showing that wide binaries are rare. The formation rate of binaries in the Galactic disk with a stellar density number of $n \sim 0.1 \text{ pc}^{-3}$ via a three-body encounter is extremely small. Statistically less than one solar-type binary with a separation of more than 2000 AU has been formed over the age of the Galaxy (Mansbach 1970).

Today star formation primarily is observable in clusters with high density and lower relative velocities (than in the Galactic disk). The three-body encounter certainly still plays a role in those systems to form binaries. Open cluster T Tauri stars have an approximated stellar number density of $n \sim 10 - 10^2 \text{ pc}^{-3}$ (Wilking & Lada 1983) or e.g. the Lynds 1641 dark cloud was calculated to have a stellar density of $n \sim 7 \times 10^3 \text{ pc}^{-3}$ (Strom et al. 1989). Mansbach (1970) showed that even with $n = 10^4 \text{ pc}^{-3}$, a mean relative velocity of 1 km s^{-1} resulting in a maximum separation of 200 AU is still too small for binaries to form through three-body encounters over a lifetime of 10^6 yr of a cluster.

Valtonen & Mikkola (1991) reviewed the three-body interaction scenario and divided it into 3 classes: (1) interplay: 3 members perform completely random motions with no periodicity; (2) close triple approach: 3 bodies brought close together. During that event an energy exchange mostly happens; (3) ejection: a close triple approach leading to the formation of a binary and a third star getting absorbed its potential energy and therefore losing its ties to the system.

Another possibility of forming a binary star through capture is the occurrence of **tidal friction** leading to the 2 stars dissipating relative kinetic energy that maybe leads to capture. Because the tidal capture cross section is ~ 10 times larger than the geometrical cross section, this just works with very close encounters within the Roche radii of the stars. This method, however, is completely negligible, because the mean time between tidal encounters for solar-type stars in the Galactic plane with $n = 1 \text{ pc}^{-3}$ and relative velocities of $v_r = 10 \text{ km s}^{-1}$ is more than 10^{19} yr and for dense clusters with $n = 10^4 \text{ pc}^{-3}$ and $v_r = 1 \text{ km s}^{-1}$ more than 10^{16} yr for any star.

Gas disk interaction is also possible if one considers 2 protostellar disks, both inhabiting a protostar, having a close encounter. Dissipation of energy could be produced by gas drag, gravitational drag, tidal forces, shock heating, and radiation. Knowing the hydro- and thermodynamics of the processes, one can assume that such encounters are in fact highly dissipative and could lead to bounded binaries. Note that such an

outcome is still not ensured, since a collision between rotating clouds can e.g. produce mergers too. Pre-main sequence-binaries could form this way, but it would be limited to a separation of 10 to 100 AU, representing protostellar disk sizes. Gravitational drag could lead to decaying orbits, however, to form closer binaries (Larson 1990).

All 3 possibilities could be applied to several observations. It is believed that binary formation via capture involves a wide range of masses and eccentric orbits. Multiple capture is believed not to be very frequent.

2.3.3 Fission

Kelvin and Tait suggested the formation of binaries via fission (Tassoul 1978). Fission seemed to be a good idea because of the contraction with conserved angular momentum of a rotating fluid body. The springboard for this theory is based on analyses of the equilibrium and linear stability of idealized spheroidal and ellipsoidal bodies. However, with analytic methods this theory was impossible to prove.

Numerical studies were made to get a better understanding. Hydrodynamics codes were used to calculate the 3-D, nonlinear time evolution of a rotating, self-gravitating gaseous body.

Instead of forming binaries, simulations show that it is more likely that low mass rings or disks are formed. To form at least one companion, a mass ratio of $q \ll 1$ would be needed. Our understanding of protostellar evolution also would lead to the conclusion that this method would not allow a separation larger than 10 AU. The eccentricity would be rather small. Spin-orbit and orbit-orbit alignment would be expected, but the expectations for the rest of the parameters are not fulfilled.

In the 1980s not that much was known about fission, since computerized simulations lacked knowledge of the process. However, in the last years some progress in the field of rotational fission was made with the use of different hydrodynamics codes studying the development of dynamic bar-like instabilities in initially axisymmetric fluid objects having star formation and late-type stellar evolution in mind (Imamura et al. 2000; Cazes & Tohline 2000; Durisen et al. 2000; New et al. 2000; Brown 2000; Shibata et al. 2000). The hydrodynamic simulations concluded (Tohline & Durisen 2001): (1) the dynamical bar mode instability does not lead to prompt binary fission; (2) the instability usually leads to the formation of a dynamically stable, bar-like structure that is spinning about its shortest axis and has non-trivial internal flows. The evolutionary process of the bar needs to be taken care of in more detail. Fission has been somehow abandoned as a binary formation scenario (Bonnell 2001).

2.3.4 Fragmentation

The following theories were developed in the twentieth century and are more preferred by the scientific community.

The first one of the theories is fragmentation, simply defined as breakup due to gravita-

tional instability during the collapse phase of protostellar evolution using the Jeans mass argument (Hoyle 1953). Hoyle stated that small masses able to become self-gravitating would separate out of the ongoing cloud collapse. Hunter (1962) proved analytically that a collapsing pressureless sphere can be unstable to perturbation growth and that the time scale for this growth is shorter than the collapsing cloud time scale. Layzer (1963), however, argued that perturbation may lead to turbulence in the cloud, but not to a completely independent, self-gravitating body. Larson (1972) found out that a rapidly rotating, collapsing cloud is flattening due to rotation and forms rings. He suggested this rings to fragment and he was the first one really suggesting that fragmentation is a process to form binaries and multiple systems out of rapidly rotating clouds. Boss (1993) also suggested that hierarchical systems could form through cloud collapses undergoing several fragmentation phases.

In the 1980s the problem was tried to be solved with 3D hydrodynamical codes. Boss & Bodenheimer (1979) showed that with a large enough initial density perturbation a binary protostar would evolve directly out of the collapsing cloud without the ring formation phase. On the other hand, Tohline (1980) argued that considering the Jeans equilibrium rapidly rotating clouds would even with large perturbations form a ring, before the complete fragmentation occurred. Bodenheimer et al. (1980) summarized that a wide variety of initial conditions has to be fulfilled to let a collapsing cloud form a binary system. One has to take care, since they used a uniform density initial cloud for their calculations. Also magnetic fields were not used in their calculations.

The models until 1980 just allowed the formation of equal mass binaries. New numerical models also included the possibility of forming unequal mass binaries. Compared to previous simulations the grid resolution in the crucial azimuthal direction has been increased and the symmetry through the rotational axis has been relaxed. This should give more and stronger perturbations in the simulations leading to a more realistic protostellar fragmentation. Numerical simulations generally proceed on the assumption that the initial cloud has a density distribution that is somewhat centrally condensed, e.g. Bodenheimer & Burkert (2001) observationally showed that cores have a density distribution near $\propto R^{-2}$ in the outer regions (a few thousand AU) and a distribution closer to $\propto R^{-1}$ in the inner regions. Boss (1993), Burkert et al. (1997) and Tsuribe & Inutsuka (2000) came to the conclusion that as the degree of central concentration increases, the parameter space available for fragmentation seems to shrink.

Bate & Bonnell (1997) identified the quantitative effects of gas accretion with known angular momentum in a binary with circular orbit and a given mass and separation. With this knowledge Bate (2000) published a semi-analytic method for calculating the evolution of a binary system from its initial mass (after the formation via fragmentation) to its final mass (after accretion of all gas from the envelope). His protobinary evolution (PBE) code allowed to trace the changes in mass ratio, separation, circumbinary disk-mass, and relative accretion rate. Compared to hydrodynamic calculations by Boss & Bodenheimer (1979) the PBE code works at least as accurate, but is 10^6 to 10^9 times faster (depending on the mass accretion rate). The PBE code shows that the angular

momentum in the initial cloud is of great importance to determine the evolution of the properties of the future binary.

It is generally believed that star formation happens through cloud collapse. Previous mentioned methods concerning binary fragmentation showed: (1) a magnetic field is dynamically insignificant; (2) a cloud can contain several Jeans masses; (3) relevant rotation is present; (4) the collapse does not start from a power law initial density profile. It is not known, however, to what extent these conditions are true. These points are explained in the following paragraphs.

There is just indirect proof that magnetic fields are not that important in dense cores ($n > 10^4 \text{ cm}^{-3}$, Heyer (1988)); in general the influence of magnetic fields is one of the open questions in the field. What we know from theoretical 3D models is that if you have a collapsing cloud with a magnetic field being frozen-in, then fragmentation is prohibited, but if ambipolar diffusion is able to reduce the influence of the magnetic field, then the formation process is permissible (Boss 2001).

With a bit more than 1 Jeans mass a thermally supported cloud might begin to collapse and also avoid fragmentation. If you take magnetic fields, rotation, and thermal pressure or even evolving by ambipolar diffusion into account, then the collapse could begin with a Jeans mass of $\alpha_i \sim 0.3$ already. Also a collapse caused by shock waves or cloud collisions is possible (Lattanzio & Henriksen 1988). High galactic latitude clouds are considered evidence for the cloud collision theory.

Since complex velocity fields and thermal line widths hamper the detection, observations are limited to the most rapidly rotating ones. Anyway, the rotation rates of most of the clouds are not known.

Shu (1977) showed that the theory of an embedded young star in the dense center of a cloud is consistent with his theorem of the formation of a singular isothermal sphere with the collapse starting at the center and the continuation of accretion of the cloud in a protostellar core.

The **frequency of binary formation via fragmentation** can not be answered yet, since there is no knowledge of the initial conditions leading to fragmentation.

The possibility of the formation of **multiple systems** via fragmentation was considered by Narita et al. (1984). Strong perturbation is necessary to produce more than 2 bodies out of a cloud being gravitationally attached to each other.

Considering the **separation** of the binaries formed from a rapidly rotating cloud, Boss & Bodenheimer (1979) clarified that the separation can only be slightly smaller than the initial cloud radius. Dense molecular clouds have radii up to 0.2 pc (Myers 1987) if the cloud core is rapidly rotating. Close binaries could form in clouds with slow rotating cores. The closest binary separation calculated was 1 AU. For this case a very small cloud core would start to collapse from a higher initial density and the fragmentation would stop, after the cloud gets non-isothermal and form quasi-equilibrium cores. Separations smaller than 1 AU just can be explained with additional orbital decay.

In binary systems formed by fragmentation high **eccentricities** are believed to occur, because there is not centrifugal balance expected in the collapsing clouds (Lucy 1981;

Boss 1988a). Nearly circular orbits are expected, when binaries are formed after the formation of nearly Keplerian disks. Another reason for the high eccentricities might be the pre-main-sequence stars forming out of the clouds, since the rest of the cloud (the envelope) should form more circularized orbits.

Because of the symmetry (above and below the orbital plane) imposed in simulations, they show **spin-orbit and orbit-orbit alignment**. Using particle hydrodynamics codes, symmetry was not imposed, but still could reproduce a fair degree of alignment. It was proven by Sigalotti (1990) that even if the clouds initially followed a solid body rotation, equatorial asymmetry can occur.

In the case of the **mass ratios**, with taking symmetry into account, binaries with mass ratios of $q = 1$ were preferently formed. Using particle hydrodynamics codes in this case, the mass ratio also became unequal. Mass ratios in fragmented systems were not that much of a topic in the literature up to now; the distribution of secondary masses for a given primary mass is still unknown.

The fragmentation during the collapse of a rotating cloud is considered the most likely process for the formation of wide binaries (Boss 1988b). The newest calculations of the occurrence and understanding of the fragmentation process, however, showed that the process is more complex than previously thought. There is still a number of open questions to be answered (Bodenheimer 2001). The general observed properties of binary and multiple systems still need to be properly explained. The distribution of binaries according to their frequency, period and eccentricity are not yet well understood. Concerning the wide binaries it is not clear if the fragmentation happens spontaneously or is induced through cloud-cloud collisions. It also can be that fragmentation leads to the formation of a small cluster and is then followed by interaction and capture scenarios. In combination with this theory, the question of the importance of hierarchical fragmentation arises. Another open question is the evolution of orbits after the formation. We know that most stars form in clusters, nevertheless numerical simulations do not or cannot yet consider this (because of the complexity), they just assume a collapse of individual cloud cores. The theory of the formation of wide binaries via fragmentation has advantages (concerning observed binary systems), but also has a number of problems. On one side, a wide range of orbital momenta and eccentricities can be predicted, the presence of circumstellar and circumbinary disks can be predicted and explained. On the other side, as mentioned before, the role of magnetic fields is still unclear. Many calculations up to now assumed adiabatic heating of the cloud center at an assumed critical density to let the fragmentation begin. Maybe also the consideration of radiation transfer is important. And finally, numerical simulations are not well compared with observations. While numerical simulations can handle the general formation process of wide binaries, for close binaries it is not perfectly applicable, but it is unlikely that there are 2 completely independent binary formation processes.

However, fragmentation of clouds has different possible outcomes: Binary formation (Boss 1993; Bate et al. 1995), induced fragmentation by an initial central binary system of further fragments in a surrounding disk (Bonnell & Bate 1994), formation of small

clusters (Monaghan & Lattanzio 1991), fragmentation of filaments (Monaghan 1994; Inutsuka & Miyama 1997) or the formation of a binary system with additional low-mass fragments (unpublished theory by Bodenheimer & Burkert)

2.3.5 Cloud clump collisions

Pringle (1989) was thinking about the possibility of binary formation via the collision between the clumps formed in molecular clouds. He mentioned the largest clumps to be the cloud cores normally associated with their embedded young stellar objects. Concerning the embedded object and the cloud envelope a relative motion of about 0.5 km s^{-1} between them was considered to be enough evidence of past external influences on the cloud collapse process. A collision with another cloud clump could be one reason for this relative motion. This is true if the clouds are thermally or magnetically supported and should lead to collapse and also fragmentation (Lattanzio & Henriksen 1988). Pringle also theorized about the clouds having long enough lifetimes, so they can accrete gas and then form stars in the centers caused by collisions.

This theory is basically a mix of the separate nuclei and fragmentation theories. Pringle (1989) assumed collisions with relative velocities up to the sound speed c . Lattanzio & Henriksen (1988) used head-on and off-center collisions also up to the sound speed c , but especially with spherical, rotating clouds with equal masses and this always resulted in the formation of a nearly spherical clump beginning to collapse. The fragmentation did not get a lot of attention in the cloud clump collision scenario, but it is believed that it happens just if the Jeans mass value is low enough in the post-collision era. If the collapse yields to a more asymmetric body, then fragmentation becomes more likely, still considering a low enough Jeans mass.

Some simulations of cloud-cloud collisions have been done with Smoothed Particle Hydrodynamics codes (SPH) by Whitworth (2001), Pongracic et al. (1992), Turner et al. (1995), Whitworth et al. (1995), and Bhattal et al. (1998). The simulated models assumed self-gravitating isothermal spheres in a hot, low-density interclump medium. The spheres alone are stable, but when they collide with other spheres at a Mach number $M < 10$ and the sound speed is reduced by radiative cooling (pre-shock and post-shock scenario), then fragments form still being influenced by ram pressure of inflowing gas. It has been suggested by R.I. Klein at the IAU Symposium about binary formation in 2001 that instead of fragmentation, the process may rather lead to cloud shredding, but Klein used smooth inviscid fluids in his simulations, not considering the complex internal structure of interstellar clouds.

For the observation of those cloud clump collisions the same as for the fragmentation is valid, meaning that there is not enough knowledge a.k.a. observation to reinforce this theory. Theoretically the frequency of binary formation via this collisions is depending on the velocity, the degree of magnetic support, the internal density and the angular velocity fields. However, cloud clump collisions could explain young and wide binaries. Again, as for previous theories, the formation of close binaries systems needs an addi-

tional decay of the orbits. Highly eccentric orbits and a wide range of mass ratios might be expected. Spin-orbit and orbit-orbit alignment may occur in some cases. Even the formation of multiple systems can not be excluded.

2.3.6 Eccentric disk instability

Adams et al. (1989) were thinking about the possibility of the formation of binary stars via spiral gravitational instability in circumstellar disks.

Shu et al. (1990) investigated the physical basis of eccentric instability further. They showed that in some cases the marginally unstable disk could reach a mass of $0.24 M_{\odot}$ for a central star with a mass of $0.76 M_{\odot}$. The disk should have approximately the same mass as the central star in order to let gravitational instability to form another body. Shu also pointed out that an eccentric instability depends strongly on a positive feedback process through wave reflection off a “sharp” outer disk boundary. This may not be the case in real disks.

Numerical studies of Adams et al. (1989) were not very successful, because they were based on linear perturbation theory and could not reproduce a growth of the eccentric instability of the $m = 1$ modes into the nonlinear regime, where the binary formation theory could be explained. Norman & Wilson (1978) and Cassen & Moosman (1981) studied nonlinear growth of gravitational instability in thin, massive disks with a central star. Cassen & Moosman (1981) did not use the $m = 1$ modes, but Norman & Wilson (1978) found using the $m = 1$ modes rotating isothermal ring.

Despite all the calculations, a non-linear growth of the gravitational instability does not mean that a binary star is forming. If the growth happens on the time scale of the rotation period of the outer edge of the disk, angular momentum can be transported by trailing spiral arms outside the corotation radius and this could result in a relatively rapid disk evolution preventing the formation of a (stable) binary system. The possibilities for the numerical treatment of this problem are not exhausted.

Like for previous methods, without good proof a good theory including the frequency of binary formation with the help of eccentric disk instabilities can not be calculated. We only can guess that for this case the formation of very young binaries could be explained if instabilities happen before the star even reaches the pre-main-sequence track. Spin-orbit and orbit-orbit alignment could possibly be applied. Due to the sizes of circumstellar disks the binary separation would have a limit of 10 to 100 AU. Wider binaries are definitely not forming through this instabilities.

There may not be a universal mechanism forming binary systems, but perhaps a mix of the mentioned mechanisms play a role for certain types of binaries. Table 2.1 summarizes the positive and negative results for the different methods, the question mark indicates that too little is known to make a conclusion.

The newest tool regarding the binary stellar evolution is called BINSTAR (Siess et al.

Table 2.1: Summary of binary formation theories, pro and contra (J. Sahade 1993). Although the table is from 1993, it is still valid.

Constraint	Separate Nuclei	Capture	Fission	Fragmentation	Clump Collisions	Eccentric Disk
Dynamics	?	+	-	+	?	?
Frequency	?	?	-	?	?	?
$10^5 age$	+	+/-	+	+	+	+
System type	?	-	-	+	?	?
Separation	-	+/-	+/-	+	+/-	+/-
Eccentricity	?	+	-	+	?	?
Spin-orbit	-	-	+	+	?	+
Orbit-orbit	-	-	+	+	?	+
Mass ratio	+	+	-	+	?	?

Six theoretical hypotheses as universal mechanisms for explaining binary and multiple star formation.

2011), an extension of the stellar evolution code STAREVOL. It simultaneously can calculate stellar components and the binary orbit. It can be used to describe the mass transfer, the tidal interaction of the orbital evolution, the chemical and angular momentum transport, semi-convection, and thermohaline and rotationally induced mixing.

2.4 Interacting binary stars

We know now that if 2 stars are interacting gravitationally, so that they move in closed (elliptical) orbits around a common center of mass, this stars are defining a binary system. In general one can distinguish between visual, spectroscopic, eclipsing and astrometric binaries. Consider that a binary can be e.g. a visual and a spectroscopic one at the same time, etc..

One of the most important parameters considering the binary evolution is the separation of the stars. Is the separation large, they orbit each other, but won't influence each others' evolution. In the case of a close binary, it is very likely that the 2 components are interacting and that the primary (which is in most cases a red giant star) is influencing the companion (which is in most cases a WD).

The majority of binary stars show signs of tidal distortions (due to gravitational interaction) and mutual irradiation (which also can be used to identify binarity). The term "interacting binary" refers to the 2 components interacting stronger and so the evolution of the binary members and the binary system as a whole are affected. This interactions are caused by at least one of the stars being unstable and ejecting mass. The instability has not to be caused by the other star, instead it is more likely that the star ejecting mass is at a mass-losing evolutionary state. In many cases expelled matter from the unstable star is caught by the 2nd star's gravitational field; in this picture

this star being referred to as the companion star. Because of the infalling material the companion, also called the secondary, can be affected in its evolutionary track. Matter from the mass-losing (primary) star can either be ejected into the binary system, can flow to the companion directly or can (not necessarily) immediately leave the system into the ISM. This is partly depending on the masses of the interacting stars together with the orbit velocities and wind outflow velocity of the mass-losing star. If the binary separation is small enough, the companion can trigger a change in the atmosphere of the mass-losing star and so form different outflow morphologies.

In 1941 Struve and Kuiper were the first to find evidence for mass loss in binary stars by observing the system β Lyrae. They originally wanted to find out, why this star showed the peculiar spectral features typical for this star. At the same time the concept of the zero-velocity surface was developed. In β Lyrae they also observed gaseous streams, later corrected to one stream from the B8II component feeding the thick disk around the companion. Also for U Cephei, SX Cassiopeiae and AU Monocerotis gaseous streams were found, in every case the stream arising from the larger, less massive star. Soon it became clear that this larger, less massive stars lose a lot of mass during their evolution. A second mass-loss period may occur, as is the case for cataclysmic binary stars, barium stars and X-ray binaries.

To interpret the period changes in β Lyrae, Kuiper (1941) and Wood (1950) suggested that the mass loss is causing period changes. Finally the mass loss was considered to be the reason for the observed gas streams, that can end as circumstellar disks around the companions or as circumbinary envelopes.

Gas streams can be identified through 4 main effects:

- A distortion in the velocity curve in the direction, where the stream is heading. Gas streams have a larger relative velocity.
- Weakening or veiling of the spectrum of the companion caused by the stream crossing its orbit.
- Emission lines at quadratures.
- Abnormalities in the light curve of eclipsing binaries caused by e.g. depressions starting about $1/4 P$ before the primary eclipse, etc..

2.4.1 Circumstellar envelopes

A circumstellar envelope was firstly discovered by Joy (1942) for the system RW Tauri. This envelopes are generally disk-shaped and their densities differ from system to system. For cataclysmic variables (CV), with one highly evolved star and a white dwarf (WD), the circumstellar envelope is always thick. For binaries with no compact component,

there are known cases for thin and thick envelopes; it may depend on the mass-loss rate in the system. One can still see stellar spectral features, when observing a thin envelope, but one can just observe emissions if the envelope is thick.

The stellar envelopes rotate in the same direction as the orbital motion, but particles in the envelopes follow a non-Keplerian motion. Emission line strength differences show that there is also a difference between the trailing and leading part of the envelope. This changes in the strength are likely broadened by turbulences. A circumstellar envelope always surrounds one of the stars in the binary system.

2.4.2 Circumbinary envelopes

The first observations of circumbinary envelopes confirmed the theory that mass-losing stars also eject matter to the binary system. The presence of diluted lines in the spectrum give a velocity range of -1300 to -170 km s⁻¹ for different binary types. Also the detection of broad H emissions (with a steep Balmer decrement) and/or emission lines corresponding to forbidden or semi-forbidden transitions lead to the presence of a circumbinary disk.

2.4.3 Mass loss through wind

Mass loss via a gaseous stream is one possibility. Stellar mass can also be ejected from the stellar surface via the stellar wind. Together with radiation pressure, the mass loss via stellar wind is important for late-type stars. The fact that wind collisions occur in binary systems, is also interesting concerning the shape of some outflow morphologies.

The theory of the mass transfer in close binaries was developed by Edouard Roche, a French mathematician, in the mid-1800s. In the following the his theory about the equipotential of a binary system will be presented regarding AGB stars.

2.5 Binary AGB stars

Close binary stars are interesting regarding their interactions. If there is additionally an AGB in the system, then the interactions become even more prominent, also for the companion. It has been assumed for long that binary stars contain stars currently ascending the Asymptotic Giant Branch, especially if one thinks about the mass loss (mass transfer in the case of a binary), which has been observed in binary systems for some time now.

The addition of an AGB star to a binary system changes not only the evolution of the companion, but of the AGB star itself. The intrinsic properties of an AGB star like the pulsation, the mass loss, the dust formation, etc., can be changed dramatically. There

are some types of stars like barium stars, CH stars or Te-poor stars, which were identified to be the successors of binary AGB stars. The most important characteristic of a binary AGB system is the presence of a mass transfer from the AGB star to the companion, which is in almost all cases a WD. Through this mass transfer the AGB star strongly influences the companion's surface. In time the companion will slowly dominate the light of the system, since the AGB star will become a WD itself.

The distinction of 2 (3) different classes of binary AGB systems is necessary: (1) the primary is the AGB star (dominating the visible spectrum) and the secondary an unevolved dwarf; (2) the secondary is a WD and the primary is at any evolutionary stage (except WD) and was influenced by the WD, when the primary still was on the AGB; (3) possible, but believed to be rare: both stars being AGB stars. It is highly unlikely, since the AGB phase is a very short phase compared to the evolutionary time scale of a star; also this case requires special physical conditions, which are not very frequent in binaries.

2.6 The Roche equipotential

2.6.1 The Roche lobe

Consider a binary system with 2 stars of masses M_1 and M_2 , which rotate around their center of mass in circular orbits. Also consider the gravitational field they generate is one of 2 point masses. It is a good assumption e.g. for cataclysmic variables (CV), since the WD component has a very small radius compared to the binary separation. Further the stars may corotate with the binary. The potential for this case can be described (with a coordinate system static in the rotating frame) with

$$\phi = -\frac{GM_1}{|r - r_1|} - \frac{GM_2}{|r - r_2|} - \frac{1}{2}(\Omega_B \wedge r)^2. \quad (2.1)$$

r_1 and r_2 are the position vectors of the 2 stellar centers, Ω_B is the angular velocity vector of the binary system and G the gravitational constant. If you consider ν to be the velocity of a fluid element relative to the rotating frame, the Euler equation (equation of motion) can be written as

$$\frac{\partial \nu}{\partial t} + (\nu \nabla) \nu = -\nabla \phi - \frac{1}{\rho} \nabla p - 2\Omega_B \wedge \nu. \quad (2.2)$$

The last term on the right-hand side is the Coriolis acceleration. Ω_B can be described with Kepler's law:

$$\Omega_B = \left[\frac{G(M_1 + M_2)}{a^3} \right]^{1/2}, \quad (2.3)$$

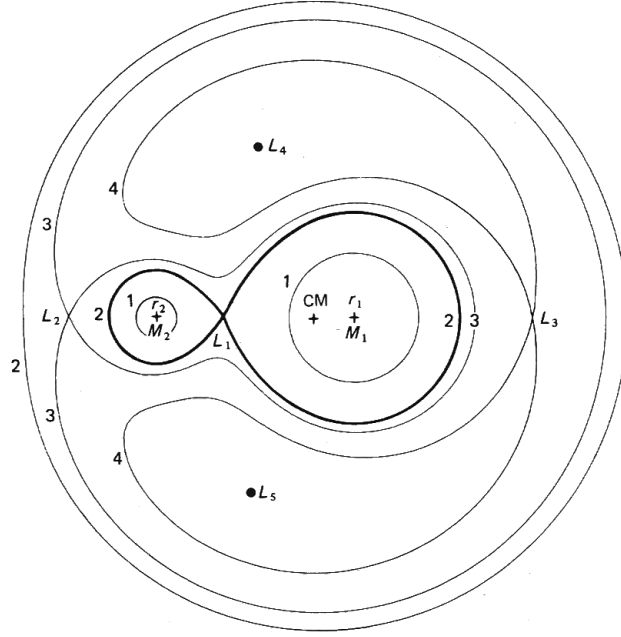


Figure 2.6: The orbital plane of Roche equipotentials (in this case for a mass ratio $q = M_2/M_1 = 0.2$). L_1 to L_5 are the respective Lagrange points. The equipotentials (1 to 4) are labelled in order of increasing Φ (Abt & Levy 1976).

since the angular velocity is correlated to the binary separation a . It becomes clear that the shape of the Roche equipotential is governed by the mass ratio $q = M_2/M_1$ if you convert the potential to the Cartesian coordinate system:

$$-\frac{GM_1}{(x^2 + y^2 + z^2)^{1/2}} - \frac{GM_2}{[(x - a)^2 + y^2 + z^2]^{1/2}} - \frac{1}{2}\Omega_B[(x - \mu a)^2 + y^2] = \text{constant}, \quad (2.4)$$

where $\mu = M_2/(M_1 + M_2)$. Figure 2.6 shows an equipotential in the orbital plane ($z = 0$). Each star has a gravitational potential with almost spherical surfaces. Farther away from the stellar centers 2 effects occur: a tidal effect of the companion, causing an elongation in the direction of it, and a flattening by the centrifugal force.

From a binary stars evolution-point of view there is one important equipotential surface, the so-called critical surface seen as a “figure-of-eight” cross section (as can be seen in Figure 2.6). This important surface passes through Lagrange point L_1 . The 2 volumes enclosed by this surface are the respective Roche lobes of the objects. Figure 2.6 represents the case of a *detached* system, where the stars are within their Roche lobes. A *semi-detached* system has one star filling its Roche lobe and a *contact binary* is a system, where both components fill their Roche lobes.

The size of the Roche lobe can be calculated if you assume a sphere having the volume of the lobe, with

$$\frac{R_{RL}}{a} = \frac{0.49q^{2/3}}{0.6q^{2/3} + \ln(1 + q^{1/3})}, \quad (2.5)$$

where R_{RL} is the Roche lobe radius.

2.6.2 Limitations of the Roche lobe concept

The Roche lobe concept is a good description for mass-losing stars in a binary system by describing 2 stars as point masses, which seems perfect for the central body of an AGB star. The forces in this concept acting upon a mass corotating in the binary system are the centrifugal pseudo-force and the gravitational forces of the 2 objects. A problem arises, when one adds radiation pressure and the momentum of the outflowing matter imparted by shock waves, making the outflowing wind stronger. If you include mass-losing AGB stars in a binary system, you have to consider this physical parameters and that is not the case in the Roche model. An outflowing wind being much stronger than the actual gravity of an AGB star renders the Roche model redundant. The radiation pressure dP_r/dr on the wind and the gravitational force decrease with the distance to the AGB star r_2 , as r_2^{-2} . A wind particle experiences a reduction of the effective gravity of the AGB star by a factor of $(1 - f)$, f being the ratio of the radiation pressure force per unit mass to the gravitational attraction (per unit mass) of the AGB star at any given point:

$$f \equiv \frac{1}{4\pi cGM_2} \int_0^\infty \kappa_\nu L_{\nu,2} d\nu. \quad (2.6)$$

With the radiation pressure

$$\frac{dP_r}{dr} = -\frac{1}{c} \int_0^\infty \kappa_\nu \rho \frac{L_{\nu,2}}{4\pi r_2^2} d\nu, \quad (2.7)$$

where κ_ν is the absorption coefficient per unit mass at a frequency ν , c is the speed of light and $L_{\nu,2}$ the luminosity of the AGB star in the frequency range $(\nu, \nu+d\nu)$; the formula for the equipotential surfaces can be rewritten into

$$\phi = -\frac{\tilde{\mu}}{r_1} - \frac{(1 - \tilde{\mu})(1 - f)}{r_2} - \frac{x^2 + y^2}{2} = \text{constant}, \quad (2.8)$$

now assuming a radiation pressure working on the outflowing wind of the AGB star, $\tilde{\mu} = M_1/(M_1+M_2)$. Figure 2.7 shows the modified Roche equipotentials with the extra force driving the outflowing mass. If f becomes larger than the critical value f_c , no critical Roche equipotential is surrounding the binary anymore. In the case of $f = f_c(\tilde{\mu})$ the critical Roche equipotential forms into a surface, which not just includes L_1 , but also

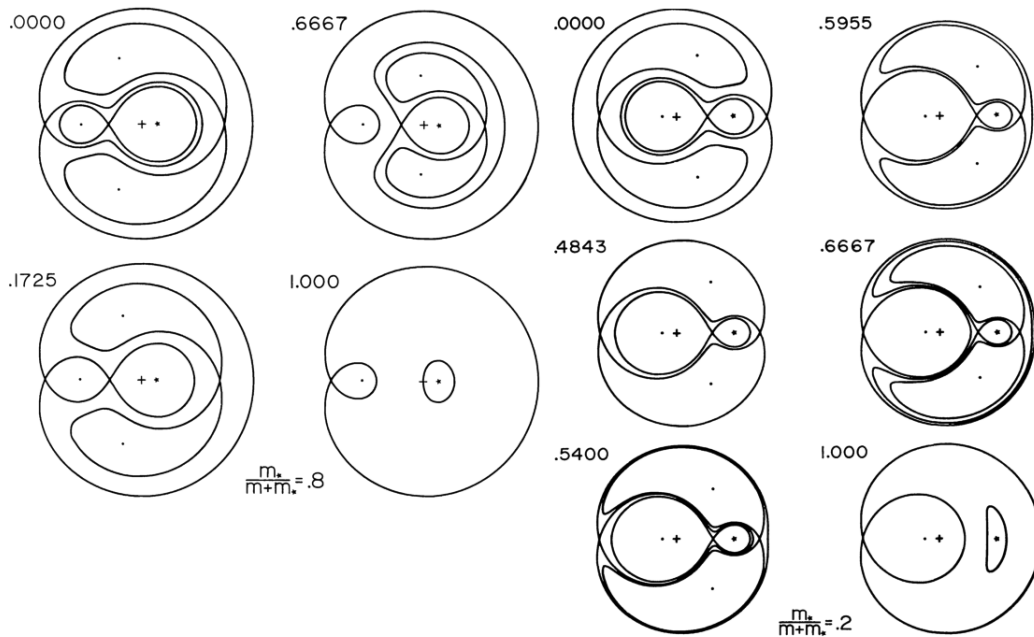


Figure 2.7: The modified Roche equipotentials with an extra force driving the mass outflow from the AGB star (filled square symbol).

Left four equipotentials 1 - $\tilde{\mu} = 0.8$, $f_c = 0.1725$.

Right six equipotentials 1 - $\tilde{\mu} = 0.2$, $f_c = 0.5955$ (Schuerman 1972).

L_2 , the outer Lagrange point opposite to the AGB star. This means that matter can flow through the outer Lagrange point too and so can escape the equipotential region and may form a circumbinary disk. Those disks are frequently observed around post-AGB stars. It has to be emphasized that this change in the Roche lobe behaviour just takes effect if the wind remains optically thin; if not, the induced force will disappear, because of the shielding from the irradiating star.

Cataclysmic variables

A direct and extreme example of a short-period binary containing a Roche lobe-filling low-mass star is a cataclysmic variable (CV, figure 2.8). A CV is a star showing strong irregular variations in brightness. CVs have an accreting WD as primary and a low-mass companion. This 2 objects are members of a very close binary system, so that the WD gravitationally influences the secondary. Because the companion is the mass transferring object, it is called the donor star, being slightly out of thermal equilibrium (Mobberley 2009). For most CVs an accretion disk is observable via the detection of strong UV or X-ray emission. The accretion of the WD can lead to it reaching the Chandrasekhar limit and explode as a Type Ia supernova.

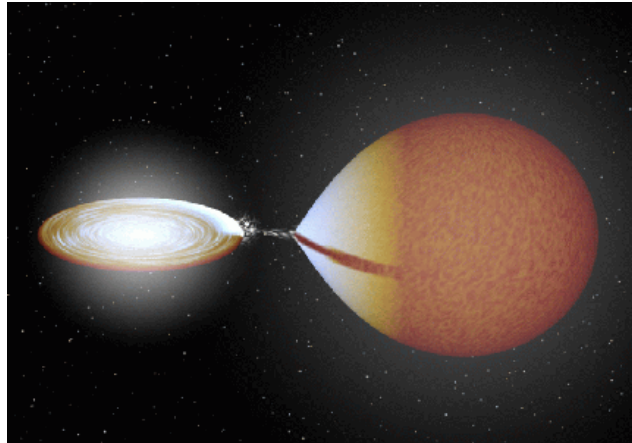


Figure 2.8: Physical structure of CVs. On the left is an accreting disk surrounding a WD, on the right is a roughly MS Roche lobe-filling companion. *Courtesy of Rob Hynes*

The mass transfer process seems to be stable on long time scales, requiring a mass ratio $q < 1$ and an angular momentum loss (AML) shrinking the system and keeping the Roche lobe in touch with the companion. The orbital period decreases with the CV evolution. The period distribution is therefore a good indicator of the current evolutionary state of those systems. This distribution is defined by 2 important features: (1) the “period gap” between $P = 2 - 3$ hr, (2) a sharp cut-off around a minimum period of $P = 80$ min (Knigge 2011). Mass transfer above this gap is driven by AML together with a weak, magnetized stellar wind from the secondary, called “magnetic braking”. Mass transfer below the gap is caused by gravitational radiation. At the period minimum a stellar object transforms into a sub-stellar object like a brown dwarf, that in the end of the process has undergone the mass-loss and experienced an increase in radius, and possibly a change in the direction of orbital period evolution. The resulting systems are called “period bouncers”.

2.7 Detecting binaries with AGB stars

AGB stars in general have a strong mass loss and exhibit nucleosynthesis processes. When it comes to binary systems, the mass loss, especially the outflow morphology gains more importance. The mass loss gets more complex, e.g. symbiotic activity is developing, associated X-ray emissions show up or maser emissions can be detected, which can be suppressed by perturbations induced by a companion. The companion also plays an important role in the detection of the AGB star in the system, since via a mass transfer, the companion (or the atmosphere of the companion), mostly a WD, gets enriched by elements like C, F and other elements heavier than iron produced in

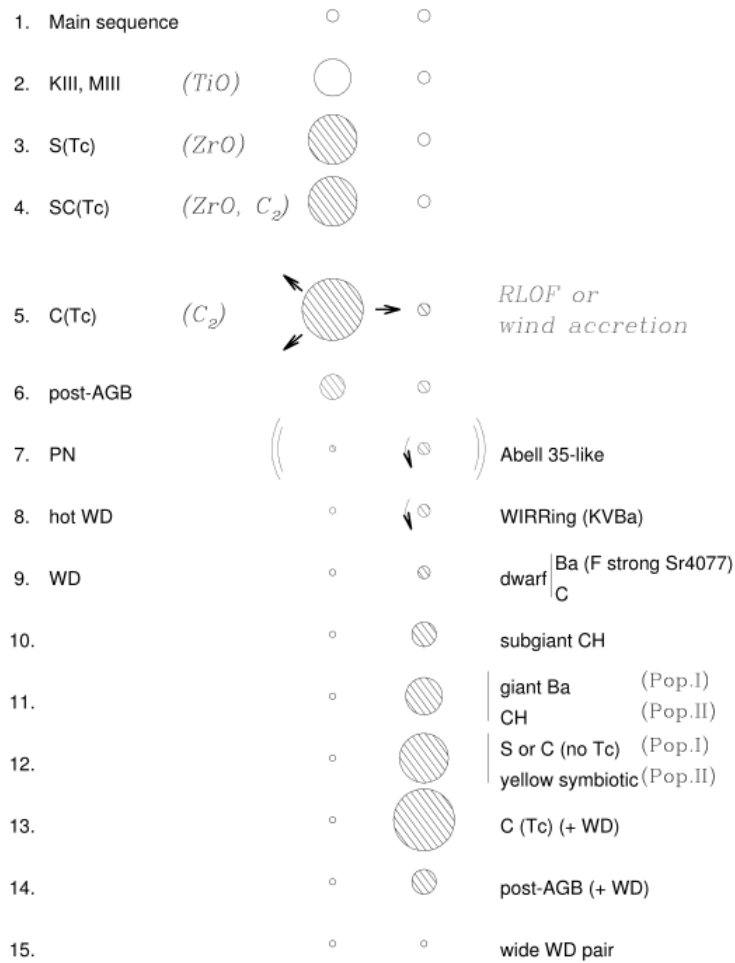


Figure 2.9: Binary evolution of low- to intermediate-mass stars. The left column corresponds to the normal evolutionary sequence of a single star, the right column represents the evolution induced by the mass transfer (H. J. Habing 2003).

the atmosphere of the AGB star through the s-process of nucleosynthesis.

Figure 2.9 shows the classification scheme (in this case the temporal sequence) of low- and intermediate-mass binary systems. This scheme requires one star in the binary system to evolve/to be evolved to an AGB star. Both stars being AGB stars is possible, but highly unlikely. There are 9 methods to detect an AGB star in a binary system:

- Radial-velocity variations
- A visual companion
- Composite nature of the spectrum and/or symbiotic activity
- X-ray emissions

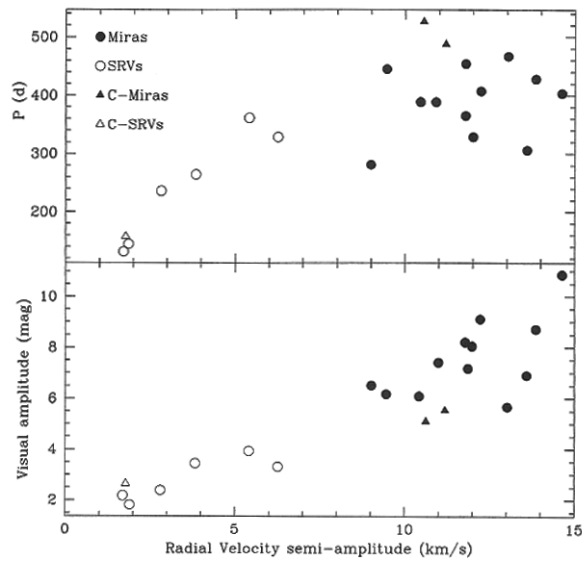


Figure 2.10: **Top panel)** Correlation between the radial-velocity semi-amplitude and the period of the visual light curve for stars from various classes of LPVs. **Bottom panel)** Same as top panel for visual amplitude (Hinkle et al. 1997).

- Shallow light curves from Mira variables
- Light variations associated with orbital motion
- Lunar occultations
- Imaging of CSE asymmetries
- Interferometric detection

In the following the different methods are briefly described.

2.7.1 Radial-velocity variations

Figure 2.10 shows the semi-amplitude of radial-velocity variations associated with the pulsation of Mira and semiregular variables. One can see a good correlation between the radial-velocity amplitude and the visual amplitude. Miras show little correlation between the period and the radial-velocity semi-amplitude (ranging from 10 to 15 km s⁻¹). On the other hand semiregular variables have a radial-velocity semi-amplitude increasing with period (ranging from few km s⁻¹ to values for Miras).

Comparing Figure 2.10 with Figure 2.11, Mira variables are located in the forbidden (RLOF, Roche-lobe overflow) region of the period-semi-amplitude diagram of binary

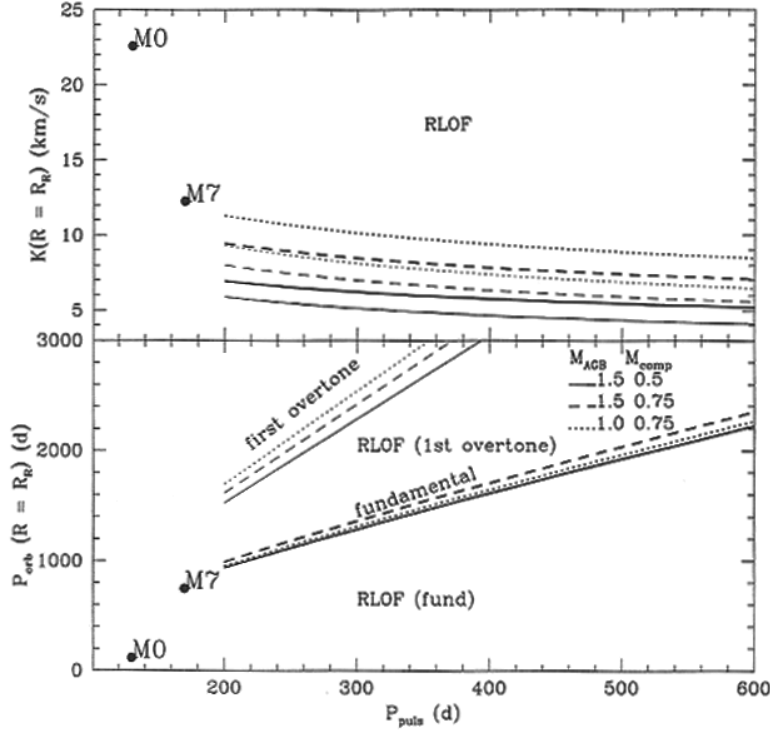


Figure 2.11: **Top panel)** Orbital radial-velocity semiamplitude versus pulsation periods for Miras in circular semidetached systems with $\sin i = 1$. Thick line: fundamental line, thin line: first overtone.

Bottom panel) Orbital periods versus pulsation periods for Miras in semidetached systems. The filled circles (M0 and M7) are critical periods to median radii of non-Mira M0 and M7 giants (H. J. Habing 2003).

systems. There is no overlap between the orbital and intrinsic radial-velocity variations of Miras. Still, orbital variations are difficult to detect, because for the masses of Miras in detached binary systems used in Figure 9.4 in H. J. Habing (2003), these variations are smaller than the semi-amplitudes of the intrinsic radial-velocity variations.

Detecting a binary system with a Mira variable with this method is difficult, since the time scales involved are long (years) and the orbital radial-velocity variations are smaller than the intrinsic variations. This method requires a lot of observation time to classify a binary system.

There are not many surveys, which used this method and just a few binary systems are believed to be found with it.

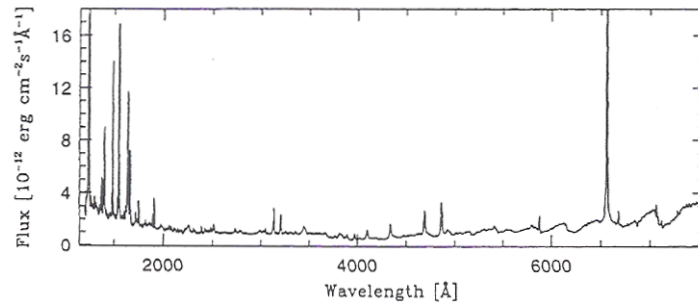


Figure 2.12: Optical/ultraviolet spectrum of the symbiotic star AG Peg showing a hot UV continuum, the emission lines, the Balmer continuum in emission, the cool-star continuum and its absorption bands (Mikołajewska 1997).

2.7.2 A visual companion

The Third Catalogue of Interferometric Measurements of Binary Stars was scanned for Mira variables and C stars. Only one visual binary, X Oph, could be found, the other 38 objects are questionable or non-detections. Some C stars are listed as binaries in the Hipparcos Catalogue, but speckle observations did not confirm the binarity. Also with this method the detection of binary systems seems to be rare. To get a visual confirmation is very difficult, because the mass loss and mass transfer, causing a stellar wind, hamper the possibility of detection. The wind morphology caused by space motion and the binary system itself additionally makes it harder. The stars need to have a large enough separation to be detected visually.

2.7.3 Composite nature of the spectrum and/or symbiotic activity

This method is more successful than the previous ones. Rare discoveries of non-symbiotic AGB stars may be understandable if one considers the symbiotic activity caused by the interaction of a strong wind with a companion. Most, if not all, of the binary systems with an AGB star might be symbiotic stars. For example, the Eighth Catalogue of the Orbital Elements of Spectroscopic Binary Stars shows 14 out of 20 systems with M giant or supergiant primaries to be symbiotic systems. Another binary system, Mira Ceti, shows some symbiotic activity despite its large orbital separation.

Symbiotic stars show peculiar spectra merging low-excitation absorption features, including TiO bands or neutral metal lines, with high-excitation emission lines like H II $\lambda 4686$ (Figure 2.12).

Symbiotic stars are binary systems involving a cool giant and a hot companion (generally a WD, but also main-sequence stars), as is proven by observed nebular features like forbidden lines, which occur frequently and require low densities; and far-UV spectroscopy shows a blackbody continuum, which is characterized by temperatures of max. 10^5 K with luminosities of 10 - 1000 L_{\odot} . The companion, heated by the wind accretion

from the primary star, emits the continuum.

Symbiotic activity is induced through eruptions by thermonuclear flashes at the WD's surface at a slow rate ($< 10^{-9} M_{\odot} \text{ yr}^{-1}$), by instabilities in the accretion disk (if the secondary is a main-sequence star accreting mass from a Roche lobe-filling primary), by dust obscuration episodes like in symbiotic Miras (e.g. R Aqr) and reflection effects (heating of the cool giant's atmosphere in direction of the hot companion).

Symbiotic stars can further be classified into subgroups:

- Yellow symbiotics: G or K giants
- Red symbiotics: M giants
- d-type symbiotics (“dusty”): IR excess indicating circumstellar dust, generally hosting a Mira variable
- d' -type symbiotics: dusty yellow symbiotics
- s-type symbiotics (“stellar”): infrared colors consistent with their photospheric temperatures

All samples of symbiotic stars show the majority to be long-period Miras. The reason for that is unclear.

2.7.4 X-ray emission

In general, 2 processes may cause X-ray emissions to appear: The shocks resulting from the collisions of streams coming from the wind accretion in a detached binary system inhabiting an AGB star and when gravitational energy from the AGB wind is falling in the potential well of the companion star and is converted into radiative energy, when reaching the companion's surface. The so-called accretion luminosity

$$L = GM_{acc} \frac{M_2}{R_2}, \quad (2.9)$$

were G is the gravitational constant, M_{acc} is the accretion rate and M_2 and R_2 the mass and radius of the companion, will be converted into hard X-rays if the matter is optically thin, or into thermal energy and radiated in form of blackbody radiation if the matter is optically thick.

The search for X-ray emitters and symbiotic activity is equally effective, since symbiotic stars show strong X-ray emissions.

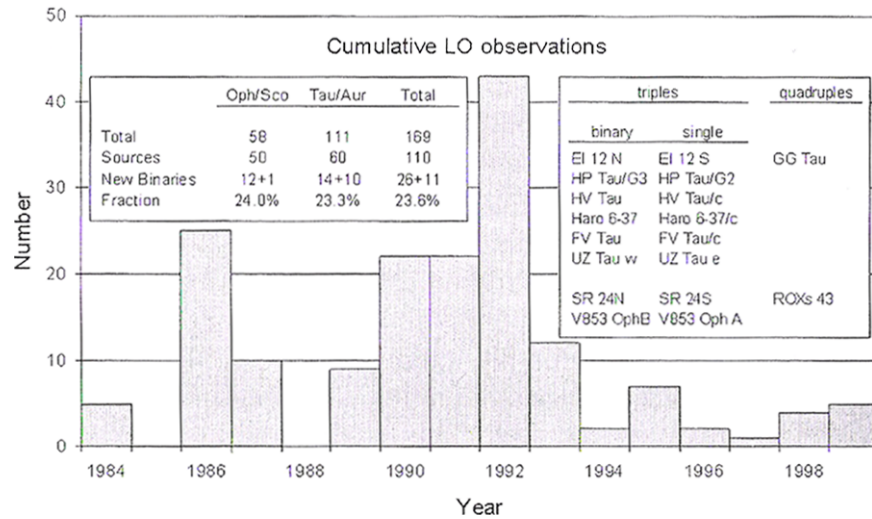


Figure 2.13: Statistics of the LO observations of young stars, and of the binary and multiple systems discovered by this method (Richichi 2001).

2.7.5 Shallow light curves from Mira variables

Light curves of long-period variables, including AGB stars, may have shallow or wide, flat minima indicating a companion, which dominates the light at minimum. Those results should be treated with caution, since this indications were not made by spectroscopic inspection, which show composite spectra for some objects. Just a few S and M stars were found to have composite spectra.

2.7.6 Lunar occultations

During a lunar occultation (LO), the limb of the Moon acts as a diffracting edge. Moving over the occulted source, a characteristic light curve is produced. LO must be recorded with high temporal resolution usually with sampling rates between 100 and 1000 Hz. To detect binaries via LO, several parameters need to be fulfilled (Richichi 2001). Important are the separation, the brightness ratio and the signal-to-noise ratio (SNR) used to record the light curve. Richichi et al. (1996) mentioned the broad rule that the LO method is sensitive enough to resolve binary separations above 5 mas, but not more than 20 mas. Brightness ratios can range from 1 to 4 mag. Figure 2.13 shows the detected binaries until 2000. This statistics will not change significantly, because in the near future the orbit of the Moon will not cross a star-forming region and large interferometric facilities such as the VLTI and Keck are having equal or even surpassing sensitivity and resolution to outpace the LO method.

2.7.7 Imaging of CSE asymmetries

Through mass loss of the AGB star, its circumstellar envelope (CSE) can grow. It is known that CSEs are not perfectly homogeneously spherical, but an even stronger asymmetry can be expected in binary systems, plus specific flow patterns indicate the presence of a companion. Through the detection of asymmetries with direct imaging a binary system can be identified .

Circumbinary disks can be detected through very narrow CO radio line emissions.

2.7.8 Interferometric detection

Interferometers like the Keck Interferometer or ESO VLTI instruments MIDI (Mid-Infrared Interferometric instrument, a mid-infrared (8-13 μm) 2-way beam combiner giving one visibility (and photometric) spectrum per observation, spectral resolution $R = 30$ (prism) and $R = 230$ (grism)) and AMBER (Astronomical Multiple BEam RE-combiner, a near-infrared (NIR, 1 - 2.5 μm) 3-way beam combiner giving 3 visibility spectra (in J, H and K) and 1 closure phase spectrum per observation, spectral resolution $R = 30$ (low), $R = 1500$ (medium) and $R = 12000$ (high) can and will be used to allow more sensitivity for high spatial resolution imaging, to gain photometry measurements at different pulsation phases and to get visibility spectra. The new generation of instruments for VLTI includes PRIMA (Phase Referenced Imaging and Microarc-second Astrometry), PIONIER (Precision Integrated-Optics Near-infrared Imaging Experiment), Gravity (NIR instrument for astrometry and interferometric imaging of faint objects) and MATISSE (Multi-AperTure mid-Infrared SpectroScopic Experiment). Due to improvements in measuring radial velocities and higher spatial resolution in imaging, more spectroscopic binaries with visual orbits were found. Interferometry can help to increase the resolution again (resolving orbital parameters in more detail) and may be able to produce a direct image of a binary, especially for Mira variables due to their large diameters and high luminosities. NIR interferometry can be used to gain information from near the continuum-forming photosphere of Miras such as effective temperature, center-to-limb intensity variations, the stellar photosphere diameter, and its dependence on wavelength and pulsation phase. Mid-infrared observations are used to study molecular shells and the dust formation zone of evolved stars; the appertaining interferometry can tell something about the chemical composition, the geometry, the temperature, the inner radii, the radial distribution, and the mass loss rate of dust shells (Karovicova et al. (2011) and references therein).

AGB stars are very bright in the red and IR and are perfect for optical or IR interferometry, because they also have large diameters. Using this method, one can check for discrepancies in the atmospheres (or CSE) of AGB stars being able to be caused by a companion. Interferometry provides images of highly structured CSEs, thin or thick disks.

Recent examples for interferometric studies of (binary) AGB stars can be found in Deroo

et al. (2006); Deroo & Van Winckel (2007); Deroo et al. (2007); Karovicova et al. (2011).

2.8 AGB mass loss in a binary system

The wind outflow of AGB stars shows a different pattern if a companion star is involved. In detached systems the geometry of the outflow or rather the mass flow is bounded to the wind velocity ν_∞ , which is typically of the order of 15 km s⁻¹, being more or less of the same order of magnitude as the relative orbital velocity ν_{orb} . Additionally Coriolis effects make the flow pattern even more complex. Normally the flow is believed to be plane-parallel at infinity and does not show traverse density or velocity gradients as e.g. is the case for X-ray binaries with fast winds from the hot star with $\nu_\infty \gg \nu_{orb}$.

The compact star’s gravitational field bends the mass flow and causes the streams coming from the AGB star and passing on each side of the companion to collide with each other resulting in a so-called accretion column at the rear side of the compact star. From this rear side the matter falls into the compact star with the rate $\dot{M}_{acc,B-H}$, where B-H stands for “Bondi-Hoyle”:

$$\dot{M}_{acc,B-H} = -\alpha\mu^2 \frac{k^4}{[1 + k^2 + (c_s/\nu_\infty)^2]^{3/2}} \dot{M}_{AGB}, \quad (2.10)$$

where α is a parameter of order unity, c_s the sound speed and \dot{M}_{AGB} the AGB mass-loss rate. The Bondi-Hoyle accretion happens, when a mass flow to a compact object occurs and finally the matter enters the accretion radius. No accretion disk is expected for the Bondi-Hoyle accretion, because the flows from the AGB star to the compact object are expected to be symmetric and there is no accretion of spin momentum to form a disk.

For detached systems with an AGB star and $\nu_\infty \gg \nu_{orb}$, it gets more complex than in the Bondi-Hoyle regime. It can be investigated numerically.

Figure 2.14 shows a 3D hydrodynamical simulation of a detached binary system with a mass-losing AGB star. A lot of parameters need to be considered including orbital separation, the 2 masses, the AGB star mass-loss rate, the AGB star corotating with the orbit or not, wind/orbital velocity ratios, the presence of a strong wind blowing off the companion’s atmosphere and a lot more. A lot of parameters are difficult to calculate and therefor remain unexplored for the time being. 4 general flow features can be seen in Figure 2.14:

2.8.1 Funneling through L_1

The funneling through L_1 occurs because of the geometry of the Roche potentials. The gas is getting heated because of the density enhancement around L_1 . The wind leaving the AGB star in direction of the companion is denser anyway, but it was not taken into account in the simulation of Figure 2.14. The funneling is visible in the figure as a curved

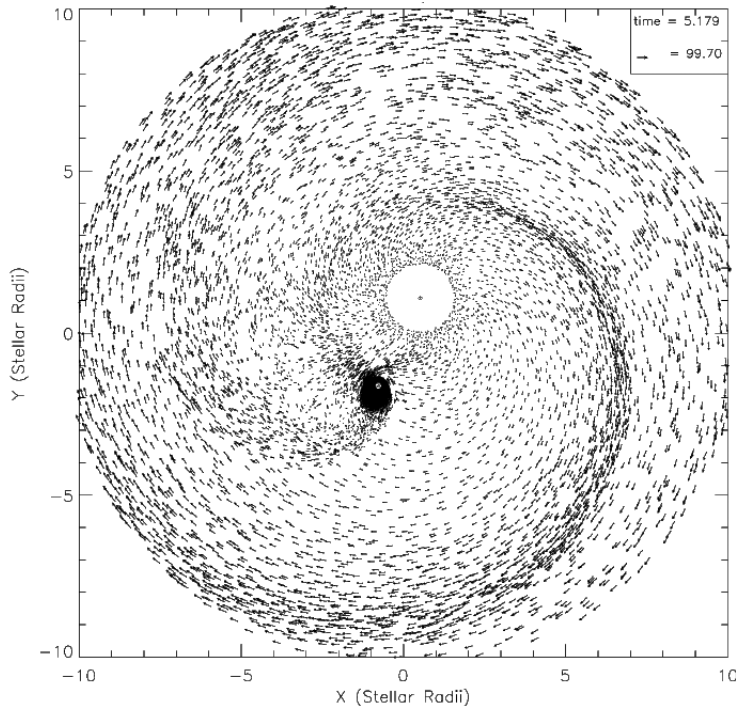


Figure 2.14: AGB binary accretion wake in the orbital plane in the corotating frame (Mastrodemos & Morris 1998).

stream between the 2 stars. A stream like this may have been detected for Mira Ceti A pointing towards Mira B as hook-like structure observed in the UV. The Coriolis force is responsible for the axisymmetry causing the appearance of an accretion disk around the secondary. In the Bondi-Hyole regime no accretion disk would form. The accretion disk is stable, thin and tilted with respect to the orbital plane. Mira and post-AGB stars additionally have polar jets and together with the companion's accretion disk a bipolar or quadrupolar structure could form, as observed in several symbiotic stars. Bipolar structures seem to be very common and the formation of the accretion disk is important in the sense, that not only RLOF is causing this structures. *o* Cet shows observational evidence for an accretion disk around the companion.

2.8.2 The spiral arm

In Figure 2.14 a double spiral arm is visible, caused by the collision of the AGB wind with the accretion wake, and curved by Coriolis force.

2.8.3 Disk

Circumbinary disks are especially formed in binary systems involving (post-) AGB stars (e.g. HD 44179, otherwise known as “Red Rectangle”). Those disks can be inferred from orbital modulations as seen in the light curves of post-AGB systems, which show as variable obscurations from trapped dust in the disks, and very narrow CO circumstellar lines ($\text{FWHM} < 5 \text{ km s}^{-1}$) observed in many post-AGB stars pointing to gas orbiting in a circumbinary disk.

It also may be that the spiral arm mimics a circumbinary disk. Such a disk can also form during RLOF, when matter is additionally ejected through L_3 .

2.8.4 Dust formation in the outflow zone

As described in the previous Subsections, there are several regions, which are denser and reach higher temperatures. The formation of dust can occur if the temperature in this regions is not higher than the condensation temperature of the specific dust species.

Dust formation may indeed happen more frequently in binary systems than in single AGB stars. Also dust formation is considered to be one reason for observed light variations in binary systems. Formed dust may be stored in the circumbinary disks in systems involving post-AGB stars or silicate J-type carbon stars.

2.9 The successors of AGB stars in binary systems

Consider a binary system with an AGB star as the primary and a WD as the companion. When an AGB star loses mass, the WD is directly affected through interaction within the binary system. Its physical (e.g. faster rotation) and chemical properties (anomalies in the atmosphere) can change dramatically.

The evolution of an AGB star in a binary system is shown in Figure 2.9, which illustrates the binary evolution of low- to intermediate-mass stars. In this figure the phases 3 to 5 and 13 show a binary with an AGB star as defined in Chapter 1 as primary. One has to note that the nature of the companion differs. To investigate the successors of AGB stars in binary systems, one has to consider the evolution after the mass transfer at phase 5. This evolution depends on how the mass transfer took place, either through RLOF or wind accretion.

The theory of mass transfer was introduced to explain the chemical anomalies of barium stars (phase 11 in Figure 2.9, for the following description always consider the phases described in this figure). Barium stars, being G and K giants, show an overabundance of s-process elements and this is not explicable only by internal nucleosynthesis. Mass transfer is thought to be the reason of barium stars showing the overabundance. The theory is that the envelopes of barium stars were polluted by the mass flow from an AGB star, which is now a WD.

Mass transfer was also introduced to explain the existence of Tc-poor S stars. In the

spectra of S stars technetium was found, which indicates some S stars to be TP-AGB stars running nucleosynthesis. The mass transfer scenario was used to explain the Tc-poor spectra of the other S stars. This resulted in the allocation of extrinsic and intrinsic S stars. Intrinsic TP-AGB S stars have Tc lines in their spectra (phase 4) and extrinsic S stars show no Tc lines, but their chemical anomalies can be explained by the mass transfer like for Barium stars (phase 12). Tc decays fast and is absent in the extrinsic S stars, since the time scale between phase 4 and 12 is longer than the Tc half-life time. The introduction of the mass transfer model gave rise to other questions: (1) Are all barium and Tc-poor S stars members in binary systems? (2) What kinds of extrinsic stars exist further (phases 7 to 12, right column)? (3) Is the companion of an extrinsic star always a WD? (4) Can rapidly rotating stars be formed also from accretion of spin angular momentum (phases 7 and 8)? (5) What is the evolutionary link between dwarf Ba and C stars, giant barium stars and Tc-poor S stars?

2.9.1 Technetium and intrinsic/extrinsic S stars

Technetium, with the elemental abbreviation Tc and atomic number 43, is one of 2 chemical elements with no stable isotope. It has two isotopes: ^{98}Tc with a half-life of 4.2×10^6 yr and ^{99}Tc with a laboratory half-life of 2.1×10^5 yr, being the only one produced in the s-process of nucleosynthesis. The presence of Tc in the spectra of stars may be the only reliable signature of the AGB nature, as it is for e.g. R And. Surveys have shown that most Tc-rich stars are LPVs and there is a significant fraction of Tc-poor S stars and Tc-rich M stars (like Mira). Calculations show that sometimes Tc is detectable in the atmospheres of M stars, before they turn into S stars, so Tc-rich M stars are theoretically possible to exist.

Besides the already known difference between intrinsic and extrinsic S stars there is more to know. They also differ in average luminosity, effective temperature, infrared colors and even Galactic scale heights. These differences lead to 2 totally different evolutionary tracks. In general one can say that intrinsic S stars are low- to intermediate-mass stars on the TP-AGB and extrinsic S stars are mostly low-mass stars on the RGB or E-AGB.

In the case of C stars, it is also assumed that there are intrinsic and extrinsic C stars, but no clear evidence has been found yet. 3 Tc-poor C stars are known (Little et al. 1987).

2.9.2 Successors

The phases 5 to 14 in Figure 2.9 show successors of AGB stars in binary systems.

Silicate J-type carbon stars (phase 5)

J stars are a subclass of carbon stars having a C-rich photosphere and an O-rich CSE. Very narrow CO(2–1) lines give a hint to the presence of a circumbinary disk in this systems. J stars may evolve out of some kind of binary induced mixing, since they lack Tc and other s-process elements being able to cause overabundances, but they have C and Li overabundances, with a low $^{12}\text{C}/^{13}\text{C}$ ratio. R-type carbon stars may be the predecessors of luminous J stars, because they show some similar abundances, but R stars were not yet discovered in binaries.

Binary nuclei of PNe (phase 7)

Planetary nebulae can contain a binary nuclei. There are especially four objects (LW Hya, LoTr1, LoTr5, WeBo 1), which show in their optical spectra to have late-type stars, but in their UV spectra to also have WDs, per definition extremely hot ($> 10^5$ K, young companions). In all the cases the late-type star is rapidly rotating and showing chromospheric activity. The fast rotation could be caused by the binary interaction, during a CE phase or by accreting some spin angular momentum, as mentioned before. Additionally WeBo 1's late-type star seems to be a barium star.

WIRRing systems (phase 8)

WIRR stands for wind-induced rapidly rotating stars describing rapidly rotating, magnetically active K dwarfs with a WD companion. This class of stars was firstly discovered by surveys of the ROSAT Wide Field Camera and the Extreme Ultraviolet Explorer (EUVE). There are no short-term radio velocity variations visible in the spectra of those K dwarfs, which leads to the systems having periods of at least a few months. Also the proper motions and the lack of photospheric Li indicate that the K dwarf is in fact an old object. The dwarf must have gotten some spin from the wind of the former AGB star, which is now a WD (this can happen in detached binary systems). Mass flow in this WIRRing systems has been confirmed by the detection of an overabundance of barium. Barium stars together with RS CVn systems have the same properties like WIRRing systems.

Dwarf Ba/C stars, subgiant CH stars (phase 9 and 10)

Most extrinsic stars form as dwarfs, because stellar lifetimes are simply longer on the main sequence (MS) than on the AGB and the cross-section for wind accretion does not depend on the stellar radius.

The Sloan Digital Sky Survey (SDSS, Margon et al. (2002)) and the Two Micron All Sky Survey (2MASS Lowrance et al. (2003)) found some dwarf C stars. Some dC stars have halo kinematics. In some systems barium overabundances were found.

The Michigan spectral survey revealed dwarf Ba stars (some of them with $C/O > 1$) among “FV strong Sr 4077” stars. Near or above the MS CH subgiants and blue metal-poor stars can be found.

This are stars , whose chemical peculiarities are still a mystery, in post-mass-transfer binaries.

Giant Ba stars (phase 11)

As mentioned before, the theory of mass transfer was introduced to explain the overabundance of Ba at the surface of giant barium stars. This stars only make 1 % of giant G-K stars.

Tc-poor S and C and yellow symbiotics (phase 12)

Tc-poor S stars have been described already in the introduction to this subsection. An interesting question is the coherence of Tc-poor S stars and symbiotic stars, both having a mass-losing giant and a WD companion in their binary systems. Additionally the systems have similar orbital periods. 2 questions arise: (1) Do symbiotic systems show s-process elements overabundances? (2) Can there be symbiotic activity in Tc-poor S stars?

The answer to question 1 is rather simple. Red symbiotics do not show overabundances, but yellow s-type symbiotics do. It is a mystery, why there are no red symbiotics known to have S stars. A possible explanation is the fact that red symbiotics are more metal-rich than binary S stars. And in fact Ba and C stars are not found very frequently in high-metallicity environments. On the other hand in the Magellanic cloud carbon symbiotics are very frequent in the low-metallicity environment. To answer this question, one has to do more research on the kinematics and metallicities of Tc-poor S stars and red symbiotics.

As for question 2: some Tc-poor S stars show some weak symbiotic activity.

Binary post-AGB stars (phase 6 and 14)

Binary post-AGB star atmospheres do not show evidence for (previous) s-processes of the third dredge-up. This may be, because the star left the AGB earlier, leaving the s-process no chance to be ignited, or because of chemical fractioning. Such fractioning is not observed in barium stars. It can be because the star left the AGB earlier, so that barium stars can not be classified as successors of post-AGB stars in binary systems.

Carbon-enhanced metal-poor stars

The occurrence of carbon-enhanced metal-poor (CEMP) stars could be explained by mass accretion from an AGB binary companion, supported by the fact that CEMP stars are mostly found in spectroscopic binary systems. 4 different categories of CEMP stars can be distinguished depending on the presence of elements heavier than iron, s-process elements (e.g. barium) and r-process elements (e.g. europium). Most CEMP stars are s-process rich stars (Abate et al. 2011). Mohamed & Podsiadlowski (2007) showed in their hydrodynamical simulations taking the AGB wind acceleration mechanism into account that an intermediate model between wind accretion and Roche-lobe overflow (RLOF) is very efficient, in the case of a slow wind, in accreting material. The maximum efficiency of this wind Roche-lobe overflow (WRLOF) was estimated to be approximately 50 %, meaning that up to half of the material from the AGB star could be transferred to the accreting star.

Binary AGB stars have a wide variety of features. A lot is already known about the AGB and binary systems, yet some physical and chemical processes still need to be determined for both fields. The identification of binary systems is still problematic in some cases and can be very time-consuming (depending on the detection method), especially if an AGB star is involved. Different space- and ground-based observatories have special possibilities to observe binary AGB stars. Optical and interferometric observations can be conducted very good with ground-based observatories like the ESO VLT(I) or the Keck Observatory. IR and UV observations can (and could) be performed very good via space observatories like IUE, GALEX, AKARI, Spitzer or Herschel (and all others covering the IR and UV wavelengths). The following chapter summarizes the observations of binary AGB candidates in the Herschel MESS sample and gives an insight into the Herschel observations.

3 Binary AGB candidates in the Herschel MESS sample

The Herschel Space Observatory (Herschel) observed among others 14 AGB stars believed to be part of binary systems, some of them confirmed and the rest believed to show evidence for a companion. Because of the nature of this AGB stars one can sometimes not observe the primary and its secondary directly (e.g. in the visual), because gas and dust are obscuring the central star, caused primarily by mass loss and wind-ISM interaction scenarios. Although it is difficult to prove the binarity of AGB stars, since they have large radii, long orbital periods and low velocity semi-regular amplitudes and they (strongly) pulsate, in the IR and UV wavelength ranges we can look through the dust and gas surrounding the objects to make their morphologies visible. Also other methods using spectroscopy, CO line outflow measurements, composite spectra or theoretical assumptions predicted from physical properties of e.g. the wind outflow are applied. The following objects were investigated in the past by several techniques and sometimes led to different outcomes and interpretations concerning the binary state. It goes from U Cam, a star claimed not to be a binary by the majority of scientific papers, to VY CMa, which is one of the most luminous stars known and has a very large estimated mass loss rate. Included in the sample is also *o* Cet, better known as Mira, which was defined to be the prototype evolved star and is maybe the most studied object in the history of AGB observations, being a confirmed binary still with a lot of secrets to unveil, like the latest publications show.

Herschel's resolution made it possible to reveal complex structures in the circumstellar environment of binary AGB stars, which show an outflow morphology (e.g. jets (bipolar outflow), spiral structure) indicating a companion.

In the following sections the stellar properties are shown and the binarity of the objects is discussed in more detail, including the results from Herschel.

The table at the end of this chapter summarizes all the important parameters.

3.1 U Cam

The semiregular variable (SRb) U Camelopardalis is a N-type carbon star. U Cam's luminosity is $7000 L_{\odot}$ with a temperature of 2700 K (Schöier et al. 2005). The General Catalogue of Variable Stars (GCVS) gives an amplitude of 1.8 mag (11 to 12.8 mag) with a pulsational period of 400 d. The star is designated to have a spectrum of type C3,9-C6,4e(N5) (Kholopov 1987). U Cam has an estimated distance of 430 pc (Knapp et al. 2003). Its space velocity with respect to the solar motion was calculated to be 9.8 km s^{-1} . The estimated present mass loss rate is $10^{-6} M_{\odot} \text{ yr}^{-1}$ (Cox et al. 2012). This value is relatively high compared to other AGB stars. An explanation for this value might be the most recent thermal pulse in U Cam. On the other hand it can be totally wrong due to uncertainties on the distance.

Past results

Radio observations showed an unusual morphology of the circumstellar envelope, indicating a short variable mass loss on a time scale of 10^3 yr (Bujarrabal & Cernicharo 1994; Lindqvist et al. 1996; Neri et al. 1998). The terminal velocity of the CO envelope amounts to 20.6 km s^{-1} (Lindqvist et al. 1999). The gas in the CSE has a lot in common with the 4 carbon stars R Scl, U Ant, S Sct and TT Cyg (Olofsson et al. 1996). Their shells have been interpreted as a result of H_2 mass loss rates on short time scales possibly due to the helium-shell flash, a matter which is still unresolved.

Proust et al. (1981) claims U Cam to be a visual binary. Furthermore the Hipparcos Double Star Solution also could give evidence for the presence of a companion or U Cam even to be a triple system (Alain Jorissen; private communication with Cox et al. (2012)). Among others Proust et al. (1981) and Jorissen assume that U Cam might be a binary system. There are, however, also arguments against the binary solution. In Barnbaum (1992b) they had a sample of 34 stars, from which 12 show an offset greater than 5 km s^{-1} between CO and optical velocities. CO radial velocities are good indicators of the center-of-mass motion, better than optical velocities. A discrepancy between the velocities could be due to atmospheric motion or due to motion in a binary system. For U Cam a clear difference of up to $\sim 3 \text{ km s}^{-1}$ is seen. They also showed that stars with offsets between optical and CO velocities greater than 5 km s^{-1} protrude from the sample by having a larger spread in multiple optical velocity measurements than do stars with a smaller offset. These 12 stars also differ in another way: (1) their IRAS and $2 \mu\text{m}$ colors; (2) variability class; (3) amplitude of optical velocity variation over several epochs; (4) The strength of the H α emission; (5) M_{kean} outflow velocity in CO. These stars have a larger $12/2 \mu\text{m}$ ratio ($2 \mu\text{m}$ flux is mostly photospheric in AGB stars, $12 \mu\text{m}$ flux is mostly due to emission from hot dust close to the object). Also stars with large offsets between optical and CO velocities tend to be more dust-obscured. In the sample the spread of the optical velocities is in general larger than the dispersion of CO velocities. The larger velocity offsets show strong H α emission (with no exception). This

emission must be very weak for U Cam. The offset between optical and CO velocities for U Cam is small, yet the star has higher mass loss rates and larger $12/2 \mu\text{m}$ colors than other stars in this group. The dispersion in optical velocities might be connected to atmospheric pulsation or to motion in a binary system, but the spread of CO velocities for the stars cannot be explained by either of these effects. More observations were requested to investigate the change of velocity with the light phase. Olson & Richer (1975) stated that U Cam is not a real binary system, because the velocity difference between the star and the companion is too large. Multi-epoch velocity measurements, photometric and polarimetric observations of binary systems and Speckle interferometry of Hipparcos binaries including U Cam are additionally discussed in Barnbaum (1992a); Docobo et al. (1997, 1998); Mason et al. (2001). The binarity of U Cam is still a matter of discussion, though theories about the star being a non-binary system prevail.

Herschel view

For U Cam a very young CO shell was found and is assumed to have an age of only ~ 800 yr. The interacting (fast-slow) wind scenario is part of the picture, since a star can have multiple mass ejections during its lifetime on the AGB leading to the estimated mass loss range losing significance. The latest far-IR observations with Herschel show U Cam to have a wind-ISM interaction of the type “*eye*” (Cox et al. (2012), Figure 3.1). Deconvolved Herschel images of U Cam show both a wind-ISM interaction and a detached ring. U Cam and several other objects show a small detached ring besides the bow shock region further away from the star. The predicted and observed stand-off distances, respectively, of the bow shock with respect to the star are 0.66 and 0.12 pc.

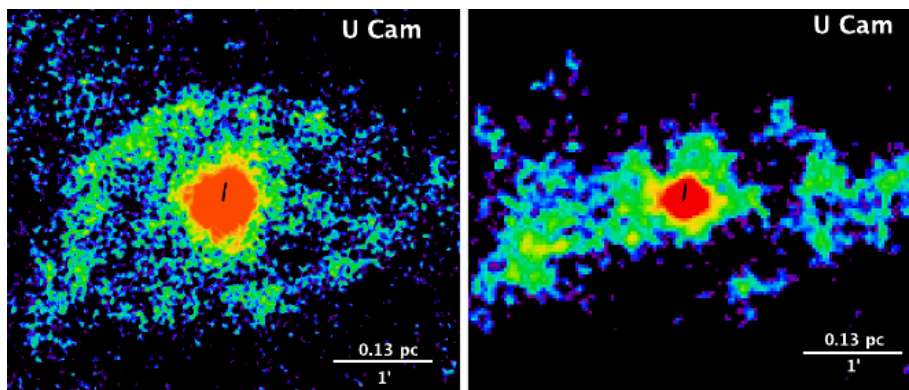


Figure 3.1: U Cam: **left**) PACS $70 \mu\text{m}$ **right**) PACS $160 \mu\text{m}$. The inner shell is not visible (Cox et al. 2012).

3.2 VY CMa

VY Canis Majoris is a very luminous cool O-rich hypergiant associated with the young cluster NGC 2362, the H II region Sharpless 310, and the dark cloud L1667 (Monnier et al. 2004). This giant is believed to have a radius of about $1.8\text{-}2.1 \times 10^3 R_{\odot}$ and a mass of $30\text{-}40 M_{\odot}$. It has an approximate luminosity of $4\text{-}5 \times 10^5 L_{\odot}$ and so is one of the most luminous stars known in our Galaxy with a temperature of 3000 K. It is a semiregular variable with an amplitude of 3.1 mag (6.5 to 9.6 mag, GCVS) and a period of ~ 2200 d (Jura & Kleinmann 1990a). Its spectral type is M4III. The latest values (Cox et al. 2012) are a distance of 562 pc and a space velocity of 42 km s^{-1} (De Beck et al. 2010). The mass-loss rate is estimated to be $2.8 \times 10^{-4} M_{\odot} \text{ yr}^{-1}$ (De Beck et al. 2010). Kastner & Weintraub (1998) concluded that the mass loss is highly anisotropic.

Past results

The star's envelope is asymmetric. Observational data shows that VY CMa consists of an unresolved and a resolved extended component. The structure of the non-spherical envelope can also be interpreted as a bipolar outflow. Visible and near-IR emissions are also very asymmetric (Monnier et al. 2004). The unresolved component, believed to be optically thick, was ruled out to contain a close binary. The axial geometry of the circumstellar environment can also be caused by the star's rotation. The presence of an extended reflection nebula around VY CMa lead to the conclusion that its envelope is flattened or the star is surrounded by a massive circumstellar disk.

Muller et al. (2007) found 2 kinematic components in the envelope: a slowly expanding shell and a high-velocity bipolar outflow. The optical and infrared morphology of the nebula around the star is found to be very complex with arcs and filaments, and bright knots in an unusual arrangement. The kinematics of the $^{12}\text{C}(2-1)$ emission do not show a typical spherical expanding shell. Also Humphreys et al. (2007) gave evidence for multiple and asymmetric mass loss at different times and copied the observations of kinematically separated ejections from the star.

Baudry et al. (1995) suggested the presence of a companion, which is together with VY CMa embedded within a complex nebular structure. That is why VY CMa is not perfect for optical astrometry, because it appears not as a simple round stellar object.

Herbig (1972) argued, using polarizing filters, that the suggested companion is just light scattered from dust condensation in the nebula near to VY CMa. This result was confirmed by Worley (1972) and Holden (1976, 1978) via visual observations. Smith et al. (2001) showed a composite distribution of knots and filamentary arcs in the reflection nebula around the star. The arcs may be a result from multiple, asymmetric ejections from VY CMa possibly caused by its magnetic field and convection. The star's spectroscopic history also does not show any sign of a hot companion. If there is a companion, then with very low mass moving through the extended envelope. Humphreys et al. (2005) discussed the detection of very slow, nearly stationary gas and dust in the ejecta.

That was a strange discovery because of the strong wind and the high mass loss measured. They did not provide an answer to the problem, but suggested that the material must have been slowed down by some process and is falling back, but no physical reason was found to confirm it. The referee of their paper suggested the slow-moving gas being gravitationally bounded in circular orbit. This can be found primarily in carbon-rich red giants and post-AGB stars that are (possible) binary systems.

Herschel view

Cox et al. (2012) did not find an obvious bow shock for VY CMa. Herschel stated that it may be a point source strongly affected by surrounding material. VY CMa, however, is not a simple round stellar object and there is a clear offset between the optical and radio positions (Figure 3.2). The following figure shows VY CMa to be at the edge of a cloud. It was processed with *Scanamorphos*, an interactive tool within the Herschel pipeline. Cox et al. (2012) believe the star to be a visual binary (Proust et al. 1981), though the presence of a companion is still an open question.

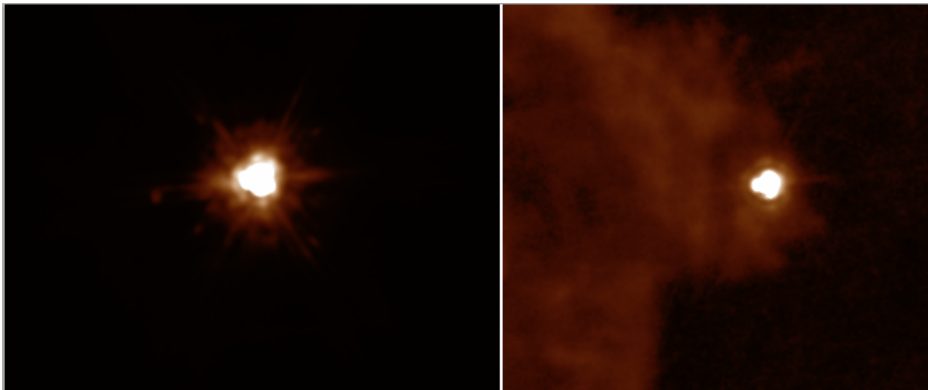


Figure 3.2: *Scanamorphos* map of VY CMa: **left**) PACS 70 μm **right**) PACS 160 μm .

3.3 TX Cam

TX Cam is a Mira variable with an amplitude of 6.05 mag (11.6 to 17.68 mag) and a period of 557.4 d (Kholopov 1987). The star has a mass of $\geq 1.5 M_{\odot}$ and a temperature of ≈ 2500 K. The luminosity is $> 3300 L_{\odot}$. Vibrational and rotational transitions (Jewell et al. 1987) show SiO maser emissions, which also were detected through SiO isotopes (Barcia et al. 1989; Cho & Ukita 1995). Some C- and S-rich molecular species were also found (Lindqvist et al. 1988), giving the possibility that TX Cam might be transitioning from an O-rich to a C-rich star. Its spectrum is M8.5 (Cox et al. 2012). At a distance of 380 pc its mass loss has been calculated to $65 \times 10^{-7} M_{\odot} \text{ yr}^{-1}$ (De Beck et al. 2010). The space velocity corrected for solar motion is $\geq 10.8 \text{ km s}^{-1}$ (Cox et al. 2012).

Past results

Lindqvist et al. (1988) described an oxygen-rich star with unusual infrared and chemical characteristics with an appearing round circumstellar envelope with a terminal CO envelope velocity of 21.2 km s^{-1} (De Beck et al. 2010), but with signs of asphericity at different scales. Diamond & Kemball (2003) concluded that the morphology and evolution of the SiO maser emissions measured for TX Cam show evidence for a non-spherical symmetry of the envelope. For different models a spherical envelope was a bad approximation for TX Cam. Kastner & Soker (2004) suggested a companion to be responsible for the magnetic field, TX Cam shows. The role of magnetic fields in shaping the wind outflow of AGB stars is still debated. Marvel et al. (2001) said TX Cam to have complex motions in the extended photosphere.

Castro-Carrizo et al. (2010) carried out a mapping of ^{13}CO $J=1-0$ and $J=2-1$ emission in AGB and post-AGB CSEs and found for TX Cam concentric arcs and a broken spiral density pattern (could point to a binary) and in general a very large envelope. Interferometric observations of the HC_3N $J=5-4$ line emission indicate the presence of a helicoidal gas distribution and the presence of a binary is so far the only suggested solution (Dinh-V.-Trung & Lim 2009; Mauron & Huggins 2006). Groenewegen & Whitelock (1996) and Groenewegen & de Jong (1998a) copied Mauron's and Dinh's conclusion.

Herschel view

The newest observations with Herschel do not give a conclusive picture. TX Cam images are hard to interpret (between point source and bow shock, Figure 3.3)

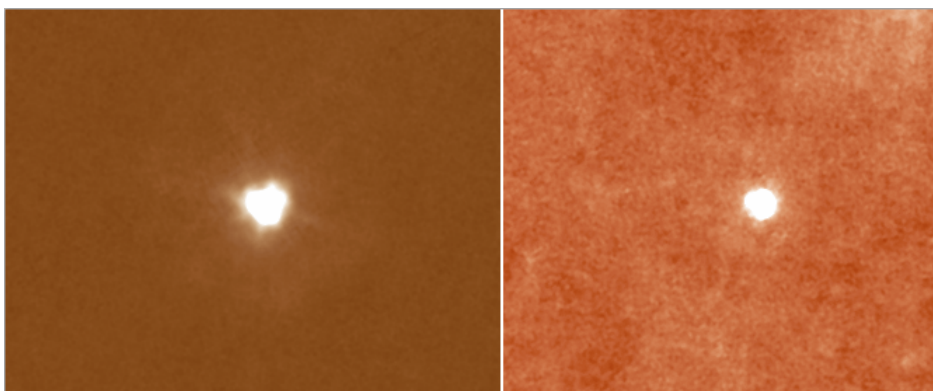


Figure 3.3: *Scanamorphos* map of TX Cam: **left**) PACS $70 \mu\text{m}$ **right**) PACS $160 \mu\text{m}$.

3.4 VY UMa

VY UMa is a Tc-rich carbon star with an irregular period. This Lb (GCVS) variable has a luminosity of $4000 L_{\odot}$ with a temperature of 2700 K (Schöier & Olofsson 2001). The variability ranges from 5.87 to 7 mag (Kholopov 1987) with periods of 125 and 190 d (Percy et al. 2001). These were suggested to be 2 alias periods, but since the autocorrelation diagram (AD), which does not suffer from aliasing, also suggested 2 periods of the same order, the before mentioned periods are possibly 2 real periods. Other scientists recalculated the periods and came up with approximately the same values. Its spectral type is C5II. A space velocity corrected for solar motion of 28.2 km s^{-1} and a terminal velocity of 7.9 km s^{-1} were found by Loup et al. (1993). At a distance of $380 \pm 51 \text{ pc}$ (van Leeuwen 2007) one can find 2 values for the mass loss in the literature: $1.5 \times 10^{-7} M_{\odot} \text{ yr}^{-1}$ (Wannier et al. 1990) and $7 \times 10^{-8} M_{\odot} \text{ yr}^{-1}$ (Schöier & Olofsson 2001); in both cases a rather small mass loss.

Past results

Mason et al. (1999) listed VY UMa as unresolved Hipparcos binary. Sahai et al. (2008) may have proven the binarity through UV excess findings.

Herschel view

Cox et al. (2012) identified the star as a double arc object, a strong eye shape (Class II in their classification, Figure 3.4). For VY UMa the arcs seem to be connected and there is maybe a jet structure in the mid plane.

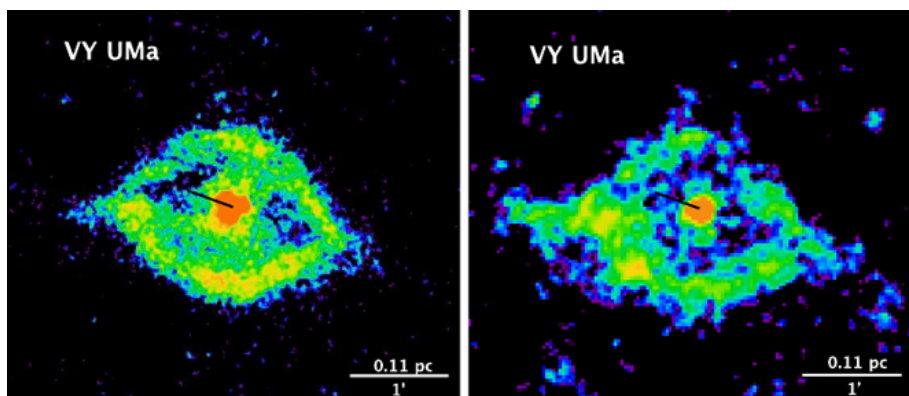


Figure 3.4: VY UMa: **left**) PACS $70 \mu\text{m}$ **right**) PACS $160 \mu\text{m}$ (Cox et al. 2012).

3.5 V Eri

V Eri is an O-rich semi-regular (SRb/SRc) pulsating star (Ivezic & Elitzur 1995). Due to the short pulsational period of 97 d it can not be very luminous. It's not expected to have more than $5 \times 10^3 L_{\odot}$; the temperature was calculated to 3000 K (Hashimoto 1994). Its amplitude is 1.6 mag (8.8 to 10.4 mag, Kholopov (1987)). The spectral class was categorized as M6IV (van Leeuwen 2007). With a distance of 439 ± 133 pc (van Leeuwen 2007) a mass loss of $1.5 \times 10^{-7} M_{\odot} \text{ yr}^{-1}$ (Young et al. 1993) could be calculated. A space motion corrected for solar motion of 39.8 km s^{-1} and a terminal CO velocity of 13 km s^{-1} (Loup et al. 1993) are given.

Past results

De Beck et al. (2010) claimed V Eri to be a binary system. Sahai et al. (2008) questioned the companion. NUV and FUX excesses measurements from V Eri may lead to a companion, which would be certainly hotter than the primary star. A Hipparcos parallaxe of 4.56 ± 1.08 mas for V Eri would result in distance of 220 pc and imply a luminosity of $6 L_{\odot}$ for the companion, but it would be too low for V Eri and the other stars in their sample (which covers 10-15 L_{\odot}). The discovery of an UV excess near V Eri does not give direct evidence for a gravitationally bound object, but it is the most likely explanation, since the UV sky is rather “empty” around V Eri and the chance of a FUV-emitting object to have a similar position as V Eri is small. The $I_{60\mu\text{m}}/I_{100\mu\text{m}}$ ratio stops decreasing at a radius of 0.9 pc indicating that in the outer envelope the dust is externally heated.

Herschel view

Herschel images (Figure 3.5) show a point source (Groenewegen et al. 2011b).

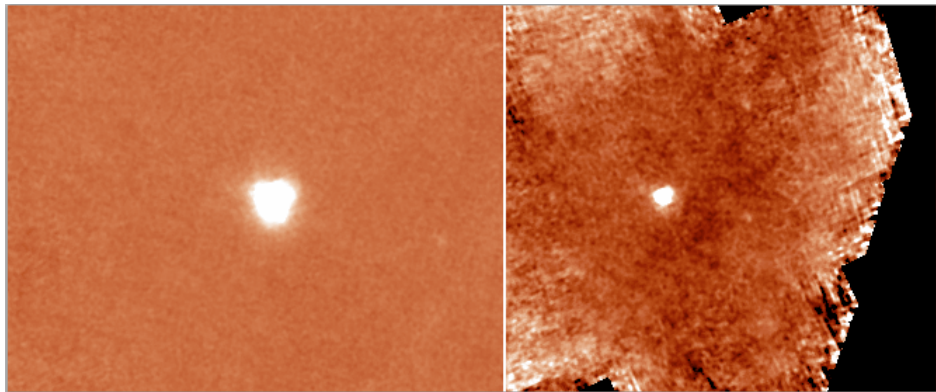


Figure 3.5: *Scanamorphos* map of V Eri: **left**) PACS 70 μm **right**) PACS 160 μm .

3.6 W Aql

W Aql is a S-type variable star of Mira Cet type. It has a pulsational period of 490.43 d. The variability ranges from 7.3 to 14.3 mag (Kholopov 1987). Its spectrum is S6.6. With a distance of 340 pc (Guandalini & Busso 2008a) a mass loss of $1.3 \times 10^{-5} M_{\odot} \text{ yr}^{-1}$ (De Beck et al. 2010) can be inferred. A corrected space velocity of 51.4 km s^{-1} and a CO envelope terminal velocity of 20.0 km s^{-1} (De Beck et al. 2010) are given.

Past results

Danchi & Bester (1995) found the dust shells with inner radius at 8 and 19 R_{*} . Tatebe et al. (2006) described the circumstellar dust to be unevenly distributed and the maximum dust density to be at or near the star. An asymmetry is seen to the east of the star relative to the west side. Tatebe suggested this rather to be an asymmetric dust emission than to be caused by external effects on the outflow. Magnetic effects may play a role in this environment, since they would lead to several outflows or to turbulences in the stellar atmosphere. W Aql pulsates strong, so dust not close to the photosphere would mean that the chemistry in the atmosphere has to be very dependent to the dust formation to run regularly. Knapp et al. (1998) discussed the presence of a double wind profile for W Aql. It is unlikely that this is caused by a binary system, because the frequency of the appearance of a double wind seems to depend on the stellar chemistry and the variable type, both parameters are intrinsic to the star. Double winds maybe occur when the period changes and so the chemistry and also the pulsation lead to a change in mass loss. Jorissen & Knapp (1998) may have identified W Aql as binary with a main-sequence companion as it was revealed by composite spectra at minimum light. Jorissen & van Eck (2000) claimed that W Aql is a binary intrinsic S star, which is eventually becoming Tc-rich.

Herschel view

This object was observed with Herschel and shows a bow shock shape with a possible detached shell and other instabilities. The stand-off distance of the bow shock was theoretically calculated to 0.40 pc and observed at 0.08/0.13 pc (Cox et al. (2012), Figure 3.6).

3.7 EP Aqr

EP Aqr is an O-rich semiregular (SRb) variable of spectral type M8III with a period of ~ 55 d (Matthews & Reid 2007). The variability ranges from 6.37 to 6.82 mag (Kholopov 1987). The stellar effective temperature is 3236 K. The star has an estimated distance of 114 ± 8 pc (van Leeuwen 2007), a calculated mass loss of $3.1 \times 10^{-7} M_{\odot} \text{ yr}^{-1}$ (De

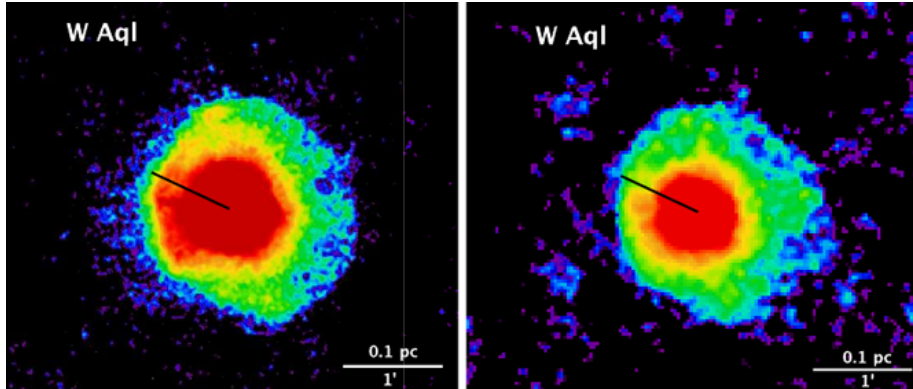


Figure 3.6: W Aql: **left**) PACS 70 μm **right**) PACS 160 μm (Cox et al. 2012).

Beck et al. 2010) and a space velocity of 40.2 km s^{-1} (Cox et al. 2012), the terminal CO velocity being 11.5 km s^{-1} (De Beck et al. 2010).

Past results

Le Bertre & Gérard (2001, 2004) and Gérard & Le Bertre (2006) conducted H I observations and found an extended envelope. Their H I emission profile was decomposed into 3 components with LSR velocities of -31.0 , -26.4 and -31.0 km s^{-1} . The HI data shows a large asymmetry leading to the assumption that those asymmetric structures may occur in the E-AGB phase (e.g. EP Aqr and X Her). In the SiO $J=2-1$ and $J=3-2$ lines the broad feature can be clearly seen, but not the narrow one (González Delgado et al. 2003). This may conclude that the narrow feature has a different origin, while the broad feature comes from the “normal” CSE. Winters et al. (2007) showed the central velocities to be -33.0 to -34.0 km s^{-1} for CO, -32.0 km s^{-1} for SiO, and -31.0 km s^{-1} for H I. This means a difference of the central velocities of 2 to 3 km s^{-1} . The narrow CO and H I features do not overlap. This observed profiles can neither be explained by a spherically symmetric model with constant mass loss rate and outflow velocity nor a simple two-wind model to reproduce the observed structures and the shape of the spectra along the central and other lines of sight.

Libert et al. (2010) defined EP Aqr to have a bipolar outflow interpreted through CO observations. The CO(1–0) and CO(2–1) spectra showed the same two components Winters et al. (2007) tried to reproduce the CO emissions by assuming a spherical flow with a slow, spatically extended and a fast, unresolved component. This wind-model could not reproduce the observed spectral shape along the lines of sight toward EP Aqr. A bipolar outflow could be an explanation for the observed CO profiles. Also Kahane & Jura (1996), Josselin et al. (2000) and Nakashima (2006) explained their found composite CO profiles to be a spherical envelope disrupted by a bipolar flow. EP Aqr being an E-AGB star Libert et al. (2008) showed it to already have a significant circumstellar

envelope. This suggests that mass loss can already occur strongly on the E-AGB. Knapp et al. (1998) indicated the 2 different CO profiles to simply come from 2 major mass loss episodes, showing a normal double wind profile. This hypothesis is supported by the presence of both broad and narrow-line components (two-component wind model), as also shown in Kerschbaum & Olofsson (1999), Winters et al. (2003), and Nakashima (2006). There was no evidence of physical interaction between the 2 components. In the catalogue of multiplicity among bright stellar systems (Eggleton & Tokovinin 2008) EP Aqr was listed as single star. Pourbaix et al. (2003) showed the star not to be a binary either.

Herschel view

The latest Herschel images show a bow shock with instabilities. The wind-ISM morphology was classified as a “*fermata*” interaction, representing Class I in Cox et al. (2012) (Figure 3.7). EP Aqr in particular shows a bullet-like shape with some flow emission in opposite direction of the bow shock. Also RT and KH instabilities are identifiable in the form of density knots in the bow shock. Cox et al. (2012) considered EP Aqr to be a solid candidate for being a binary system. If the difference of the predicted and observed stand-off distance of the bow shock (0.07 and 0.018 pc) points to binarity, is not clear.

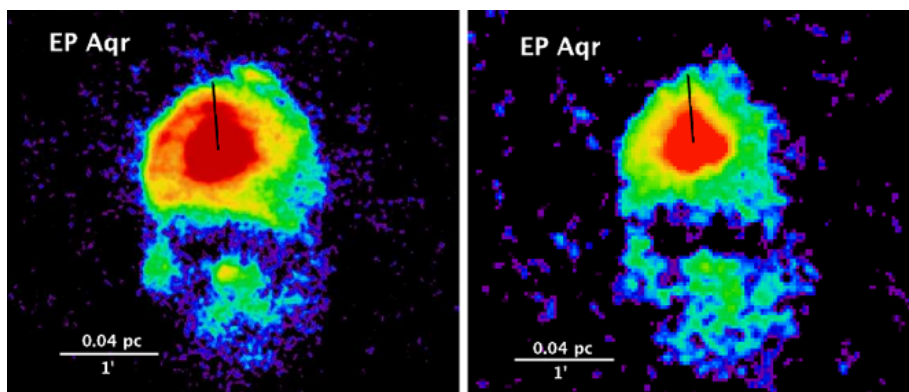


Figure 3.7: EP Aqr: left) PACS 70 μm right) PACS 160 μm (Cox et al. 2012).

3.8 LL Peg

LL Peg is a C-type variable star of Mira Cet type. It has a luminosity of $1.3 \times 10^4 L_{\odot}$ (Winters et al. 1997) with a temperature of 2200 K. The variability amplitude is 1.74 mag ranging from 9.86 to 11.60 mag, as shown in the CGVS by Kholopov (1987). Winters et al. (1997) gave a pulsational period of 696 d. LL Peg has a space velocity corrected

for solar motion of 31 km s^{-1} (Cox et al. 2012) and a terminal velocity of 16 km s^{-1} , and an estimated distance of 980 pc with a mass-loss rate of $3.1 \times 10^{-5} M_{\odot} \text{ yr}^{-1}$ (De Beck et al. 2010). Morris et al. (2006) even claimed the star to lose mass with a rate of $10^{-4} M_{\odot} \text{ yr}^{-1}$, making it an extreme, mass-losing carbon star (Winters et al. 1997). This high value was gained from infrared observations, because LL Peg is surrounded by a thick dust photosphere.

Past results

Winters et al. (1997) found a thin, continuous spiral arc winding 4 to 5 times around the star and interpreted this as nested spiral shells, which theoretically occur, when the star has a companion to form a binary system. At a distance of 1 kpc they found with the NIRC2 camera of the Keck II telescope 2 components, a very red one being LL Peg and a blue one, presumably the companion, with a separation of 109 AU or $0.11''$. The shell spacings visible in the Keck II images would also suggest a binary system with the separation they found. Maunon & Huggins (2006) observed LL Peg with the VLT. Neither the V- nor the B-Band images showed the central star, but the asymmetric distributed envelope, which may contain a cool dust shell with 300 K and is convex to the north-west, possibly caused by a companion star. Additional Hubble Space Telescope (Hubble, HST) images showed the before mentioned spiral pattern. With long wavelengths observations (2MASS and HST far red F814W images) the central star could be spotted at the center of the observed pattern, which was identified as a true Archimedes spiral (see Fig. 8 in Maunon & Huggins (2006)). This spiral could be due to mass loss in a binary system, as investigated by Mastrodemos & Morris (1999) and Soker (1994). In both cases the evolution of spiral pattern is described as an interplay of the motions of the mass-losing AGB star and the companion. The pitch of the pattern directly gives the companion's period. The presence of those spiral patterns also could help to understand the formation of some planetary nebulae. Herschel does not show any spirals in the IR wavelengths.

Herschel view

Cox et al. (2012) listed LL Peg as binary candidate, as was suggested by Knapp et al. (1998) and De Beck et al. (2010). Figure 3.8 shows a PACS image of the object.

3.9 R Aqr

R Aqr is an O-rich symbiotic LPV of spectral type M7IIIpev. The variability amounts to 7.2 mag (5.12 to 12.4 mag, Kholopov (1987)). Its pulsational period corresponds to 390 d. R Aqr has a distance of 214 pc (Kamohara et al. 2010) and an appertaining

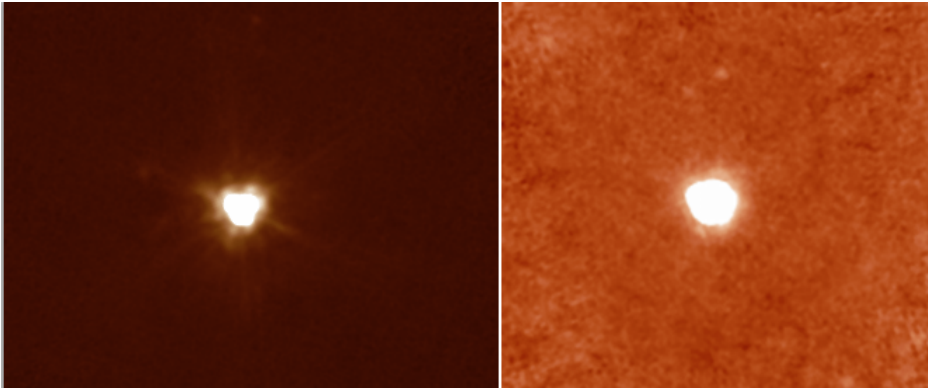


Figure 3.8: *Scanamorphos* map of LL Peg: **left**) PACS 70 μm **right**) PACS 160 μm .

mass loss of $0.6 \times 10^{-7} M_{\odot} \text{ yr}^{-1}$ (Matthews & Reid 2007). Its space velocity corrected for solar motion and terminal outflow velocity are 45 (Cox et al. 2012) and 16.7 km s^{-1} (Groenewegen et al. 2002), respectively.

Past results

Merrill (1921, 1950) suggested for the first time a hot companion around the AGB star from bright emission lines in optical wavelength. Hollis et al. (1997) found a resolved binary system with a separation of 55 mas (11 AU). Hollis et al. (2000, 2001) found through SiO maser emission that the LPV rotates around the north-east south-west axis, where also jets were discovered (Wallerstein & Greenstein 1980; Kafatos et al. 1989). The axis and jets were assumed to be exactly perpendicular, however Kamohara et al. (2010) found the velocity field not to come along with the rotation, but there seems to be an axis of symmetry around $\text{PA} = 0^{\circ}$. The jets were measured to be extended more than 2500 AU in both directions with the south-west (SW) one being much fainter than the north-east (NE) one, but since 1983 the excitation increased for the NE jet by a factor of 2-3 and declined for the SW jet by a factor of 1.5. This jet may be due to an accretion disk outflow of dense material with a shock being the primary source (Meier & Kafatos 1995). The wind of the primary or the wind of the WD companion accretion disk may collide with a higher density material in the outflow pass to show, what was observed. NE jet parts broke apart maybe due to the presence of a companion (Hinkle et al. 1989). This disruptions could have been caused by collisions with more massive clouds from the side or caused due to a reverse shock because of a collision with a cloud. The mass inside the jet can be compared to the giant's mass loss in a few years.

The outflowing mass must have been accumulated in the jets, because normally not more than 1% of ejected material ends up in them. The favoured bow shock model for R Aqr is a cloudlet model, which states that the ambient medium is denser than the ejected material (Nichols & Slavin 2009). Nichols et al. (2007) found oscillations in X-

ray observations with a period of 1734 s corresponding to the rotation period of the WD companion, suggesting it to be a rapidly rotating magnetic white dwarf with $\approx 1 M_{\odot}$ favouring accretion. The binary system is believed to have a period of 44 yr (Willson et al. 1981; Wallerstein 1986) with revisited values of 34.6 and 43.6 yr by McIntosh & Rustan (2007) and Gromadzki & Mikołajewska (2009), who calculated R Aqr’s Roche lobe to have a radius of 4 AU with its slow wind to be able to fill it (Podsiadlowski & Mohamed 2007). Solf & Ulrich (1985) found a two-hourglass-nebula structure with the inner nebula (180 yr old) to be embedded in the outer (600 yr old) one with an expansion of 1 - 2'. Both structures are linked to R Aqr and may be evolved out of an explosion of the binary system. Whitelock (2003) found SiO and H₂O maser emission in R Aqr; they only occur in 3 out of 4 known symbiotics. The best fit for the emission was introduced by Cotton et al. (2006): a star surrounded by a water molecular shell and an off-axis compact feature. A hot dwarf alone can not contribute the luminosity necessary to explain observations. A possible explanation for that is heating of the secondary from the primary and its Roche lobe hot spot.

Herschel view

Cox et al. (2012) showed R Aqr to have an irregular outflow morphology (Figure 3.9).

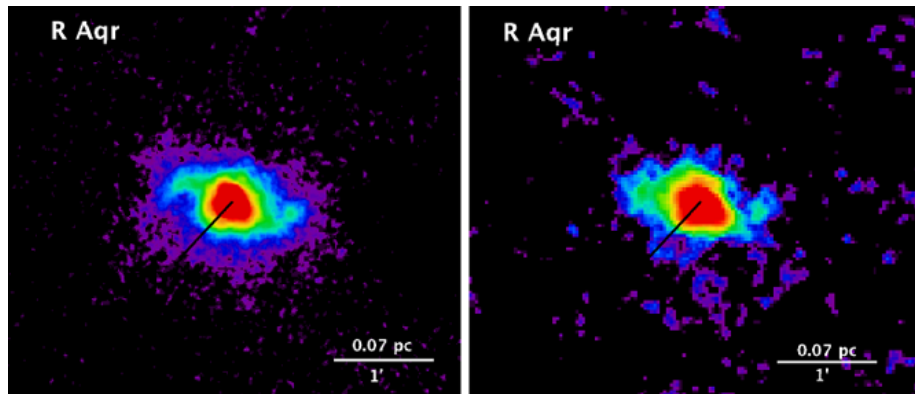


Figure 3.9: R Aqr: **left**) PACS 70 μm **right**) PACS 160 μm (Cox et al. 2012).

3.10 θ Aps

θ Aps is an O-rich semi-regular pulsating star of spectral class M6.5III, at a distance of 113 ± 6 pc, leading to a mass loss of $1.1 \times 10^{-7} M_{\odot} \text{ yr}^{-1}$ (Cox et al. 2012). According to the GCVS the star’s variability ranges from 6.4 to 8.6 mag and the pulsational period is 119 d (Kholopov 1987). It has a space velocity corrected for solar motion of 34.2 km s^{-1} and a CO emission thermal velocity of 4.5 km s^{-1} (Schöier & Olofsson 2001).

Past results

Pourbaix et al. (2003) found it to be a VIM (Variability-Induced Mover) binary, showing the motion of the photocenter to be correlated with its brightness variation.

Herschel view

Herschel observations show an elliptical bow shock shape. Cox et al. (2012) assigned θ Aps to their morphological class I, “*fermata*” (Figure 3.10), and indicated the star to be a solid candidate for binarity.

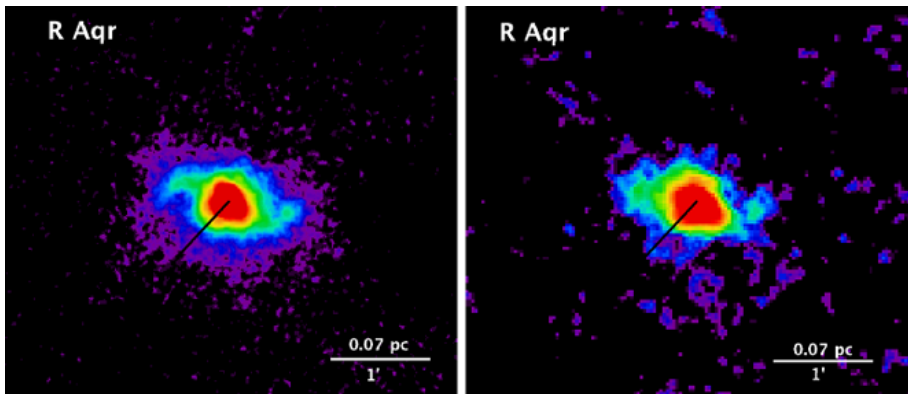


Figure 3.10: θ Aps: **left**) PACS 70 μm **right**) PACS 160 μm (Cox et al. 2012).

3.11 TW Hor

TW Hor is a semi-regular (SRa/SRb) pulsating star designated to have spectral type C. Its luminosity is $9 \times 10^3 L_{\odot}$ with an effective temperature of 3250 K and a radius of 300 R_{\odot} (Bouchet 1984). The pulsational period is 158 d with a variability range of 0.43 mag (5.52 to 5.95 mag, (Kholopov 1987)). The measured mass loss is $0.24 \times 10^{-7} M_{\odot} \text{ yr}^{-1}$ (Groenewegen et al. 2002) at 322 ± 38 pc. It moves with $v_{\text{LSR}} = 52.4 \text{ km s}^{-1}$ through space with an outflow velocity of 7.5 km s^{-1} (Ramstedt et al. 2006).

Past results

Eggleton & Tokovinin (2008) referred TW Hor in their catalogue of multiplicity to be a single star. Sahai et al. (2008), however, claimed to have found a hot companion through UV excess. Therefore TW Hor was observed with long-wavelength and short-wavelength instruments on-board the Galaxy Evolution Explorer (GALEX). They found NUV and FUV excesses, which could refer to the presence of a companion being hotter than the primary. For TW Hor they saw significant flux at wavelengths longer than $\sim 2500 \text{ \AA}$.

The rise in the spectrum toward the red end of the bandpass identified this flux to be caused by the primary star. This UV excesses, however, do not mean to have found a gravitationally bound object (see also V Eri). This AGB star is assumed to be a member of NGC 1252, an open cluster (Bouchet 1984).

Herschel view

Herschel images revealed a point source (Figure 3.11).

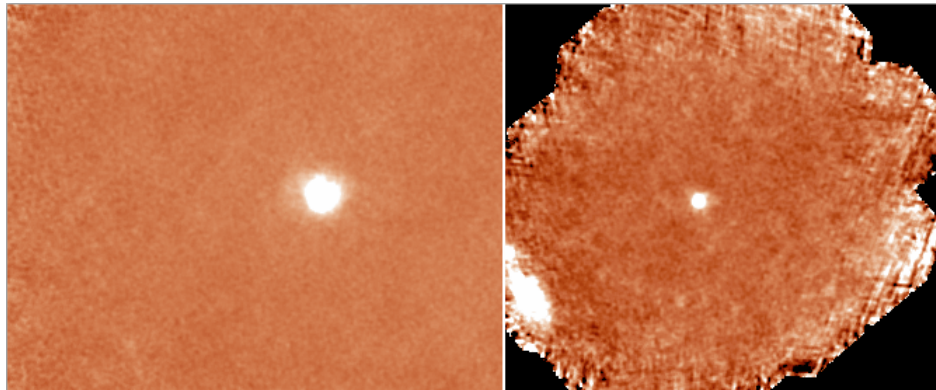


Figure 3.11: *Scanamorphos* map of TW Hor: **left**) PACS 70 μm **right**) PACS 160 μm .

3.12 π^1 Gru

π^1 Gru is a semi-regular (SRb) pulsating star of spectral type S5,7e. It is one of the brightest intrinsic S stars known with a variability ranging from $V = 5.41$ to 6.70 mag with a pulsational period of 150 d (Kholopov 1987). Its mass loss was calculated to $8.5 \times 10^{-7} M_{\odot} \text{ yr}^{-1}$ (De Beck et al. 2010) with a distance of 163 ± 20 pc, a space velocity of 11.9 km s^{-1} (van Leeuwen 2007) and an outflow terminal velocity of 30.0 km s^{-1} (De Beck et al. 2010).

Past results

Evidence for binarity was firstly published by Bidelman (1958) describing the S-type star π^1 Gru (HR 8521) to be similar to a normal M giant with a faint companion of late spectral type. No more conclusions could be made at that time. Proust et al. (1981) listed the star in their catalogue of variable-visual binary stars. Stars in that catalogue show peculiarities in their variability and evidence to be part of visual multiple systems. Jorissen et al. (1993) found Tc in π^1 Gru. Together with its binary properties and IR fluxes for stars they concluded that for Tc-rich S stars with low $R = F(12 \mu\text{m})/F(2.2 \mu\text{m})$,

Tc enhancement occurs before a major mass loss event. Pourbaix et al. (2003) were not sure if π^1 Gru is a VIM binary, but the companion seems to be separated at about $2.7''$. The AGB star was the only S star (Frankowski et al. 2007) in the Hipparcos catalogue to be detected as $\Delta\mu$ binary. In Huggins et al. (2009) and references therein π^1 Gru is explained to show an equatorial torus and jets as can be seen in proto-PNe. Numerical simulations were made to understand the influence of the companion on large scale structures.

Herschel view

The star has an irregular outflow morphology as pointed out by Cox et al. (2012) as shown in Figure 3.12.

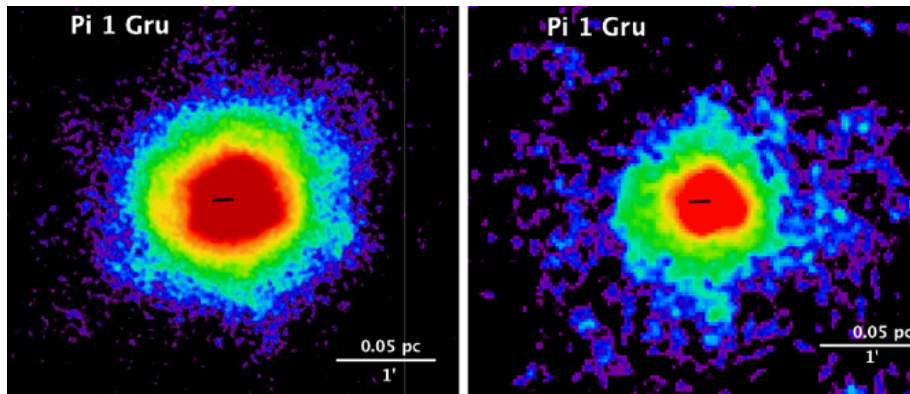


Figure 3.12: π^1 Gru: **left**) PACS 70 μm **right**) PACS 160 μm (Cox et al. 2012).

3.13 σ^1 Ori

The object is an O-rich LPV (SRb) of spectral type M3 with periods of 30 and 120 d and a variability ranging from 4.65 to 4.88 mag (Kholopov 1987). Its luminosity was calculated by Ake & Johnson (1988) to $M_V = -0.7 \pm 0.4$ mag. A mass loss of $0.4 \times 10^{-7} M_\odot \text{ yr}^{-1}$ was measured by Groenewegen & de Jong (1998a). The distance corresponds to 200 ± 28 pc. The star moves with $v_{LSR} = 38.8 \text{ km s}^{-1}$ through the ISM.

Past results

σ^1 Ori was already observed with the International Ultraviolet Explorer (IUE) and this satellite found a white dwarf companion through ultraviolet spectra (Ake & Johnson 1988); follow-up observations were done in the radio with the VLA (Drake et al. 1991). The primary was identified as an optical variable star, as was seen in the UV variability

in LWP spectra; 3 SWP images showed the secondary to be constant in light. Mg II and C II emission lines were found as expected for single red giant stars, they may originate in the chromosphere. This fact suggests σ^1 Ori to be a simple binary with a non-interacting companion. The detection of the secondary in this system gave rise to the question of the evolution of σ^1 Ori. It is not known if the surface composition changed in time caused by accretion from the secondary, what could have been a red giant itself. The Tc-rich star σ^1 Ori was found to have a significant H I absorption in the spectra probably due to the WD companion. Brown et al. (1990) estimated the WD to have $T = 22,000$ K and an absolute visual magnitude of 11.0 mag. This values lead to cooling times much longer than Tc could be detected because of its shorter lifetime if the WDs progenitor was a TP-AGB star responsible for the formation of this element. In the sample of Johnson (1992) σ^1 Ori was the only Tc-rich star with a hot WD companion. Mason et al. (2001) listed the star as an unresolved Hipparcos binary and Pourbaix et al. (2003) identified it as a red VIM binary.

Herschel view

Herschel's first observations showed σ^1 Ori as a point source with an irregular outflow morphology (Figure 3.13).

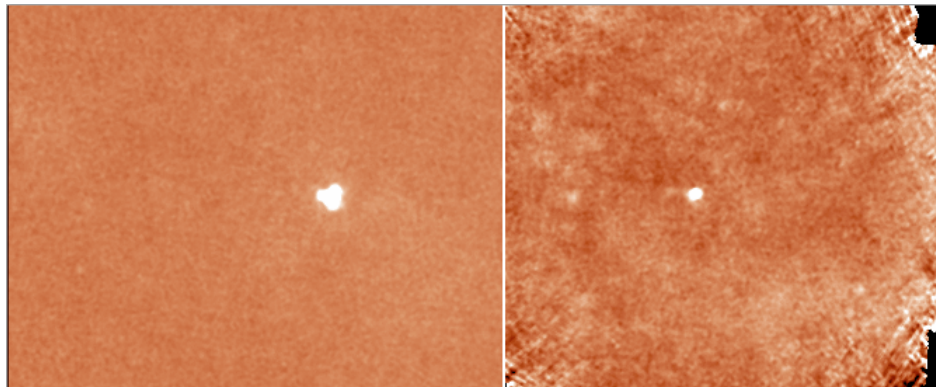


Figure 3.13: *Scanamorphos* map of σ^1 Ori: **left)** PACS 70 μm **right)** PACS 160 μm .

3.14 σ Cet (Mira)

σ Cet or Mira (Latin adjective meaning “Wonderful”) was one of the first variable stars discovered and is in many ways a template for the evolution of low- to intermediate-mass stars, also concerning binary systems involving red giants. Its appearance on the night sky gave rise to a new class of objects: Mira variables, defined to have very red colors, long periods (>100 d) and large light amplitudes (>1 mag). Scientists still discover new

facts about this famous AGB binary every year. Its observations reflect the advances in Instrumental Astronomy in time.

o Cet is an O-rich star. The variability of Mira was first recorded by David Fabricius beginning around 1600. Kholopov (1987) in the GCVS list a variability amplitude of 8.1 mag (2.0 to 10.1 mag) and a pulsational period of 331.96 d. The strong variation in variability also causes a bright spectrum change. Near brightness maximum the spectrum was measured to be M6III, near brightness minimum it is M9III. At a distance of 91 ± 10 pc a mass loss of $2.5 \times 10^{-7} M_{\odot} \text{ yr}^{-1}$ (De Beck et al. 2010) was derived. The accretion rate of Mira B was estimated to be $10^{-10} M_{\odot} \text{ yr}^{-1}$. The actual space velocity of the binary system was calculated to 107.7 km s^{-1} (van Leeuwen 2007).

Past results

Infrared interferometry at $11 \mu\text{m}$ showed a complex extended atmosphere and an inner dust envelope ($\leq 10R_*$, (Lopez et al. 1997)). That could infer to two or more spherical dust shells. Lopez1997 mentioned that the observed axis of the bipolar outflow found by Reimers & Cassatella may be perpendicular to Mira B's orbital plane. It was also theorized that the presence of asymmetries in the Mira system is possibly due to an asymmetric mass loss caused by non-radial pulsation or giant convection cells and/or magnetic spots on the stellar surface. Martin et al. (2007) reported for the first time the detection of an UV-emitting bow shock and a turbulent wake extending over 2° on the sky with GALEX, caused by Mira's large space velocity and the interaction between its wind and the ISM. This wake is just visible in the far-UV and represents 30,000 years of Mira's mass loss. Mira is an extremely well studied object, but this long tail and the bow shock were not detected before. 3 major morphological features were outlined: the tail, the southern bow shock, and the southern and northern streams breaking up in knots farther away from the star. Far-UV and near-UV emissions were detected in the bow shock and the knots, the tail only showed far-UV emission with one near-UV region associated with the northernmost knots. The knots show higher density and more developed radiative shocks and occur in the region of the bipolar outflow components. The source of the long-lived ultraviolet tail emission is an open question. Martin et al. (2007) suggested it could be due to dust scattering of interstellar light, molecular hydrogen emission, hydrogen two-photon continuum, or coronal line emission from shocks or gas at $\approx 10^5 \text{ K}$. Wareing et al. (2007) mentioned for the first time surrounding arclike structures. The slow terminal outflow velocity of 8.1 km s^{-1} (De Beck et al. 2010) explains why the ejected material is still within 4 pc of Mira. There is also evidence that Mira entered the Local Bubble: (1) a narrowness and rebrightening of the tail starting about $40'$ from Mira, and (2) the bend in the tail starting at the same position. This changes can be due to the higher ISM density in the Local Bubble. Entering a higher density environment caused the bow shock to disappear and it had to re-establish itself in $\approx 10^4 \text{ yr}$ according to calculations corresponding to a gap in the tail between $25'$ and $35'$ downstream. Wareing in a separate paper described the instabilities

at the head of the bow shock as von Karman-like vortex shedding into the ram pressure-stripped tail. Also variations in the ISM could cause the instabilities. Recently a H I counterpart to the extended tail of Mira was found (Matthews et al. 2008). H I is common in CSEs and also can extend to very large distances from the star. For a long time Mira was the only AGB star to be known to have H I emissions. The H I emission detected with the VLA overlaps with FUV observations by GALEX, but it is unclear why. However, most FUV emissions do not have a H I counterpart, especially the bow shock. The gas in the knots may be partly ionized due to the detection of H α emission. Mira has also been observed with the Spitzer Space Telescope (Spitzer) and AKARI Infrared Astronomy Satellite. Spitzer images resolved the structure of Mira’s astropause (Ueta 2008): (1) the circumbinary disc envelope; (2) the termination shock; (3) the astroheath. Meaburn et al. (2009) stated that Mira A is currently in its AGB phase and will become a complex planetary nebula (PN) soon, possibly with multiple bipolar lobes. Mira B was confirmed to be a white dwarf by Sokoloski & Bildsten (2010), showing that the rapid optical variability of Mira AB gives Mira B as a WD. The companion’s amplitude of the optical brightness fluctuations on time scales of minutes correspond to accreting WDs in cataclysmic variables (CVs).

The binarity was already confirmed in 1923 by Joy (1926) through spectroscopy with a period of 14 yr for the secondary. The companion (Mira B) was first identified as a faint blue star showing variable emissions in H, He I and Ca II, as well as sharp Fe II emission lines. Reimers & Cassatella (1985) made spectroscopic observations with IUE especially of Mira B (VZ Cet) and assigned the observed UV continuum at Mira A minimum to the companion. The binary period was first estimated to be longer than 100 d (van Biesbroeck 1959) with a first approximation of 400 yr by Coureau in 1981 (private communications with Reimers & Cassatella (1985)); this value was corrected to \approx 500 yr by Martin et al. (2007). Reimers & Cassatella were the first ones pointing out that Mira B could be a “simple” case of an accretion disk around a WD formed in the wind from the AGB star Mira A with a separation of 0.4”. The first Hubble images of the binary system are presented in Karovska et al. (1997). They mentioned that the primary does not fill its Roche surface, so the mass transfer must happen per wind and not per tidal interaction. Mira AB was described as a special binary, because as an accreting system its parameters for accretion rate and luminosity calculations can be conclusively won by observations, since this system is resolvable from X-ray to radio wavelengths. Mira was therefor observed with FOC, the Faint Object Camera on-board Hubble, in the near-UV and optical. FOC images together with NUV and FUV objective-prism spectra gave the first complete sample of continuum and line emissions from Mira A and B. With the FOC images asymmetries in the Mira A atmosphere were noted for the first time in the UV. The images were deconvolved using images of Mira B as point source. This asymmetries were already seen using interferometry (Karovska et al. 1991; Haniff et al. 1992). It was suggested that they come from unresolved bright spots on the surface of Mira A or from the extended atmosphere, or are an indication of non-radial pulsation of the primary atmosphere causing geometrical asymmetries in temperature and density

non-uniformities. The first Hubble observations of the wind-accreting system *Mira* AB concluded: (1) the SEDs of *Mira* A and B uncontaminate by each other, especially in the region of a found Balmer jump; (2) first direct images of *Mira* A and B in the UV; (3) asymmetries in *Mira* A atmosphere. Josselin et al. (2000) found strong asymmetries in the neutral envelope. They discussed asymmetries on all scales. Following Karovska et al. (1997) they also thought about the UV images revealing an interaction between *Mira* A and B, a hook-like structure extending towards *Mira* B. This interaction could be the reason for the accretion disk around the white dwarf detected by Reimers & Cassatella (1985).

Herschel view

In Cox et al. (2012) *o* Cet shows RT and/or KH instabilities in the outflow morphology type “fermata” (Figure 3.14), thanks to Herschel.

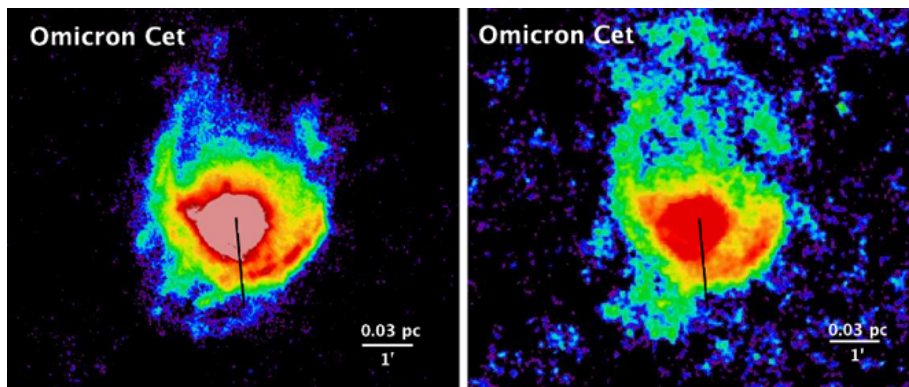


Figure 3.14: *o* Cet: **left**) PACS 70 μm **right**) PACS 160 μm (Cox et al. 2012).

Thanks to the high spatial resolution of the Herschel PACS instrument (with a point-spread function of $5.6''$ full-width at half-maximum at 70 μm) it was possible to give a more detailed view on *Mira*’s circumstellar shell(s). In general clumpy broken arcs could be resolved. The newest detailed description of this arcs can be found in Mayer et al. (2011), on which the following summary is based on.

The circumstellar environment shows several arc-like structures, labelled A to E in Figure 3.15. The brightest arc, C, is clearly detached from the star and stretches over position angles (PAs) $\sim 190^\circ$ to 270° (south-west to west). Its angular separation is $67''$ at the closest point at 6100 AU to $85''$ at 7800 AU, being the most distant point. The radial intensity profile (Figure 3.16) shows the arc C as a plateau in the diagram.

Arc C seems to be non-circular; it could be circular, but then not centered on the position of the star. Arc D is found in the same direction, but not that stretched as C. In the radial intensity profile arc D is visible as a bump at a distance of 1900 to

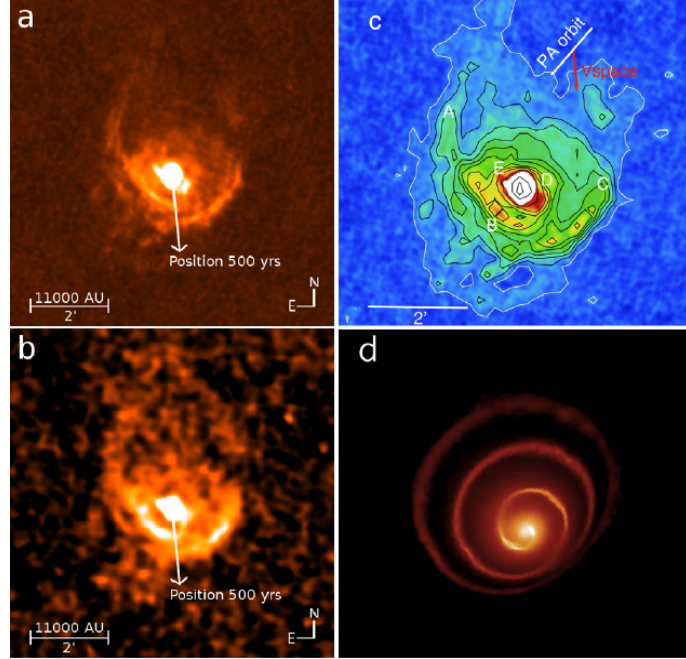


Figure 3.15: **a)** Deconvolved PACS image at $70 \mu\text{m}$. The arrow shows the space motion and the position in 500 yr. **b)** Same for a deconvolved PACS image at $160 \mu\text{m}$ **c)** $70 \mu\text{m}$ deconvolved PACS image with contours and the arcs A, B, C, D, E. The lowest contour is the 3σ threshold (white), the arrow shows the space motion, the bar labelled PA orbit gives the orientation of the major axis of the apparent orbit. **d)** A “toy model” based on hydrodynamical simulations of Mohamed & Podsiadlowski (2007, 2011).

2600 AU (21-28''). In the south-east direction, arc B is closer to the star than C and D at PAs of $75\text{-}180^\circ$. It is more circular than arc C and is seen as a narrow peak in the radial intensity profile at a distance of 2800 AU (corresponding to 41°) from the binary system. Arc A can be found in the north-east direction at a distance of 6200 to 8200 AU ($68\text{-}89^\circ$). The radial intensity profile suggests that the arcs A and C may have a common history. There may be also another arc E in the south-east direction very close to the star (1400 AU, corresponding to $15''$). Just the edge at a position angle of 65° can be seen. It is interesting to recognize that the arc sequence E-D-B-C-A corresponds to an increasing distance from the star and an increasing PA range; E is the shortest and closest and A the longest and farthest arc seen.

The overall 3σ emission above the $70 \mu\text{m}$ IR background of Mira can be seen in Figure 3.15c as the outermost contours. It is worth mentioning that the extension of the emission is towards a PA of $\approx 160^\circ$ and differs significantly from Mira’s space motion in the direction of PA = 185° .

Assuming the binary state of Mira, the observed arcs can be a direct result of the binary

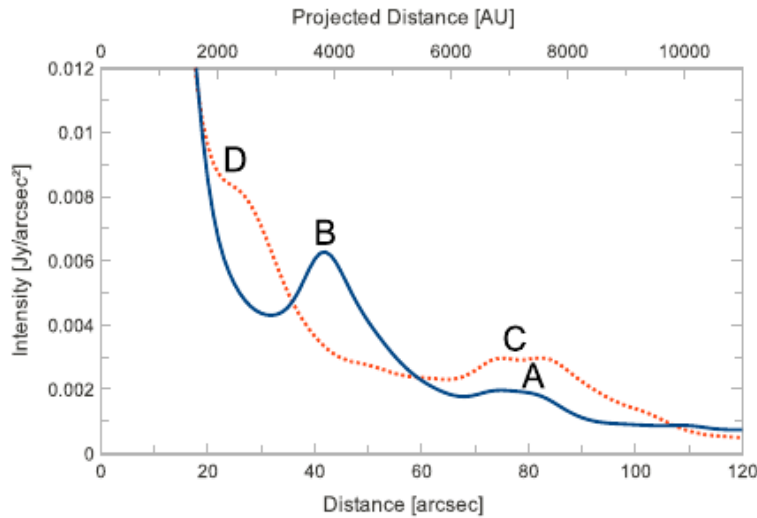


Figure 3.16: Radial intensity profile

interaction.

Figure 3.15d shows a “toy model” based on hydrodynamical simulations of Mohamed & Podsiadlowski (2007, 2011). The fast bipolar outflow of Mira of 160 km s^{-1} could be responsible for disrupting the arcs with its high velocity. The arcs B, C and D are located along the southern jet, as can be seen in GALEX far UV images obtained by Martin et al. (2007) (Fig. 3 in the paper by Mayer et al.). The outermost arcs A and C show evidence of an interaction with the ISM by forming together a bullet-like structure in direction of the space motion. Martin et al. (2007) showed the curvature of the bipolar-outflow southern stream to confirm the bullet-like shape found with Herschel. It is thought that the arcs are a result of both an interaction of Mira with its companion and an interplay with the ISM. This combination was used to simulate the AGB star *o* Cet nearly filling its Roche lobe and losing mass through slow wind. The resulting 3D structure (as seen in Figure 3.15d) shows a typical wind outflow shape of a binary system (Archimedean spiral).

All parameters of all objects are summarized in the following table including the distance from the Galactic plane z and the proper motion μ .

3 Binary AGB candidates in the Herschel MESS sample

Table 3.1: The MESS AGB binary sample (values are if not stated from Cox et al. (2012))

IRAS id	Name	Type ^{b,31}	Distance [pc]	z [pc]	L [10 ⁴ L _⊙]	Variability ³¹			Period ³¹ [d]	[10 ⁻⁷ M _⊙ yr ⁻¹]	v _w [km s ⁻¹]	v _{LSR} ¹ [km s ⁻¹]	μ ^a [mas yr ⁻¹]	Binarity					
						V _{min} [mag]	V _{max} [mag]	31											
14003-7633	θ Aps	O - M6.5III	113 ± 6.0	-13	-	8.6	6.4	119	1.1	1.1	4.5	34.2	63.3	variability induced mover ³					
21439-0226	EP Aqr	O - M8III	114 ± 8.0	-70	-	6.82	6.37	5 ³³	3.1	4	11.5	40.2	31.2	complex CO profile ^{5,6,7}					
19126-0708	W Aql	S - S6.6+FY	340	8	35	14.3	7.3	490.43	130	4	20.0	51.4	27.6	composite spectra ^{9,10} / CO profile ⁵					
02168-0312	o Cet	O - M7IIIe	91 ± 10	-63	-	10.1	2	331.96	2.5	4	8.1	107.7	223.3	visual ¹³					
03374-6229	U Cam	C - C3.9-C6.4e	430	11	60	7.26	12.8	400	10	10	20.6	9.8	4.2	Hipparcos					
10416-6740	VY UMa	C - C5II	380 ± 51	286	4	2	7	5.87	125, 190	30	7.2	7.9	14	28.2	15.6	UV excess ¹⁵			
22196-4612	π ¹ Gru	S - S5+G0V	163 ± 20	25	-119	-	6.70	5.41	150	150	8.56	4	30.2	4	11.9	25	8.4	visual	
04497+1410	o ¹ Ori	O - M3 S	200 ± 28	25	-36	-	4.88	4.65	30, 120	0.4	16	-	38.8	41.1	27.5	41.1	UV excess ¹⁵		
23412-1533	R Aqr	O - M7IIIpev	250	23	-220	-	12.4	5.12	390	0.6	17	16.7	18	45	27.5	27.5	symbolic ^{19,20,21}		
03112-5730	TW Hor	C - -	322 ± 38	25	265	0.9	29	5.95	5.52	158	0.24	18	7.5	22	52.4	25	34.4	UV excess ¹⁵	
04566+5606	TX Cam	O - M8.5	380	4	72	3.3	17.68	11.6	557.4	65	4	21.2	4	10.8	-	-	34.4	spiral? ³⁴ / interferometry ³⁵	
04020-1551	V Eri	O - M5/M6IV	439 ± 133	25	-290	0.5	10.4	8.8	97	32	1.5	26	13	14	39.8	16.7	16.7	UV excess ¹⁵	
07209-2540	VY CMa	O - M3/M4III	562	-35	40-50	27	9.6	6.5	2200	2800	4	46.5	4	42.9	12.4	12.4	12.4	UV excess ¹⁵	
23116+1655	LL Peg	C - -	980	4	-620	1.3	28	11.6	9.86	696	28	310	4	16.0	4	31.0	-	31.0	visual ²⁴

References: 1: if not stated, from Johnson & Soderblom (1987), 2: Schöier & Olofsson (2001), 3: Poutaiax et al. (2003), 4: De Beck et al. (2010), 5: Knapp et al. (1998), 6: Nakashima (2006), 7: Winters et al. (2007), 8: Gaundalini & Busso (2008b), 9: Herbig (1965), 10: Culver et al. (1974), 11: Knapp et al. (2003), 12: Lindqvist et al. (1999), 13: Karovska et al. (1997), 14: Loup et al. (1993), 15: Sahai et al. (2008), 16: Groenewegen & de Jong (1998b), 17: Matthews & Reid (2007), 18: Groenewegen et al. (2002), 19: Whilson et al. (1981), 20: Hinkle et al. (1989), 21: Gromadzki & Mikolajewska (2009), 22: Ramstedt et al. (2006), 23: Groenewegen & Whitelock (1996), 24: Morris et al. (2006), 25: van Leeuwen (2007), 26: Schöier et al. (2005), 27: Jura & Kleinmann (1990b), 28: Winters et al. (1997), 29: Bouchet (1984), 30: Percy et al. (2001), 31: (spectral type) if not stated, from Kholopov (1987), 32: Jura & Kleinmann (1990b), 33: Matthews & Reid (2007), 34: Castro-Carrizo et al. (2010), 35: Dimh-V-Tung & Lim (2009); Mamon & Huggins (2006))

Notes: a: Proper motion (van Leeuwen 2007), b: CSE chemistry: oxygen-rich (O), carbon-rich (C) and S-type (ZnO₂ lines in addition)/instead of TiO₂ - and spectral type of the central star.

4 Discussion

The binarity of most of the objects in Chapter 3 was known before the MESS program came into existence. For some objects the binary state is not clear yet, e.g. for U Cam. This star shows signs of binarity, but they are a matter of discussion in the community so far.

Herschel is not very efficient at detecting binaries because of its moderate resolution not being able to resolve the binary separations. In the MESS sample discussed in Cox et al. (2012) there is little evidence for binarity. As a matter of fact, many identified binaries show an irregular morphology. In the “*fermata*” class only Mira is known to be a binary showing an interesting, peculiar shape (Mayer et al. 2011). U Cam, believed to be a binary in Cox et al. (2012), can be found in the “*ring*” class. It may be noteworthy that 6 out of 30 objects with no detected outflow morphology are confirmed binaries. If one especially considers visual binaries, 3 binaries can be found for the “*fermata*”, “*eyes*”, and “*non-detection*” classes, respectively. 4 visual binaries are known to have a “*ring*” morphology. In total one finds 5 out of 7 “*eye*” morphologies to be confirmed binaries. Herschel may not be very effective at detecting binaries, but concerning the proper motion vector and the inclination of Mira, which is part of the sample in this Thesis, and μ Cep, it could give some indications on the binary nature. The majority of proper motion vectors (if known) point to the observed bow shock apexes within an angle of 20-30°, but this is not the case for Mira and μ Cep. It might be that both stars are long-period binaries and that the proper motion vectors observed with Herschel are not pointing to the present bow shock because the angle of the vector changed over time. However, this theory requests further testing and observations and modelling. The morphology does not show any dependency on the inclination angle, i , either. VY UMa, also part of the sample in the previous chapter, classified as “*eye*” morphology, is the only one in the mentioned class to have an inclination of $i = -1^\circ$, the rest of the objects having an eye-shaped morphology with $i > 28^\circ$.

5 out of the 14 objects in the previous chapter are “*non-detections*”, 4 objects show a “*fermata*” morphology, 3 have an “*irregular*” outflow morphology, and one object is a member in the “*ring*” and “*eye*” class, respectively.

4.1 Chemistry

In Chapter 3 the majority of binary candidates have O-rich atmospheres (VY CMa, TX Cam, V Eri, EP Aqr, R Aqr, θ Aps, o^1 Ori, Mira), 4 objects have a C-rich atmosphere (VY UMa, LL Peg, TW Hor, U Cam) and 2 are classified as S stars (W Aql, π^1 Gru). At this point one can just speculate about what distinct processes are responsible for the AGB stars keeping an O-rich atmosphere, since 4 of 14 objects also have a C-rich CSE. Despite its binary state, the C-rich CSE of U Cam could be explained by the fact that its “ring” morphology may be caused through an interaction of a fast wind with an older slower wind or simply by an extreme mass-loss event (caused by a thermal pulse; in fact all “ring” morphologies in the MESS sample are TP-AGB stars). The same explanations could be adopted for the “eye” morphology of VY UMa. In the MESS sample O-rich stars are dominated by “fermata” and “irregular” morphological types. In the subsample of this Thesis the O-rich binaries contain most of the “non-detections”, “fermata”, and “irregular” types. The C-rich binaries have one “ring” and one “eye” type and 2 “non-detections”. The 2 S stars in the subsample have a “fermata” and an “irregular” morphology.

Cox et al. (2012) and references therein also discussed the gas-to-dust ratios, which showed a lower value for O-rich than for C-rich dust. Since O-rich stars have been found to have a wider range of mass-loss rates than C-rich stars (previous to the Cox paper), mass loss for O-rich stars may be easier detectable. In Cox et al. (2012) the majority of “fermata” and “eyes” morphologies contain O-rich stars.

4.2 Magnetic field

It may be that a bow shock shows signs of magnetic field effects, e.g. Heiligman (1980) theorized that ISM magnetic pressure could lead to the spherical halos of PNe to be “lemon”-shaped. VY UMa, with its “eye” morphology, could be an example of an out-flow morphology influenced by the magnetic field, assuming that the ISM magnetic field is parallel to the Galactic plane (but the star’s symmetry axis is not aligned to it). VY UMa also could have its own magnetic field causing axisymmetric mass loss, its morphology could be caused by a rotating star with a magnetic field (private communications of Cox et al. (2012) with A.-J. Van Marle).

4.3 Stand-off distance of the bow shock

Stand-off distances of observed bow shocks for some objects in the MESS sample have been calculated before within the scope of the IRAS, Spitzer and AKARI mission. PACS measurements of the angular stand-off distance agree well with earlier observations. The uncertainties of predicted stand-off distances depend on stellar and interstellar parameters like the space and wind velocity, or the mass loss together with a possible inaccurate

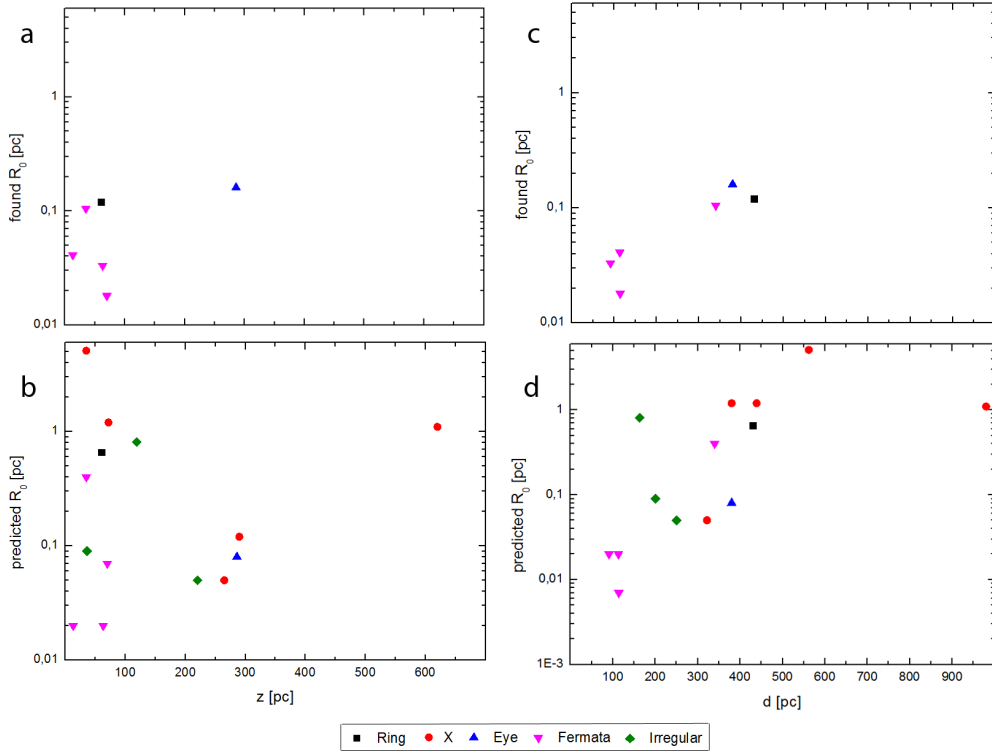


Figure 4.1: Predicted and found stand-off distances for the bow shocks of binary AGB candidates in the MESS sample described in Cox et al. (2012) as a function of the height above the Galactic plane z and the distance d . Description in the text.

distance (Figure 4.1). Finally, to derive the density of the surrounding ISM out of the stand-off distance is observationally difficult, since one should know what ISM phase an object is traversing. In the MESS sample there are some discrepancies concerning some stars showing higher ISM densities than expected from calculations from Dickey & Lockman (1990) and Loup et al. (1993), as will be explained in the next paragraph. On the other hand the high ISM densities go with high mass-loss rates, as it is the case for W Aql with a space velocity of 51.4 km s^{-1} , but not for e.g. R Leo, which shows a low mass-loss rate with a space velocity of 15 km s^{-1} , but its bow shock revealed that it should have a higher space velocity according to the existence of instabilities in the shock. It may also be that the ISM itself obeys a specific flow pattern in the Galactic context to alter the results. Despite the limited sample one can try to state some conclusions. Figure 4.1 shows the predicted and measured stand-off distances of the binaries discussed in Chapter 3. Be aware that not for all stars (in the complete MESS sample, but also for the binary candidates) stand-off distances were found and that a qualitative and quantitative analysis is not possible because of the limited sample of 14 stars.

The predicted and found stand-off-distance differences for the “*fermata*” types range from 0.011 to 0.3 pc with more divergence for objects closer to the Galactic plane. The found stand-off distance for the “*eye*” type (VY UMa) in the sample was actually twice as much as predicted. For the “*ring*” morphology (U Cam) the difference between the observed and predicted stand-off distance was calculated to be 0.54 pc. Since the previous 2 morphologies are related, there could be the same reason causing this big divergence, although it is for now difficult to recognize, since for VY UMa the observed stand-off distance was twice as much and for U Cam the predicted one was far too large. For the “*irregular*” morphologies no found stand-off distances are listed. The predicted distances are in general larger than for the rest of the 14 objects.

Concerning the height above the Galactic plane one can recognize that the “*fermata*” types can be found within the limit of 100 pc for both predicted and found stand-off distances. Binaries with “*irregular*” outflow morphology show larger stand-off distances for smaller z , with one exception. The predicted stand-off distances for the “*irregular*” types seem to be randomly distributed, though the Galactic dynamics may play a role in causing their irregular outflow in a way not clear yet. To give an explanation for the “*eye*” and “*ring*” morphology is difficult because of just one respective object.

Concerning the distance to the objects the predicted stand-off distances for “*fermata*” types can be generally found within 150 pc (with one exception at 400 pc), and for the “*irregular*” types at 150 to 250 pc. Like before, for the “*eye*” and “*ring*” morphology no significance can be given. In general for larger distances larger stand-off distances can be found, but that should be a selective result rather than an intrinsic one.

For the “*irregular*” morphologies and the “*non-detections*” no stand-off distances have been found.

4.4 The ISM density

It is known that the ISM density is not uniform. Some distinct dependencies, however, exist according to Milky Way studies. It is assumed that the interstellar matter (space-averaged) volume density, n_{ISM} , depends generally on the height above the Galactic plane, z . Several papers presented different approaches. Primarily one has to take care of the different phases of the ISM (molecular clouds, CNM, WNM, WIM, H II regions, HIM). Dickey & Lockman (1990) calculated with the help of radio observations of H I in the Milky Way the structure of the CNM (Cold Neutral Medium), WNM (Warm Neutral Medium) and WIM (Warm Ionised Medium). Loup et al. (1993) made another attempt based on Spitzer (1978) and Mihalas & Binney (1981). Also Diplas & Savage (1994) calculated a relation, as can be seen in Figure 4.2, following Figure 11 in Cox et al. (2012), which shows very good consistency of the data from the binary candidates in Chapter 3 with the relation by Loup et al. (1993). The “*fermata*” types and the single “*ring*” morphology show the highest ISM densities, the “*irregular*” types are evenly distributed and the “*non-detections*” and the “*eye*” morphology show to have less dense

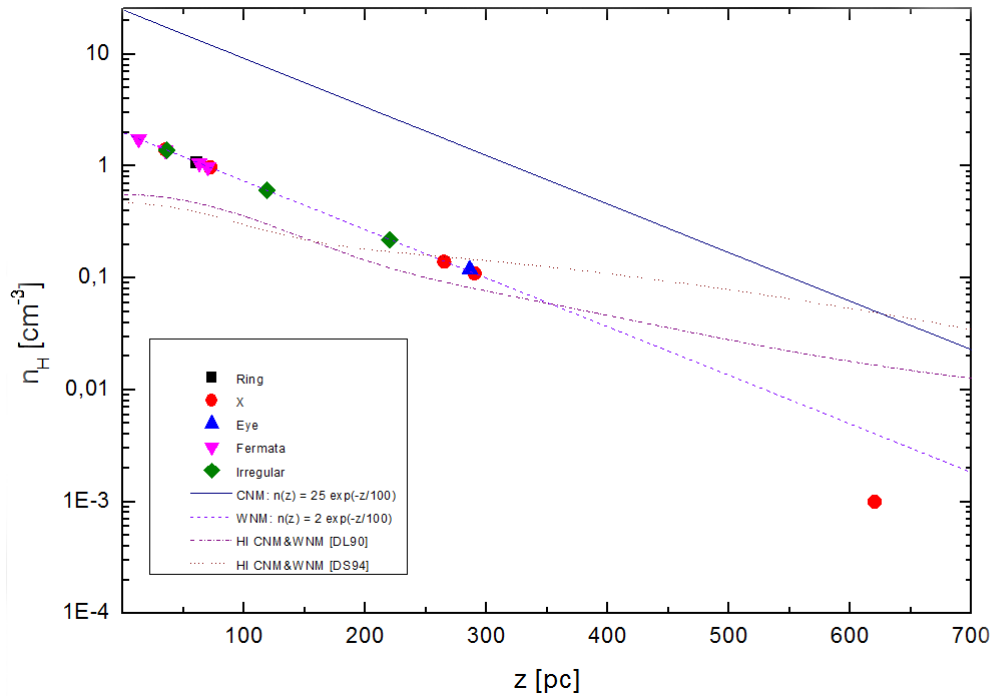


Figure 4.2: ISM density as a function of the height above the Galactic plane for the binaries following Figure 11 in Cox et al. (2012). The binary AGB candidates are indicated according to their morphologies. Different density models for the Milky Way are included: for the CNM, for the WNM (Loup et al. 1993), and for the H I gas (Dickey & Lockman (1990)[DL90] and Diplas & Savage (1994)[DS94])

environments. The outcome of the relations should be handled with caution, since the ISM (in the Milky Way) is not distributed uniformly, the different phases have different filling factors, and structures on all spatial scales exist.

5 Conclusions

This Thesis summarized the literature of binary AGB candidates in the MESS sample and presented the latest observations obtained with the Herschel Space Observatory. The Herschel images reveal different morphological structures. It was tried to find a relation between the binary state of a star and its outflow morphology. Some hints could be found connecting specific morphological types to binary AGB candidates.

Wind-ISM interaction and detached rings were observed on a frequent basis via the MESS GTKP. Observations revealed various shapes and sizes of the interacting regions divided in the 4 main morphological classes. The proposed follow-up program *Old and slow Galactic bullets: Tracing the dust in turbulent interactions regions due to AGB stars traversing interstellar space* wanted to characterize and understand the interaction of mass loss with the immediate surroundings by studying direct emissions from cold dust trapped in the interacting zone. The Herschel PACS instrument is perfect for tracing the cold dust. The proposal for this program was supported by various member of the MESS GTKP. Unfortunately it was not approved.

Following the MESS program an emphasis should be put on the fate of circumstellar dust to investigate the local ISM and the late-stage stellar evolution. Further investigation of the enrichment of the ISM via AGB wind and to search for signatures of bow-shock interactions within fast-moving stellar systems is necessary. Herschel can resolve the arising bow shocks through the detection of the cold dust in the far-IR. The MESS program already observed 70 AGB stars revealing new photometry and spectroscopy of the central star and the immediate inner surroundings. The size of the wind-ISM interacting regions, however, was in some cases larger than expected. The images obtained via the MESS program showed that there is a lot more going on at larger distances from the star. Furthermore, the map sizes and the achieved sensitivity in the MESS sample sometimes differ significantly, so a good comparison between the objects is not perfectly possible.

The “problem” with the MESS sample concerning the interpretation of the wind-ISM interaction and the mass-loss rates is that it included many variable stars with uncertain distances, making it difficult to calculate an accurate mass loss and exact relative motions. For the subsample of previous known binary AGB stars it is important to know

5 *Conclusions*

the distance to get more insight into the dimensions of the system, into the morphology and into the chemistry in those systems. A distance-limited far-IR survey of nearby AGB stars could improve the understanding of the chemistry, the evolutionary status and possible binarity by observing the shaping of the bow shocks and the detached rings on a larger scale.

Bibliography

- Abate, C., Pols, O. R., Izzard, R. G., Mohamed, S., & de Mink, S. E. 2011, in ASP Conf. Ser., Vol. 447, ASP Conf. Ser., ed. L. Schmidtobreick, M. R. Schreiber, & C. Tappert, 81
- Abt, H. A. & Levy, S. G. 1976, ApJS, 30, 273
- Adams, F. C., Ruden, S. P., & Shu, F. H. 1989, ApJ, 347, 959
- Ake, T. B. & Johnson, H. R. 1988, ApJ, 327, 214
- Anosova, J. P. 1989, Comments on Astrophysics, 14, 17
- Barcia, A., Alcolea, J., & Bujarrabal, V. 1989, A&A, 215, L9
- Barnbaum, C. 1992a, AJ, 104, 1585
- Barnbaum, C. 1992b, ApJ, 385, 694
- Bate, M. R. 2000, ArXiv Astrophysics e-prints
- Bate, M. R. & Bonnell, I. A. 1997, MNRAS, 285, 33
- Bate, M. R., Bonnell, I. A., & Price, N. M. 1995, MNRAS, 277, 362
- Baudry, A., Lucas, R., & Guilloteau, S. 1995, A&A, 293, 594
- Bhattal, A. S., Francis, N., Watkins, S. J., & Whitworth, A. P. 1998, MNRAS, 297, 435
- Bidelman, W. P. 1958, PASP, 70, 168
- Bodenheimer, P. 2001, in ASP Conf. Ser., Vol. 229, Evolution of Binary and Multiple Star Systems, ed. P. Podsiadlowski, S. Rappaport, A. R. King, F. D'Antona, & L. Burderi, 67
- Bodenheimer, P. & Burkert, A. 2001, in IAU Symposium, Vol. 200, The Formation of Binary Stars, ed. H. Zinnecker & R. Mathieu, 13
- Bodenheimer, P., Tohline, J. E., & Black, D. C. 1980, ApJ, 242, 209
- Bonnell, I. A. 2001, in IAU Symposium, Vol. 200, The Formation of Binary Stars, ed. H. Zinnecker & R. Mathieu, 23

- Bonnell, I. A. & Bate, M. R. 1994, MNRAS, 269, L45
- Boss, A. P. 1988a, Comments on Astrophysics, 12, 169
- Boss, A. P. 1988b, Comments on Astrophysics, 12, 169
- Boss, A. P. 1993, ApJ, 410, 157
- Boss, A. P. 2001, in IAU Symposium, Vol. 200, The Formation of Binary Stars, ed. H. Zinnecker & R. Mathieu, 371
- Boss, A. P. & Bodenheimer, P. 1979, ApJ, 234, 289
- Bouchet, P. 1984, A&A, 139, 344
- Brown, J. A., Smith, V. V., Lambert, D. L., et al. 1990, AJ, 99, 1930
- Brown, J. D. 2000, PhRvD, 62, 084024
- Bujarrabal, V. & Cernicharo, J. 1994, A&A, 288, 551
- Burkert, A., Bate, M. R., & Bodenheimer, P. 1997, MNRAS, 289, 497
- Casey, B. W., Mathieu, R. D., Vaz, L. P. R., Andersen, J., & Suntzeff, N. B. 1998, AJ, 115, 1617
- Cassen, P. & Moosman, A. 1981, Icarus, 48, 353
- Castro-Carrizo, A., Quintana-Lacaci, G., Neri, R., et al. 2010, A&A, 523, A59
- Cazes, J. E. & Tohline, J. E. 2000, ApJ, 532, 1051
- Chen, W. P., Simon, M., Longmore, A. J., Howell, R. R., & Benson, J. A. 1990, ApJ, 357, 224
- Cho, S.-H. & Ukita, N. 1995, PASJ, 47, L1
- Cohen, M. & Kuhl, L. V. 1979, ApJS, 41, 743
- Cotton, W. D., Vlemmings, W., Mennesson, B., et al. 2006, A&A, 456, 339
- Cox, N. L. J., Kerschbaum, F., van Marle, A.-J., et al. 2012, , 537, A35
- Culver, R. B., Ianna, P. A., & White, N. M. 1974, in Bulletin of the American Astronomical Society, Vol. 6, Bulletin of the American Astronomical Society, 427
- Danchi, W. C. & Bester, M. 1995, Ap&SS, 224, 339
- De Beck, E., Decin, L., de Koter, A., et al. 2010, A&A, 523, A18

- de Graauw, T., Helmich, F. P., Phillips, T. G., et al. 2010, *A&A*, 518, L6
- Deroo, P., Acke, B., Verhoelst, T., et al. 2007, *A&A*, 474, L45
- Deroo, P. & Van Winckel, H. 2007, *Baltic Astronomy*, 16, 145
- Deroo, P., van Winckel, H., Min, M., et al. 2006, *A&A*, 450, 181
- Dgani, R., van Buren, D., & Noriega-Crespo, A. 1996, *ApJ*, 461, 372
- Diamond, P. J. & Kembball, A. J. 2003, *ApJ*, 599, 1372
- Dickey, J. M. & Lockman, F. J. 1990, *ARAA*, 28, 215
- Dinh-V.-Trung & Lim, J. 2009, *ApJ*, 701, 292
- Diplas, A. & Savage, B. D. 1994, *ApJS*, 93, 211
- Docobo, J. A., Melikian, N. D., Tamazian, V. S., Eritsian, M. H., & Karapetian, A. A. 1998, *Ap*, 41, 254
- Docobo, J. A., Tamazian, V. S., Eritsian, M. A., Karapetian, A. A., & Melikian, N. D. 1997, *Information Bulletin on Variable Stars*, 4510, 1
- Drake, S. A., Johnson, H. R., & Brown, A. 1991, *AJ*, 101, 1483
- Duquennoy, A. & Mayor, M. 1990, *Duplicity of solar-like stars in the solar neighbourhood*, ed. Sanchez, F. & Vazquez, M., 253
- Duquennoy, A. & Mayor, M. 1991, *A&A*, 248, 485
- Durisen, R. H., Pickett, B. K., Bate, M. R., et al. 2000, in *IAU Symposium*, Vol. 200, IAU Symposium, 187P
- Eggleton, P. P. & Tokovinin, A. A. 2008, *MNRAS*, 389, 869
- Famaey, B., Pourbaix, D., Frankowski, A., et al. 2009, *A&A*, 498, 627
- Fekel, Jr., F. C. 1981, *ApJ*, 246, 879
- Frankowski, A., Famaey, B., van Eck, S., et al. 2009, *A&A*, 498, 479
- Frankowski, A., Jancart, S., & Jorissen, A. 2007, *A&A*, 464, 377
- Gérard, E. & Le Bertre, T. 2006, *AJ*, 132, 2566
- González Delgado, D., Olofsson, H., Kerschbaum, F., et al. 2003, *A&A*, 411, 123
- Griffin, M. J., Abergel, A., Abreu, A., et al. 2010, *A&A*, 518, L3

- Groenewegen, M. A. T. & de Jong, T. 1998a, *A&A*, 337, 797
- Groenewegen, M. A. T. & de Jong, T. 1998b, *A&A*, 337, 797
- Groenewegen, M. A. T., Sevenster, M., Spoon, H. W. W., & Pérez, I. 2002, *A&A*, 390, 511
- Groenewegen, M. A. T., van der Veen, W. E. C. J., Lefloch, B., & Omont, A. 1997, *A&A*, 322, L21
- Groenewegen, M. A. T., Waelkens, C., Barlow, M. J., et al. 2011a, *A&A*, 526, A162
- Groenewegen, M. A. T., Waelkens, C., Barlow, M. J., et al. 2011b, *A&A*, 526, A162
- Groenewegen, M. A. T. & Whitelock, P. A. 1996, *MNRAS*, 281, 1347
- Gromadzki, M. & Mikołajewska, J. 2009, *A&A*, 495, 931
- Guandalini, R. & Busso, M. 2008a, *A&A*, 488, 675
- Guandalini, R. & Busso, M. 2008b, *A&A*, 488, 675
- H. J. Habing, H. O. 2003, Book: *Asymptotic Giant Branch stars*
- H. Zinnecker, R. M. 2001, Book: *The Formation of Binary Stars*, IAU Symposium, Vol. 200 (ASP, IAU Volumes)
- Halbwachs, J. L. 1986, *A&A*, 168, 161
- Halbwachs, J. L. 1987, *A&A*, 183, 234
- Halbwachs, J. L., Mayor, M., & Udry, S. 1998, in *ASP Conf. Ser.*, Vol. 134, *Brown Dwarfs and Extrasolar Planets*, ed. R. Rebolo, E. L. Martin, & M. R. Zapatero Osorio, 308
- Haniff, C. A., Ghez, A. M., Gorham, P. W., et al. 1992, *AJ*, 103, 1662
- Hashimoto, O. 1994, *A&A*, 107, 445
- Hawkins, G. W. 1990, *A&A*, 229, L5
- Heiligman, G. M. 1980, *MNRAS*, 191, 761
- Herbig, G. H. 1965, *Veröffentlichungen der Remeis-Sternwarte zu Bamberg*, 27, 164
- Herbig, G. H. 1972, *ApJ*, 172, 375
- Herschel, W. 1802, *Royal Society of London Philosophical Transactions Series I*, 92, 477
- Heyer, M. H. 1988, *ApJ*, 324, 311

- Hinkle, K. H., Lebzelter, T., & Scharlach, W. W. G. 1997, *AJ*, 114, 2686
- Hinkle, K. H., Wilson, T. D., Scharlach, W. W. G., & Fekel, F. C. 1989, *AJ*, 98, 1820
- Holden, F. 1976, *PASP*, 88, 52
- Holden, F. 1978, *PASP*, 90, 463
- Hollis, J. M., Boboltz, D. A., Pedelty, J. A., White, S. M., & Forster, J. R. 2001, *ApJL*, 559, L37
- Hollis, J. M., Pedelty, J. A., Forster, J. R., et al. 2000, *ApJL*, 543, L81
- Hollis, J. M., Pedelty, J. A., & Lyon, R. G. 1997, *ApJL*, 482, L85
- Hoyle, F. 1953, *ApJ*, 118, 513
- Huggins, P. J., Mauron, N., & Wirth, E. A. 2009, *MNRAS*, 396, 1805
- Humphreys, R. M., Davidson, K., Ruch, G., & Wallerstein, G. 2005, *AJ*, 129, 492
- Humphreys, R. M., Helton, L. A., & Jones, T. J. 2007, *AJ*, 133, 2716
- Hunter, C. 1962, *ApJ*, 136, 594
- Imamura, J. N., Durisen, R. H., & Pickett, B. K. 2000, *ApJ*, 528, 946
- Inutsuka, S.-I. & Miyama, S. M. 1997, *ApJ*, 480, 681
- Ivezic, Z. & Elitzur, M. 1995, *ApJ*, 445, 415
- J. Sahade, G.E. McCluskey, Y. 1993, Book: *The Realm of Interacting Binary Stars*
- Jewell, C., Passvogel, T., Gageur, U., et al. 2010, in *American Institute of Physics Conference Series*, Vol. 1218, *American Institute of Physics Conference Series*, ed. J. G. WeisendExtra1Ii/Extra1, 1487–1493
- Jewell, P. R., Dickinson, D. F., Snyder, L. E., & Clemens, D. P. 1987, *ApJ*, 323, 749
- Johnson, D. R. H. & Soderblom, D. R. 1987, *AJ*, 93, 864
- Johnson, H. R. 1992, in *IAU Symposium*, Vol. 151, *Evolutionary Processes in Interacting Binary Stars*, ed. Y. Kondo, R. Sistero, & R. S. Polidan, 157
- Jorissen, A., Frankowski, A., Famaey, B., & van Eck, S. 2009, *A&A*, 498, 489
- Jorissen, A., Frayer, D. T., Johnson, H. R., Mayor, M., & Smith, V. V. 1993, *A&A*, 271, 463

- Jorissen, A. & Knapp, G. R. 1998, *A&A* SS, 129, 363
- Jorissen, A., Mayer, A., van Eck, S., et al. 2011, *A&A*, 532, A135
- Jorissen, A. & van Eck, S. 2000, in *IAU Symposium*, Vol. 177, *The Carbon Star Phenomenon*, ed. R. F. Wing, 259
- Josselin, E., Mauron, N., Planesas, P., & Bachiller, R. 2000, *A&A*, 362, 255
- Joy, A. H. 1926, *ApJ*, 63, 281
- Jura, M. & Kleinmann, S. G. 1990a, *ApJS*, 73, 769
- Jura, M. & Kleinmann, S. G. 1990b, *ApJS*, 73, 769
- Kafatos, M., Hollis, J. M., Yusef-Zadeh, F., Michalitsianos, A. G., & Elitzur, M. 1989, *ApJ*, 346, 991
- Kahane, C. & Jura, M. 1996, *A&A*, 310, 952
- Kamohara, R., Bujarrabal, V., Honma, M., et al. 2010, *A&A*, 510, A69
- Karovicova, I., Wittkowski, M., Boboltz, D. A., et al. 2011, *A&A*, 532, A134
- Karovska, M., Hack, W., Raymond, J., & Guinan, E. 1997, *ApJL*, 482, L175
- Karovska, M., Nisenson, P., Papaliolios, C., & Boyle, R. P. 1991, *ApJL*, 374, L51
- Kastner, J. H. & Soker, N. 2004, *ApJ*, 608, 978
- Kastner, J. H. & Weintraub, D. A. 1998, *AJ*, 115, 1592
- Keppens, R., Meliani, Z., van Marle, A. J., et al. 2012, *Journal of Computational Physics*, 231, 718
- Kerschbaum, F., Ladjal, D., Ottensamer, R., et al. 2010, *A&A*, 518, L140
- Kerschbaum, F., Mecina, M., Ottensamer, R., et al. 2011, in *ASP Conf. Ser.*, Vol. 445, *Why Galaxies Care about AGB Stars II: Shining Examples and Common Inhabitants*, ed. F. Kerschbaum, T. Lebzelter, & R. F. Wing, 589
- Kerschbaum, F. & Olofsson, H. 1999, *A&A* SS, 138, 299
- Kholopov, P. N. 1987, *General Catalogue of Variable Stars.*, ed. Kholopov, P. N.
- Knapp, G. R., Pourbaix, D., Platais, I., & Jorissen, A. 2003, *A&A*, 403, 993
- Knapp, G. R., Young, K., Lee, E., & Jorissen, A. 1998, *ApJS*, 117, 209

- Knigge, C. 2011, in ASP Conf. Ser., Vol. 447, ASP Conf. Ser., ed. L. Schmidtobreick, M. R. Schreiber, & C. Tappert, 3
- Ladjal, D., Barlow, M. J., Groenewegen, M. A. T., et al. 2010, *A&A*, 518, L141
- Larson, R. B. 1972, *MNRAS*, 156, 437
- Larson, R. B. 1990, in *Astrophysics and Space Science Library*, Vol. 162, *Physical Processes in Fragmentation and Star Formation*, ed. R. Capuzzo-Dolcetta, C. Chiosi, & A. di Fazio, 389–399
- Lattanzio, J. C. & Henriksen, R. N. 1988, *MNRAS*, 232, 565
- Layzer, D. 1963, *ApJ*, 137, 351
- Le Bertre, T. & Gérard, E. 2001, *A&A*, 378, L29
- Le Bertre, T. & Gérard, E. 2004, *A&A*, 419, 549
- Libert, Y., Le Bertre, T., Gérard, E., & Winters, J. M. 2008, *A&A*, 491, 789
- Libert, Y., Winters, J. M., Le Bertre, T., Gérard, E., & Matthews, L. D. 2010, *A&A*, 515, A112
- Lindqvist, M., Lucas, R., Olofsson, H., et al. 1996, *A&A*, 305, L57
- Lindqvist, M., Nyman, L.-A., Olofsson, H., & Winnberg, A. 1988, *A&A*, 205, L15
- Lindqvist, M., Olofsson, H., Lucas, R., et al. 1999, *A&A*, 351, L1
- Little, S. J., Little-Marenin, I. R., & Bauer, W. H. 1987, *AJ*, 94, 981
- Lopez, B., Danchi, W. C., Bester, M., et al. 1997, *ApJ*, 488, 807
- Loup, C., Forveille, T., Omont, A., & Paul, J. F. 1993, *A&A SS*, 99, 291
- Lowrance, P. J., Kirkpatrick, J. D., Reid, I. N., Cruz, K. L., & Liebert, J. 2003, *ApJL*, 584, L95
- Lubow, S. & Artymowicz, P. 1996, in *Bulletin of the American Astronomical Society*, Vol. 28, *AAS/Division of Dynamical Astronomy Meeting #27*, 1182
- Lubow, S. H. & Artymowicz, P. 2000, *Protostars and Planets IV*, 731
- Lucy, L. B. 1981, in *IAU Symposium*, Vol. 93, *Fundamental Problems in the Theory of Stellar Evolution*, ed. D. Sugimoto, D. Q. Lamb, & D. N. Schramm, 75–83
- Mansbach, P. 1970, *ApJ*, 160, 135

- Margon, B., Anderson, S. F., Harris, H. C., et al. 2002, *AJ*, 124, 1651
- Martin, D. C., Seibert, M., Neill, J. D., et al. 2007, *Nature*, 448, 780
- Marvel, K. B., Diamond, P., & Kemball, A. 2001, *JAAVSO*, 29, 154
- Mason, B. D., Hartkopf, W. I., Holdenried, E. R., & Rafferty, T. J. 2001, *AJ*, 121, 3224
- Mason, B. D., Martin, C., Hartkopf, W. I., et al. 1999, *AJ*, 117, 1890
- Mastrodemos, N. & Morris, M. 1998, *ApJ*, 497, 303
- Mastrodemos, N. & Morris, M. 1999, *ApJ*, 523, 357
- Mathieu, R. D. 1994, *ARA&A*, 32, 465
- Mathieu, R. D., Walter, F. M., & Myers, P. C. 1989a, *AJ*, 98, 987
- Mathieu, R. D., Walter, F. M., & Myers, P. C. 1989b, *AJ*, 98, 987
- Matthews, L. D., Libert, Y., Gérard, E., Le Bertre, T., & Reid, M. J. 2008, *ApJ*, 684, 603
- Matthews, L. D. & Reid, M. J. 2007, *AJ*, 133, 2291
- Mauron, N. & Huggins, P. J. 2000, *A&A*, 359, 707
- Mauron, N. & Huggins, P. J. 2006, *A&A*, 452, 257
- Mayer, A., Jorissen, A., Kerschbaum, F., et al. 2011, *A&A*, 531, L4
- Mazeh, T., Goldberg, D., Duquennoy, A., & Mayor, M. 1992, *ApJ*, 401, 265
- McIntosh, G. C. & Rustan, G. 2007, *AJ*, 134, 2113
- Meaburn, J., López, J. A., Boumis, P., Lloyd, M., & Redman, M. P. 2009, *A&A*, 500, 827
- Meier, S. R. & Kafatos, M. 1995, *ApJ*, 451, 359
- Merrill, P. W. 1921, *ApJ*, 53, 375
- Merrill, P. W. 1950, *ApJ*, 112, 514
- Mihalas, D. & Binney, J. 1981, *Galactic astronomy: Structure and kinematics /2nd edition/*, ed. Mihalas, D. & Binney, J.
- Mikołajewska, J., ed. 1997, *Physical Processes in Symbiotic Binaries and Related Systems*.

- Mobberley, M. 2009, Book: Cataclysmic Cosmic Events and How to Observe Them
- Mohamed, S. & Podsiadlowski, P. 2007, in ASP Conf. Ser., Vol. 372, 15th European Workshop on White Dwarfs, ed. R. Napiwotzki & M. R. Burleigh, 397
- Mohamed, S. & Podsiadlowski, P. 2011, in Asymmetric Planetary Nebulae 5 Conference
- Monaghan, J. J. 1994, *ApJ*, 420, 692
- Monaghan, J. J. & Lattanzio, J. C. 1991, *ApJ*, 375, 177
- Monnier, J. D., Millan-Gabet, R., Tuthill, P. G., et al. 2004, *ApJ*, 605, 436
- Morris, M., Sahai, R., Matthews, K., et al. 2006, in IAU Symposium, Vol. 234, Planetary Nebulae in our Galaxy and Beyond, ed. M. J. Barlow & R. H. Méndez, 469–470
- Muller, S., Dinh-V-Trung, Lim, J., et al. 2007, *ApJ*, 656, 1109
- Myers, P. C. 1987, in Astrophysics and Space Science Library, Vol. 134, Interstellar Processes, ed. D. J. Hollenbach & H. A. Thronson Jr., 71–86
- Nakashima, J.-i. 2006, *ApJ*, 638, 1041
- Narita, S., Hayashi, C., & Miyama, S. M. 1984, *Progress of Theoretical Physics*, 72, 1118
- Neri, R., Kahane, C., Lucas, R., Bujarrabal, V., & Loup, C. 1998, *A&A SS*, 130, 1
- New, K. C. B., Centrella, J. M., & Tohline, J. E. 2000, *PhRvD*, 62, 064019
- Nichols, J. & Slavin, J. D. 2009, *ApJ*, 699, 902
- Nichols, J. S., DePasquale, J., Kellogg, E., et al. 2007, *ApJ*, 660, 651
- Norman, M. L. & Wilson, J. R. 1978, *ApJ*, 224, 497
- Olofsson, H., Bergman, P., Eriksson, K., & Gustafsson, B. 1996, *A&A*, 311, 587
- Olofsson, H., Eriksson, K., & Gustafsson, B. 1988, *A&A*, 196, L1
- Olson, B. I. & Richer, H. B. 1975, *ApJ*, 200, 88
- Percy, J. R., Wilson, J. B., & Henry, G. W. 2001, *PASP*, 113, 983
- Pilbratt, G. L., Riedinger, J. R., Passvogel, T., et al. 2010, *A&A*, 518, L1
- Podsiadlowski, P. & Mohamed, S. 2007, *Baltic Astronomy*, 16, 26
- Poglitsch, A., Waelkens, C., Geis, N., et al. 2010, *A&A*, 518, L2

- Pongracic, H., Chapman, S. J., Davies, J. R., et al. 1992, MNRAS, 256, 291
- Pourbaix, D., Platais, I., Detournay, S., et al. 2003, A&A, 399, 1167
- Pringle, J. E. 1989, MNRAS, 239, 361
- Proust, D., Ochsenbein, F., & Pettersen, B. R. 1981, A&A SS, 44, 179
- Quist, C. F. & Lindegren, L. 2000, , 361, 770
- Quist, C. F. & Lindegren, L. 2001, in IAU Symposium, Vol. 200, The Formation of Binary Stars, ed. H. Zinnecker & R. Mathieu, 64
- Ramstedt, S., Schöier, F. L., Olofsson, H., & Lundgren, A. A. 2006, A&A, 454, L103
- Ratzka, T., Schegerer, A. A., Leinert, C., et al. 2009, A&A, 502, 623
- Reimers, D. & Cassatella, A. 1985, ApJ, 297, 275
- Reipurth, B. 1988, in NATO ASIC Proc. 241: Formation and Evolution of Low Mass Stars, ed. A. K. Dupree & M. T. V. T. Lago, 305
- Reipurth, B. & Zinnecker, H. 1993, A&A, 278, 81
- Richichi, A. 2001, in IAU Symposium, Vol. 200, The Formation of Binary Stars, ed. H. Zinnecker & R. Mathieu, 280
- Richichi, A., Calamai, G., Leinert, C., Stecklum, B., & Trunkovsky, E. M. 1996, A&A, 309, 163
- Roussel, H. 2012, A&A
- Sahai, R., Findeisen, K., Gil de Paz, A., & Sánchez Contreras, C. 2008, ApJ, 689, 1274
- Sasselov, D. D. & Rucinski, S. M. 1990, ApJ, 351, 578
- Schöier, F. L., Lindqvist, M., & Olofsson, H. 2005, A&A, 436, 633
- Schöier, F. L. & Olofsson, H. 2001, A&A, 368, 969
- Schuerman, D. W. 1972, ApSS, 19, 351
- Shatsky, N. 2000, in IAU Symposium, Vol. 200, IAU Symposium, 175P
- Shibata, M., Baumgarte, T. W., & Shapiro, S. L. 2000, ApJ, 542, 453
- Shu, F. H. 1977, ApJ, 214, 488
- Shu, F. H., Adams, F. C., & Lizano, S. 1987, ARAA, 25, 23

- Shu, F. H., Tremaine, S., Adams, F. C., & Ruden, S. P. 1990, *ApJ*, 358, 495
- Siess, L., Izzard, R. G., Davis, P. J., & Deschamps, R. 2011, in *ASP Conf. Ser.*, Vol. 447, *ASP Conf. Ser.*, ed. L. Schmidtobreick, M. R. Schreiber, & C. Tappert, 339
- Sigalotti, L. D. G. 1990, *MNRAS*, 246, 243
- Smith, N., Humphreys, R. M., Davidson, K., et al. 2001, *AJ*, 121, 1111
- S.N. Shore, M. Livio, E. v. d. H. 1992, *Book: Interacting Binaries*
- Soker, N. 1994, *MNRAS*, 270, 774
- Sokoloski, J. L. & Bildsten, L. 2010, *ApJ*, 723, 1188
- Solf, J. & Ulrich, H. 1985, *A&A*, 148, 274
- Spitzer, L. 1978, *Physical processes in the interstellar medium*, ed. Spitzer, L.
- Stahler, S. W. 1988, *ApJ*, 332, 804
- Stencel, R. E., Pesce, J. E., & Hagen Bauer, W. 1988, *AJ*, 95, 141
- Strom, K. M., Margulis, M., & Strom, S. E. 1989, *ApJL*, 346, L33
- Tassoul, J.-L. 1978, *Theory of rotating stars*, ed. Tassoul, J.-L.
- Tatebe, K., Chandler, A. A., Hale, D. D. S., & Townes, C. H. 2006, *ApJ*, 652, 666
- Tohline, J. E. 1980, *ApJ*, 235, 866
- Tohline, J. E. & Durisen, R. H. 2001, in *IAU Symposium*, Vol. 200, *The Formation of Binary Stars*, ed. H. Zinnecker & R. Mathieu, 40
- Trimble, V. 1990, *MNRAS*, 242, 79
- Tsuribe, T. & Inutsuka, S.-I. 2000, in *IAU Symposium*, Vol. 200, *IAU Symposium*, 184P
- Turner, J. A., Chapman, S. J., Bhattal, A. S., et al. 1995, *MNRAS*, 277, 705
- Ueta, T. 2008, *ApJL*, 687, L33
- Valtonen, M. & Mikkola, S. 1991, , 29, 9
- van Biesbroeck, G. 1959, *PASP*, 71, 462
- van der Veen, W. E. C. J. & Habing, H. J. 1988, *A&A*, 194, 125
- van Leeuwen, F. 2007, *A&A*, 474, 653

- van Loon, J. T., Zijlstra, A. A., Whitelock, P. A., et al. 1998, *A&A*, 329, 169
- Vishniac, E. T. 1994, *ApJ*, 428, 186
- Wallerstein, G. 1986, *PASP*, 98, 118
- Wallerstein, G. & Greenstein, J. L. 1980, *PASP*, 92, 275
- Wannier, P. G., Sahai, R., Andersson, B.-G., & Johnson, H. R. 1990, *ApJ*, 358, 251
- Wareing, C. J., Zijlstra, A. A., O'Brien, T. J., & Seibert, M. 2007, *ApJL*, 670, L125
- Weigelt, G., Balega, Y., Bloecker, T., et al. 1998, *A&A*, 333, L51
- Weis, E. W. 1974, *ApJ*, 190, 331
- Whitelock, P. A. 2003, in *ASP Conf. Ser.*, Vol. 303, *ASP Conf. Ser.*, ed. R. L. M. Corradi, J. Mikolajewska, & T. J. Mahoney, 41–+
- Whitworth, A. P. 2001, in *IAU Symposium*, Vol. 200, *The Formation of Binary Stars*, ed. H. Zinnecker & R. Mathieu, 33
- Whitworth, A. P., Bhattal, A. S., Turner, J. A., & Watkins, S. J. 1995, *A&A*, 301, 929
- Wielen, R., Lenhardt, H., Schwan, H., & Dettbarn, C. 2001, *A&A*, 368, 298
- Wilking, B. A. & Lada, C. J. 1983, *ApJ*, 274, 698
- Willson, L. A. & Bowen, G. H. 1998, in *Cyclical Variability in Stellar Winds*, ed. L. Kaper & A. W. Fullerton, 294
- Willson, L. A., Garnavich, P., & Mattei, J. A. 1981, *Information Bulletin on Variable Stars*, 1961, 1
- Winters, J. M., Fleischer, A. J., Le Bertre, T., & Sedlmayr, E. 1997, *A&A*, 326, 305
- Winters, J. M., Le Bertre, T., Jeong, K. S., Nyman, L.-Å., & Epchtein, N. 2003, *A&A*, 409, 715
- Winters, J. M., Le Bertre, T., Pety, J., & Neri, R. 2007, *A&A*, 475, 559
- Wootten, A. 1989, *ApJ*, 337, 858
- Worley, C. E. 1972, *ApJL*, 175, L93
- Young, K., Phillips, T. G., & Knapp, G. R. 1993, *ApJ*, 409, 725
- Zinnecker, H. 1989, in *European Southern Observatory Conference and Workshop Proceedings*, Vol. 33, *European Southern Observatory Conference and Workshop Proceedings*, ed. B. Reipurth, 447–469

Appendix

Curriculum Vitae

Personal Information

Name: Klaus Kornfeld

Birthday: August 22nd, 1985

Birthplace: Güssing, Austria

Nationality: Austrian

Address: Kienmayergasse 23/2, 1140 Wien, Austria

Telephone: +43/650/7073751

E-mail: klaus.kornfeld[at]gmail.com

Sex: male

Education

1996 - 2000 Bundesgymnasium Oberschützen (lower grade)

2000 - 2004 Bundesoberstufenrealgymnasium Güssing (senior grade)

2004 - 2005 Paramedic for Austrian Armed Forces

2005 - 2009 Bachelor study in Astronomy at University of Vienna

2009 - 2010 ERASMUS exchange at Uppsala University

2009 - 2012 Master study in Astronomy at University of Vienna

Publications

The large scale environments of binary AGB stars with case studies of R Aqr, W Aql and EP Aqr

A. Mayer, A. Jorissen, F. Kerschbaum, S. van Eck, R. Ottensamer, **K. Kornfeld**, M. Mecina, J.A.D.L. Blommaert, L. Decin, M.A.T. Groenewegen, Th. Posch, B. Vandebussche, and C. Waelkens, A&A, *subm.*

Attended Conferences

Why Galaxies Care About AGB Stars II - Shining Examples and Common Inhabitants, August 16-20, 2010, Vienna, University Campus

This Thesis was written in L^AT_EX